DIANA LUISE WESCH

Molecular mechanisms underlying the regulation of δ-epithelial sodium channel (δ-ENaC) function

Directores
DIEGO ÁLVAREZ DE LA ROSA RODRÍGUEZ
TERESA GIRÁLDEZ FERNÁNDEZ

Hereby I declare, that I have written this PhD thesis on my own and without any other sources and aids than quoted. Accordingly, all citations and borrowed illustrations are perceptibly indicated by references and listed at the end of this thesis. This thesis has not been presented in any form to another examination committee.

Part of this study was published in the *American Journal of Physiology – Cell Physiology*, entitled: "The neuronal-specific SGK1.1 kinase regulated δ-epithelial Na^+ channel independently of PY motifs and couples it to phospholipase C signaling" (2010). A publication in the same journal citing another part of this dissertation is currently under way.

La Laguna, October the 20th, 2011

To my family.

Contents

Illustration index

Table index

Abstract

The epithelial sodium channel (ENaC) is a heteromultimeric Na^+ selective ion channel member of the ENaC/degenerins family of non-voltage gated ion channels. Canonically, ENaC is composed by three analogous subunits α, β and γ and represents the rate-limiting step of Na^+-reabsorption across tight epithelia. Another subunit, named δ, is expressed in the nervous system of primates, where its role and regulation are unknown. The δ-subunit can substitute α and form functional channels either alone or with β and γ. δ-ENaC has been proposed to participate in the transduction of ischemic signals during hypoxia and inflammation. δ-ENaC exists in two isoforms, δ1 and δ2. Pyramidal neurons of the human cortex express either δ1 or δ2, with few cells co-expressing both isoforms, which suggest that they may play specific physiological roles. Heterologous expression of δ1 in *Xenopus* oocytes led to ~2.5 fold more amiloride-sensitive current than δ2. The difference in whole-cell current is based on differential plasma membrane abundance. Two sequences in the δ2 N-terminus independently reduced channel abundance in the membrane based on altered insertion rates and without involvement of PY motifs. Since Dynasore did not inhibit δ-ENaC endocytosis, it is concluded that δ-ENaC undergoes clathrin-independent endocytosis as opposed to αβγ-ENaC. αβγ-ENaC in the distal nephron is regulated by the serum- and glucocorticoid-induced kinase 1 (SGK1) and a neuronal-specific isoform, SGK1.1, was found to regulate acid sensing ion channel 1 (ASIC1), another member of the ENaC/degenerins family. Here is shown that SGK1.1 is involved in δ-ENaC regulation. Co-expression of SGK1.1 with δ-ENaC in *Xenopus* oocytes leads to enhanced amiloride-sensitive currents when compared to δ-ENaC currents alone. This effect does not require a PY motif and depends on SGK1.1 phosphorylation activity and binding to phosphatidylinositol 4,5-bisphosphate (PIP2). Further, activation of phospholipase C abrogates SGK1.1 modulation of δ-ENaC.

Resumen

El canal epitelial de sodio (ENaC) es un canal iónico heteromultimérico con selectividad para Na$^+$. Es miembro de la familia ENaC/degenerinas de canales iónicos independientes de voltage. El ENaC canónico está compuesto por tres subunidades análogas α, β y γ, y constituye el paso limitante de la tasa de reabsorpción de Na$^+$ a través de epitelios impermeables. Otra subunidad, denominada δ, se expresa en el sistema nervioso central de primates, donde su papel y regulación son poco conocidos. La subunidad δ puede sustituir a α y forma canales funcionales bien sola o en combinación con β y γ. Se ha propuesto que δ-ENaC participa en la transmisión de señales isquémicas durante hipoxia e inflamación. Existen dos isoformas de δ-ENaC, δ1 y δ2. Las neuronas piramidales de la cortiza cerebral humana expresan δ1 o bien δ2, mientras que pocas células co-expresan ambas isoformas, lo cual sugiere que tengan papeles fisiológicos específicos. La expresión heteróloga de δ1 en oocitos de *Xenopus* produjo corrientes sensibles a amiloride ~2.5 veces superiores a δ2. La diferencia en corriente macroscópica se basa en la diferente abundancia de las isoformas en la membrana. Dos secuencias en el N-terminal de δ2 disminuyeron independientemente la abundancia del canal en la membrana, a consecuencia de tasas de inserción alteradas y sin implicación del motivo PY. Dynasore no inhibió la endocitosis de δ-ENaC, lo cual lleva a concluir que la endocitosis de δ-ENaC es independiente de clatrina, a diferencia de la de αβγ-ENaC. En la nefrona distal αβγ-ENaC está regulado por la quinasa inducida por suero- y glucocorticoides 1 (SGK1). Se ha descrito una isoforma específica de neuronas, SGK1.1, que participa en la regulación del canal iónico sensible a acidez 1 (ASIC1), otro miembro de la familia ENaC/degenerinas. En este estudio se muestra que SGK1.1 está implicada en la regulación de δ-ENaC. La co-expresión de SGK1.1 con δ-ENaC en oocitos de *Xenopus* resulta en un aumento de corriente sensible a amiloride. Este efecto no requiere el motivo PY y depende de la actividad de fosforilación de SGK1.1 y su unión a fosfatidilinositol 4,5-bifosfato (PIP2). La activación de la fosfolipasa C (PLC) elimina la modulación de δ-ENaC por SGK1.1.

I.   Introduction

I. 1   Epithelial Na$^+$ channel (ENaC)

The epithelial sodium channel (ENaC) is a heteromultimeric Na$^+$ selective ion channel. ENaC is constitutively active, voltage- and ligand-independent. ENaC is inhibited by the K$^+$-sparing diuretic amiloride (Kellenberger & Schild, 2002) and belongs to the MEC/DEG/ENaC superfamily of ion channels (Alvarez de la Rosa et al., 2000). Family members share a common membrane topology, each subunit spans the membrane twice with the transmembrane domains TM1 and TM2 connected by a large extracellular loop and exhibits short intracellular N- and C-termini, with TM2 being the pore-lining domain (Canessa *et al.*, 1994a; Renard *et al.*, 1994; Snyder *et al.*, 1994). ENaC is formed by the three analogous subunits α, β and γ (Canessa *et al.*, 1994b), forming a putative trimer (Canessa, 2007; Jasti *et al.*, 2007; Stockand *et al.*, 2008), but its definitive stoichiometry remains to be elucidated (**Fig. I.1**). In this composition ENaC is expressed at the apical cell surface of tight epithelia, such as the distal colon, the distal kidney tubule and lung (Rossier *et al.*, 2002). There, its physiological role is to limit the rates of Na$^+$ reabsorption for the maintenance of body volume, blood pressure and fluid clearance (Garty & Palmer, 1997; Soundararajan *et al.*, 2010).
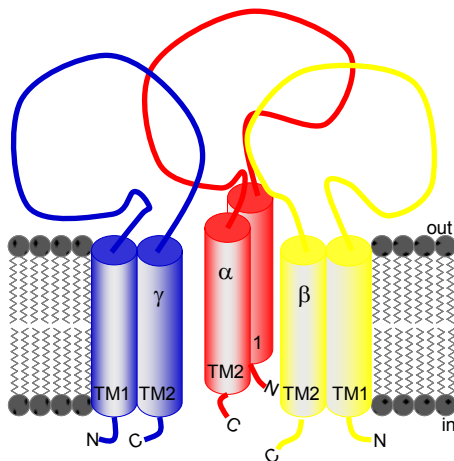
Fig. I.1 Proposed structure of ENaC composed by the subunits α, β and γ.
The canonical ENaC is a putative trimer formed by the subunits α, β and γ. Each subunit contains short N- and C-termini and two membrane spanning domains connected by a large extracellular loop. Supposedly the second transmembrane domain (TM2) of each subunit is pore lining (Su & Menon, 2001).

In the kidney ENaC is specifically expressed in cortical collecting duct principal cells of the distal nephron, where it is described to be the rate limiting step of Na$^+$ reabsorption and the principal target of potassium sparing diuretics, such as amiloride (Benos *et al.*, 1997; Horisberger, 1998). The electrochemical gradient of Na$^+$ created by the basolateral Na$^+$/K$^+$-ATPase, which pumps Na$^+$ from the cell into the blood and K$^+$ into the cell, is the driving force to allow Na$^+$ to enter the cell apically via ENaC (Loffing & Korbmacher, 2009). Once Na$^+$ has entered the cell, water moves along according to the osmotic driving force. The reabsorption of Na$^+$ in the cortical collecting tubule generates a lumen-negative potential that facilitates the secretion of K$^+$ and H$^+$ by the distal nephron.

Biophysical hallmarks of ENaC are its low conductance and its high selectivity for Na$^+$ over K$^+$ (Canessa *et al.*, 1994b; Puoti *et al.*, 1995). Further, a causal relationship between proteolytic

cleavage of ENaC extracellular domain and increased ENaC open probability (Po) has been established. Exposure to serine proteases led to a dramatic increase of ENaC Po of the near-silent channel pool (Caldwell *et al.*, 2004), and ENaC is considered to mature upon proteolytic processing (Hughey *et al.*, 2003). Therefore ENaC is thought to exist in a variety of pools within the plasma membrane (Hughey *et al.*, 2004) and also just beneath it (Lu *et al.*, 2007b). In the membrane, a mature and active pool of channels was reported opposed to a pool of near-silent channels (Firsov *et al.*, 1996), which could be activated upon proteolytic processing by proteases such as trypsin (Caldwell *et al.*, 2004; Diakov *et al.*, 2008). Cleavage may activate the channel by releasing inhibitory peptides from the extracellular loops (Kleyman *et al.*, 2009). Further, the existance of a subapical ENaC pool was correlated to the early effect of aldosterone, where ENaC was redistributed from the cytoplasm into the apical membrane within $1 – 3$ hours (Kellenberger & Schild, 2002) in a PY motif dependent manner (Lu *et al.*, 2007b). Another characteristic feature of ENaC is Na^+ self-inhibition, a mechanism to prevent intracellular Na^+ overload in transporting epithelial cells in the presence of high extracellular Na^+ concentration (Turnheim, 1991; Bize & Horisberger, 2007). Whilst the inhibitory effect of extracellular Na^+ on ENaC is rapid and caused by an acute decrease in channel Po (Na^+ self-inhibition) (Chraibi & Horisberger, 2002), the inhibitory effect of increased intracellular Na^+ concentration is a slower process and mainly involves a decrease in channel surface expression (Na^+ feedback inhibition) (Kellenberger *et al.*, 1998).

Several ENaC associated channelopathies have been reported and the importance of ENaC in Na^+ homeostasis and blood pressure control is emphasized by the direct genetic relation of its genes to diseases involving blood pressure variations: 1) Liddle's syndrome, an inherited form of human salt-sensitive hypertension (Shimkets *et al.*, 1994; Bubien, 2010), which is accompanied by hypokalemia, metabolic acidosis, and low circulating levels of renin and aldosterone (Lifton *et al.*, 2001), and 2) pseudohypoaldosteronism type 1 (PHA1), a heritable salt-wasting disease (Chang *et al.*, 1996; Edelheit *et al.*, 2010), which is further characterized by normal renal function, hypotension, hyperkalemia, metabolic acidosis and high circulating renin and aldosterone levels (Stokes, 1999). PHA1 patients suffer a life-threatening hyperkalemia, which requires balancing and can be controlled by high salt intake. PHA1 appears in several different intensities and amongst others results from varied dysfunction of the MR gene or ENaC gene (Grunder *et al.*, 1997; Berger *et al.*, 2000; Geller *et al.*, 2006).

Cystic fibrosis (CF) is also reported to be associated with ENaC dysfunction (Ji *et al.*, 2000; Chang *et al.*, 2005; Lazrak *et al.*, 2011). The characteristic symptom of CF is solid mucus in the lung. One possible explanation for CF was that in lungs of CF patients, the failure of defective CF transmembrane conductance chloride channel (CFTR) fails to inhibit ENaC. This is thought to cause hyperabsorption of sodium and fluid, contributing to the formation of dry sticky mucus (Donaldson & Boucher, 2007; Berdiev *et al.*, 2009). Indeed, airway-specific over-expression of ENaC also produces CF-like lung disease (Mall *et al.*, 2004; Kimura *et al.*, 2011) that can be prevented by amiloride (Zhou *et al.*, 2011), which supports the concept that increased ENaC activity may contribute to CF pathophysiology (Chang *et al.*, 2005). The complexity of the ENaC-CFTR

relationship is corroborated by suggestions that ENaC may have a stimulatory effect on CFTR activity (Chabot *et al.*, 1999; Ji *et al.*, 2000; Kunzelmann *et al.*, 2000).

I. 2   δ-ENaC

Another ENaC subunit is δ, which is expressed in primates in a variety of tissues not involved in body sodium homeostasis such as the skeletal muscle, heart, lung, pancreas and brain (Waldmann *et al.*, 1995; Giraldez *et al.*, 2007), where its physiological function remains to be elucidated. In rodents δ is a pseudogene (Alvarez de la Rosa, Flores & Giraldez, unpublished data). In *Xenopus* a related subunit was found, denoted as ε-ENaC (**Fig. I.2**). This ε subunit was characterized to be able to replace the α subunit and to form functional, highly selective and amiloride-sensitive Na$^+$-channels with β and γ, displaying a strong Na$^+$ self-inhibition (Babini *et al.*, 2003).
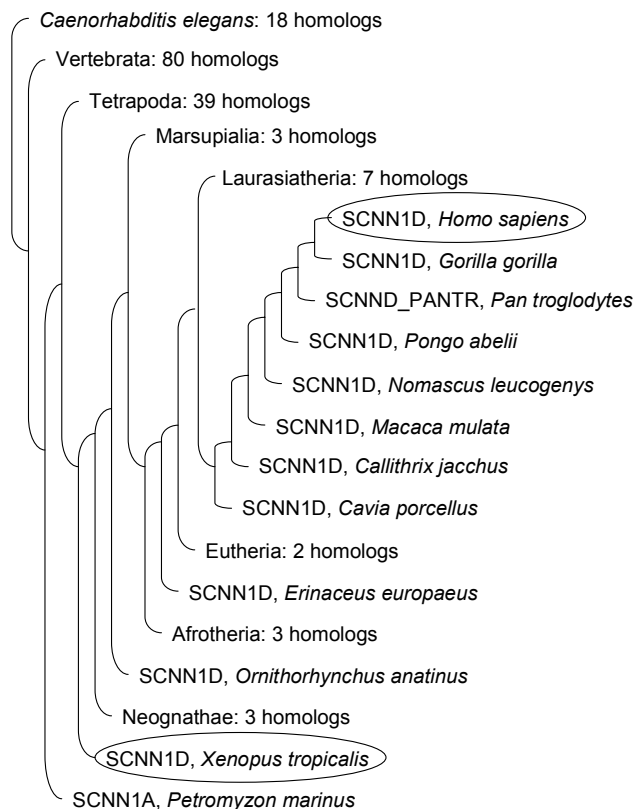
Fig. I.2 Phylogenetic tree of the SCNN1D gene encoding for δ-ENaC.
Based on the SCNN1D DNA sequences δ-ENaC appears to be frequently encoded among vertebrates. Encircled are the human gene and the *Xenopus* gene denoted as ε-ENaC, which happens to be an orthologue of δ-ENaC sharing more than 66 % of sequence identity (www.enselmbl.org).

The δ subunit shares the highest sequence identity with the α subunit (37 %) and forms functional channels either alone or in combination with the β and γ subunits, although expressed alone it yields ~50-fold smaller currents than when co-expressed with β and γ (Waldmann *et al.*, 1995; Yamamura *et al.*, 2006). In human brain, the β and γ subunits are absent or expressed in low amounts (Giraldez *et al.*, 2007), therefore they are unlikely interacting partners for δ. Rather other members of the ENaC/Degenerin family expressed in the human brain, like the acid sensing ion channels ASIC1 and ASIC2 (Lingueglia *et al.*, 1997; Alvarez de la Rosa *et al.*, 2002b; Duggan *et al.*, 2002), could be channel-forming partners for δ-ENaC. Like ASIC, δ-ENaC is potentiated by a drop in extracellular pH and therefore could serve as a pH sensor. Unlike some ASIC channels, which display a fast desensitization (Waldmann *et al.*, 1997) the response of δ-ENaC towards pH drop is sustained (Waldmann *et al.*, 1995). Both ASIC and δ-ENaC, were

proposed to integrate ischemic signals in inflamed and hypoxic tissues (Ji & Benos, 2004; Xiong *et al.*, 2004; Yamamura *et al.*, 2004b).

Further, comparison between the α and the δ subunit shows that δβγ-ENaC (IC_{50} amiloride ~2.6 µM) is more than an order of magnitude less sensitive to amiloride or benzamil than αβγ (IC_{50} amiloride ~80nM) (Waldmann *et al.*, 1995; Ji *et al.*, 2004). Additional pharmacological differences are the activating effect of capsazepine and icilin on δβγ-ENaC, and its inhibition by Evans blue (Yamamura *et al.*, 2004a; Yamamura *et al.*, 2005a; Yamamura *et al.*, 2005b). Moreover, δβγ-ENaC displays a higher single-channel Na^+ conductance (~12 pS) than αβγ-ENaC (~5 pS) (Waldmann *et al.*, 1995; Haerteis *et al.*, 2009), but a similar conductance for Li^+ (~7 pS) (Ji *et al.*, 2004). The Po of αβγ is determined to be 0.5, whereas the Po of δβγ is approximately 0.9 (Garty & Palmer, 1997; Haerteis *et al.*, 2009) and proteolytic processing of the channel has less effect on the Po of δβγ than on αβγ Po (Haerteis *et al.*, 2009). Interestingly, self-inhibition by extracellular Na^+ is less pronounced in δβγ-ENaC than in αβγ-ENaC (Ji *et al.*, 2006).

Since δ-ENaC features voltage-independence and high Na^+-selectivity, it could provide a leak sodium conductance in the central nervous system, contributing to the setting of the resting membrane potential like the sodium leak channel (NALCN) (Lu *et al.*, 2007a). This idea is supported by the observation that amiloride has a hyperpolarizing effect on the resting potential of muscles (Estrada & Sanchez, 1991). Furthermore, amiloride resulted neuroprotective in cerebral ischemia (Arias *et al.*, 2008), which is consistent with the idea that neuronal members of the ENaC/Degenerin family like δ-ENaC could be implicated neurodegenerative diseases, such as Parkinson. *In situ* hybridization (ISH) stainings of brains of the *Macaca fascicularis* (**Fig. I.3**) show a strong correlation between expression of δ-ENaC and dopaminergic neuron vulnerability as seen in Parkinson's disease, since both δ1 and δ2 are highly abundant in the ventral area of the *substantia nigra*, which is highly vulnerable, and display moderate abundance in the lateral area (moderate vulnerability), whereas δ-ENaC is low abundant in the dorsal area, which has a low vulnerability (González-Hernandez, Afonos-Oramas, Alvarez de la Rosa & Giraldez, unpublished data).
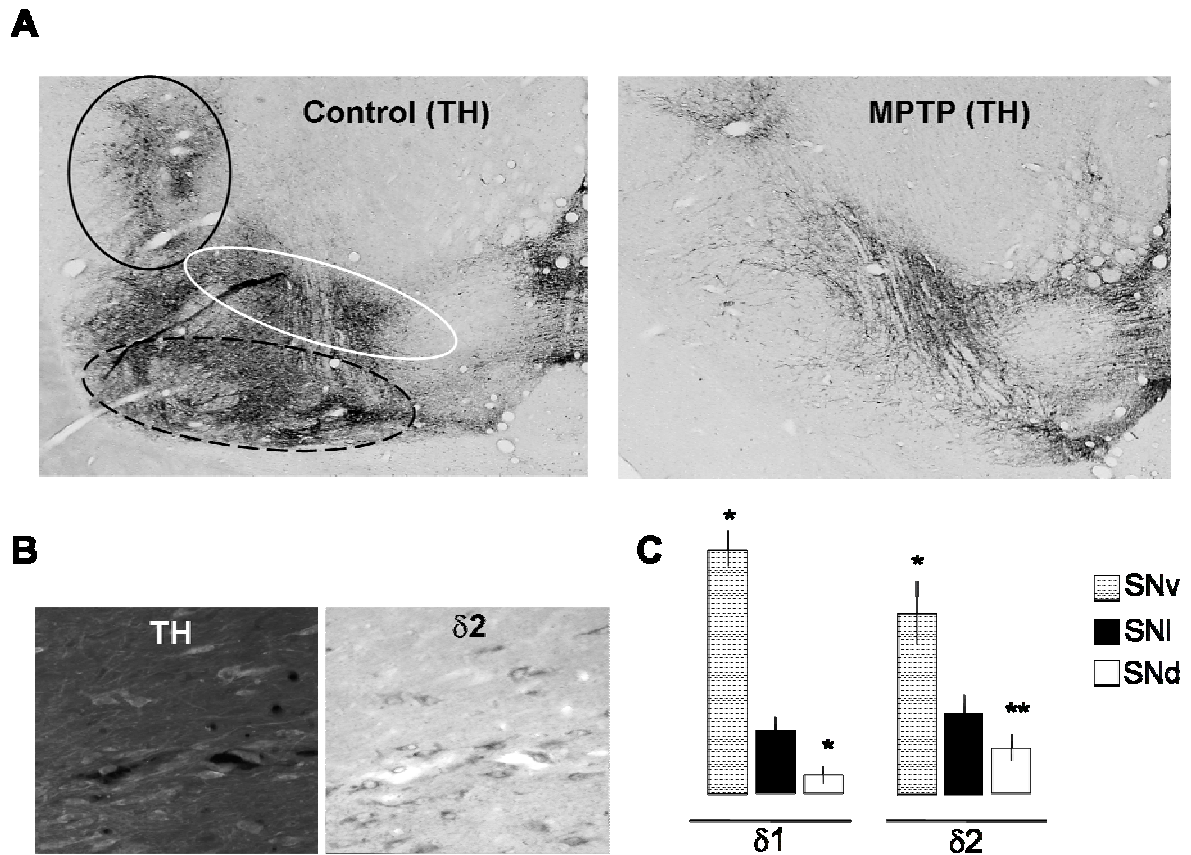
Fig. I.3 Expression of δ-ENaC in the *substantia nigra* of *Macaca fascicularis*.
A: ISH with tyrosine hydroxilase (TH) probe as marker of dopaminergic neurons in *substantia nigra* (SN) obtained from *M. fascicularis*. left, control animal; right, animal treated with the neurotoxin 1-methyl-4-phenyl-1,2,3,6-tetrahydropyridine (MPTP) to induce a Parkinson-like disease. Circles indicate the ventral (broken lined, SNv), lateral (black, SNl) and dorsal (white, SNd) areas of the SN. The ventral area is the most vulnerable (compare control with MPTP treated animal), the lateral displays moderate vulnerability and the dorsal low vulnerability. B: ISH for δ2 combined with immunohistochemical detection of TH, demonstrating the expression of δ-ENaC in dopaminergic neurons. C: Quantification of signal intensity in ISH of δ1 or δ2 (images not shown) in the different areas of *Macaca* SN.

However, in non-epithelial cells a constitutively active sodium channel like δ-ENaC requires stringent regulation to avoid cell death due to Na^+-overload and the loss of the electrochemical gradient in the membrane. Therefore, it is essential to unveil the molecular mechanisms involved in the control of δ-ENaC activity to understand its role in neurons.

Two transcript variants of human δ-ENaC have been described: δ1, which corresponds to the originally cloned sequence (Waldmann *et al.*, 1995) and δ2 (Yamamura *et al.*, 2006; Giraldez *et al.*, 2007), which exhibits a longer N-terminus.

ENaCδ1—ENaCδ2
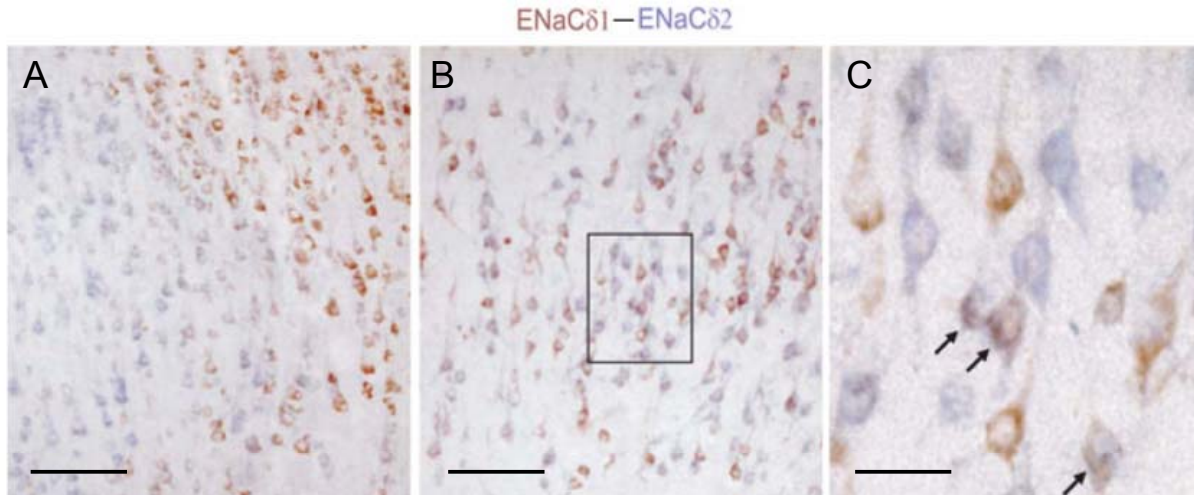
Fig. I.4 Expression of δ-ENaC isoforms δ1 and δ2 in human cerebral cortex.
Sections hybridized with both isoforms showed that most neurons expressed only one of them, forming different clusters (A) or being intermingled in the same region (B), where a few of them co-express both isoforms (arrows in C). Bar in A and B, 250 µm; in C, 40 µm.

δ2 is produced by a combination of alternative transcription start sites, a frame shift in exon 3 and alternative splicing of exon 4 (Giraldez *et al.*, 2007). **Fig. I.4** shows that in the human brain cortex, the two isoforms are expressed in pyramidal neurons and show a low co-localization level, with fewer than 10% of neurons expressing both isoforms (Giraldez *et al.*, 2007). This pattern suggests a strict regulation of isoform expression and the existence of specific functional roles for each of them. The N-terminal variation between isoforms could possibly implicate differential regulation of channel activity and/or traffic. So far no functional differences between the two splice variants have been described. According to (Yamamura *et al.*, 2006), δ1 and δ2 show similar macroscopic current levels, proton activation and amiloride-sensitivity.

Nonetheless, based on the *in situ* hybridization (ISH) stainings published by Giraldez *et al*., where the δ1 and δ2 isoforms were unequally distributed in monkey neuronal tissue (**Fig. I.4**), the question was brought up whether δ1 and δ2 show different functionality. More detailed investigation to define the cause for the differential expression pattern should also shed light into the molecular mechanisms by which δ-ENaC could be regulated.
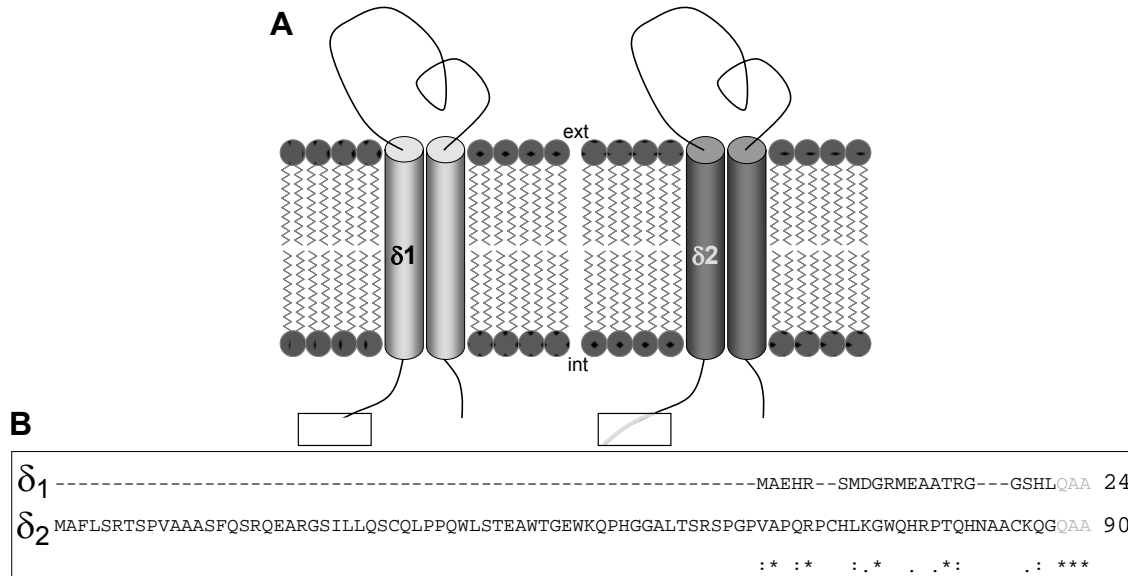
Fig. I.5 δ-ENaC isoforms.
A Sequence alignment of the primary protein sequence of δ1 and δ2 n-termini. *, identical residues, :,conserved substitutions, ., semi-conserved substitutions. B schematic representation of δ1 and δ2 topology. Divergent sequences are localized in the N-termini and are indicated in light grey (for δ1) and dark for δ2. (modified after Giraldez *et al.* 2007)

I. 3   ENaC regulation by serum- and glucocorticoid-induced kinase 1 (SGK1)

Since ENaC is the rate limiting step in Na^+ absorbing epithelia, it requires a strict regulation. This is achieved by a variety of factors including hormones (e.g. aldosterone, angiotensin II, vasopressin, insulin, insulin-like growth factor I, reviewed in (Garty & Palmer, 1997; Snyder, 2005; Verrey *et al.*, 2008), extra- and intracellular proteases (e.g. channel-activating proteases (CAP1-3), tissue kallikrein, furin, revised in (Kleyman *et al.*, 2009; Rossier & Stutts, 2009; Gaillard *et al.*, 2010). Also intra- and extracellular ion concentrations, osmolarity, tubular flow and membrane shearing play important roles in ENaC regulation (Garty & Palmer, 1997; Fronius & Clauss, 2008; Abi-Antoun *et al.*, 2011). Moreover, cyclic adenosine monophosphate (cAMP) and membrane phospholipids like phosphatidylinositol 4,5-bisphosphate (PIP2) were reported to be involved in ENaC regulation (Yue *et al.*, 2002; Snyder *et al.*, 2004; Butterworth *et al.*, 2005; Zhang *et al.*, 2010). Channel effectors comprise kinases, such as serum- and glucocorticoid-induced kinase 1 (SGK1), protein kinase A (PKA), extracellular-regulated kinase (ERK) (Bhalla *et al.*, 2006; Lang *et al.*, 2006), and interacting proteins (e.g. ubiquitine ligases, deubiquitinylating proteases, rab GTPases), which regulate membrane trafficking of the channel (Saxena & Kaur, 2006; Malik *et al.*, 2006; Butterworth, 2010; Rotin & Staub, 2010).

Here, the renin angiotensin aldosterone system, which is on of the main regulatory mechanisms underlying body Na^+ balance (Boron & Boulpaep, 2001), is partially contemplated, because the mineralocorticoid hormone aldosterone is the most important regulator of ENaC. Hormonal regulation by aldosterone leads to renal sodium and fluid retention through controlling the surface expression of the canonical αβγ-ENaC (Masilamani *et al.*, 1999; Lee *et al.*, 2008; Verrey *et al.*, 2008; Lang *et al.*, 2009). The underlying mechanism of the early response to aldosterone en-

compasses the serum- and glucocorticoid-induced kinase 1 (SGK1) (Alvarez de la Rosa *et al.*, 1999; Shigaev *et al.*, 2000; Faletti *et al.*, 2002), which is an ubiquitous serine/threonine protein kinase (Webster *et al.*, 1993; Waldegger *et al.*, 1997), that has been shown to target directly or indirectly the function of many other transport proteins (Vallon & Lang, 2005).

Aldosterone binds to the intracellular mineral corticoid receptor (MR), which upon translocation to the cell nucleus induces or represses the transcription of genes encoding proteins of the Na^+-transporting machinery (e.g. ENaC, Na^+/K^+-ATPase) and proteins that regulate the activity of the Na^+-transporting apparatus (Fuller & Young, 2005). The SGK1 promoter contains a glucocorticoid response element (GRE) to which binds the activated MR, so that SGK1 is rapidly induced by aldosterone (Chen *et al.*, 1999; Verrey *et al.*, 2008).

Aldosterone further induces K-Ras2, a small G-protein that stimulates its effector protein phosphatidylinositol 3 kinase (PI3K), which in turn phosphorylates and activates SGK1 through 3-phosphoinositide dependent kinases PDK1 and 2 (Park *et al.*, 1999; Staruschenko *et al.*, 2007). PI3K is involved in insulin signalling and both insulin-dependent and basal transepithelial Na^+ transport can be inhibited by blockers of PI3K (Alvarez de la Rosa & Canessa, 2003; Blazer-Yost & Nofziger, 2004). Moreover, it was demonstrated that PI3K-inhibitors inhibit the early action of aldosterone and phosphorylation of SGK1 (Wang *et al.*, 2001), suggesting that SGK1 may be an integrator of both the aldosterone and insulin pathways with respect to ENaC regulation (Alvarez de la Rosa & Canessa, 2003; Blazer-Yost & Nofziger, 2004; Pearce & Kleyman, 2007).

The activated SGK1 then phosphorylates the E3 ubiquitine ligase Nedd4-2 (Kamynina & Staub, 2002; Staub & Verrey, 2005) by means of its interaction with Nedd4-2 WW-domains (Wiemuth *et al.*, 2010) thereby providing docking sites for 14-3-3 proteins (Chandran *et al.*, 2011). The association of 14-3-3 proteins with Nedd4-2 is then thought to prevent binding of Nedd4-2 to ENaC (Debonneville *et al.*, 2001; Bhalla *et al.*, 2005; Flores *et al.*, 2005). ENaC suffers tonic inhibition mediated by Nedd4-2: Nedd4-2 binds to and ubiquitinates ENaC, thus marking it for endocytosis, which results in an enhanced ENaC internalization leading to a decreased cell surface expression (Kamynina *et al.*, 2001; Fotia *et al.*, 2003; Rauh *et al.*, 2006; Lu *et al.*, 2007b). This interaction is PY motif (xPPxY) dependent. The PY motif is localized in each C-terminus of the α, β and γ subunits where it serves as a recognition site (Schild *et al.*, 1996) for the binding of Nedd4-2 WW protein-protein interaction domains (Staub *et al.*, 1997; Abriel *et al.*, 1999).

Consequently, SGK1 interrupts ubiquitination of the ENaC subunits by Nedd4-2, which in turn leads to a loss of the retrieval signal into the cytosol and the channel remains longer in the membrane (Alvarez de la Rosa *et al.*, 1999; Snyder, 2005). The concerted action of ENaC, Nedd4-2 and SGK1 is summarized in **Fig. I.4**.

In Liddle's syndrome (section **I.1**), the C-termini of β or γ subunits are mutated in a manner that disrupts the PY motif. Once these PY motifs are deleted, the ubiquitination by Nedd4-2 is abolished, since without a PY motif no ENaC-Nedd4-2 interaction can take place and thus ubiquitination is reduced, which in turn leads to increased membrane stability of ENaC and enhanced Na^+ reabsorption, leading to hypertension (Goulet *et al.*, 1998).
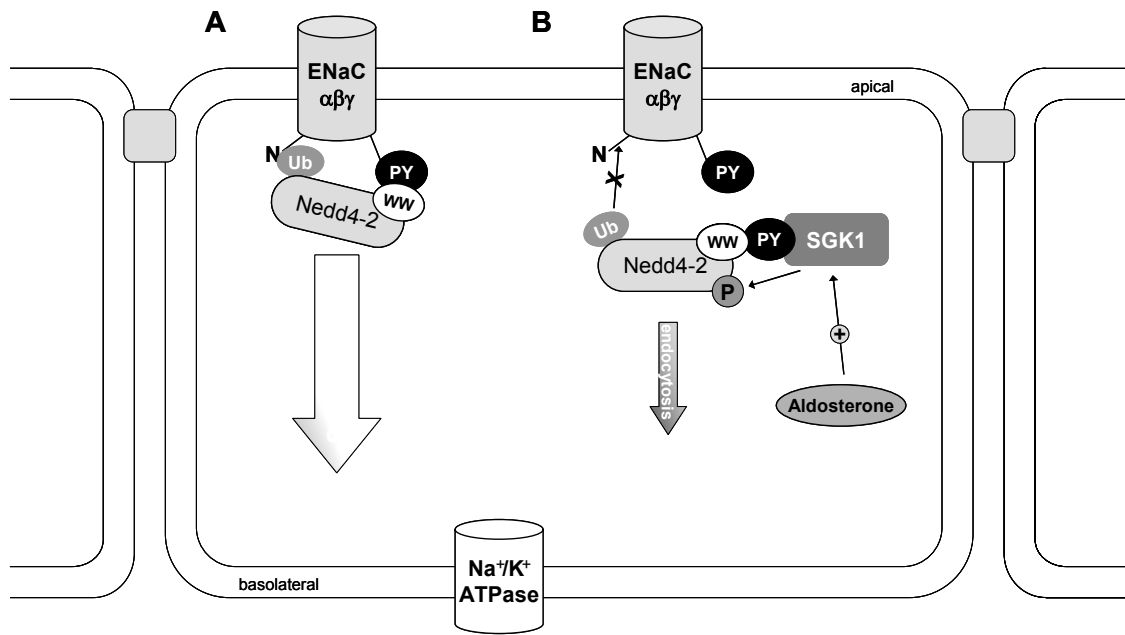
Fig. I.6 Schematic presentation of ENaC regulation by Nedd4-2 and SGK1.1.
A: ENaC cell surface expression is balanced between the insertion of more channels from vesicular stocks and new channels from the TGN and their retrieval via Nedd4-2 mediated ubiquitination. B: aldosterone induces expression of SGK1, which is activated by PI3K phosphorylation leading to SGK1 phosphorylation of Nedd4-2. This reduces ENaC-Nedd4-2 interaction and thus decreases ENaC ubiquitination, for which in turn ENaC remains longer stable in the membrane and causes enhanced Na^+ reabsorption (modified after Kamynina & Staub, 2002).

Ubiquitylation is a post-translational modification of target proteins involving the ligation of one or more ubiquitine polypeptides (Glickman & Ciechanover, 2002). It requires a cascade of enzymatic reactions: The first step of this cascade is binding of ubiquitin by a thioester to a cysteine residue of the E1 ubiquitin-activating enzyme, a reaction requiring ATP. Ubiquitin is then transferred onto an E2 enzyme, also as thioester. Finally, it is the E3 ubiquitin-protein ligase that provides substrate recognition and promotes transfer of ubiquitin to the target protein to which it is then linked by an isopeptide bond at the level of the ε-amino group of a lysine residue (Stryer *et al.*, 2003). Ubiquitylation of ENaC is reversible by de-ubiquitylating enzymes (DUBs), e. g. the aldosterone-induced Usp2-45 (Fakitsas *et al.*, 2007), which increased the channel density at the cell surface (Ruffieux-Daidie *et al.*, 2008). It was reported, that inhibition of DUBs increased ENaC ubiquitylation and reduced the activity and cell surface density of the channel at the plasma membrane (Butterworth *et al.*, 2007; Hurley & Stenmark, 2011).

I. 4 SGK1.1

SGK1.1 is a brain-specific isoform of SGK1 (Arteaga *et al.*, 2008). SGK1.1 is expressed in human brain, where it was described to down-regulate the acid sensing ion channel 1 (ASIC1), another member of the superfamily of ENaC/degenerins. At least partly, this is achieved by decreasing ASIC1 expression at the cell surface. SGK1.1 does not phosphorylate the channel protein, because ASIC1 lacks a SGK1.1 consensus phosphorylation motif (RXRXXS/T). Therefore, the ef-

fect on surface expression must be indirect, as it is the case for the regulation of αβγ-ENaC expression by the canonical SGK1. A possible regulation of δ-ENaC by SGK1.1 has not been studied so far.

Several promoters in the SGK1 gene allow induction by a varied set of conditions in a tissue-specific manner, i.e. glucocorticoids are the main stimuli for the transcription of the canonical SGK1 in epithelia (Webster *et al.*, 1993; Alvarez de la Rosa & Canessa, 2003). Unlike SGK1, the SGK1.1 transcription is not enhanced by glucocorticoids (Arteaga *et al.*, 2008).

SGK1.1 differs from SGK1 in its N-terminus, which in turn determines a higher protein stability and increased plasma membrane binding for SGK1.1 (Arteaga *et al.*, 2008; Raikwar *et al.*, 2008). The N-terminus of SGK1.1 exhibits a polybasic motif that attaches to the membrane via PIP2. SGK1.1 is required to be tethered to the plasma membrane to exert its effect on ASIC1 (Arteaga *et al.*, 2008). Consequently, SGK1.1 could be modulated by transiently decrease PIP2 levels in the plasma membrane upon activation of phospholipase C (PLC) or inositol phosphatases. Under this condition, SGK1.1 moves to the cytosol and accumulates in the nucleus using the same polybasic cluster, which also serves as a nuclear localization signal (Arteaga *et al.*, 2008).

I. 5   Aim of this dissertation

Since δ-ENaC may be implicated in neurodegenerative diseases and the transduction of noxious stimuli in the brain, its regulation and functionality are of special interest. To understand its regulation it is important to investigate more detailed interaction with other proteins and how they modulate δ-ENaC function. To unravel the underlying mechanism for δ-ENaC regulation, the aims were set as follows:

> 1) determination of functional differences between δ1 and δ2,
> 2) definition of the trafficking properties of δ-ENaC and
> 3) identification of possible regulation pathways for δ-ENaC.

II.   Materials & Methods

To investigate δ ENaC function and its underlying mechanisms, the *Xenopus laevis* oocytes heterologous expression system was used. Starting material were plasmid vectors, which contained the coding sequences for α, β, γ, δ1 and δ2 ENaC and also SGK1.1. Inserts were cloned from human lung RNA for ENaC subunits and from mouse brain total RNA for SGK1.1. cRNA of each protein was transcribed *in vitro* and injected into the oocytes for heterologous expression and further two-electrode-voltage-clamp (TEVC), confocal microscopy or other experiments.

All materials and reagents were purchased from Sigma Aldrich, unless otherwise stated.

II. 1   DNA cloning, mutagenesis, and cRNA synthesis

II. 1.1 RT-PCR and DNA cloning

The plasmid vectors pTNT (*Promega*) with the coding sequences of human α, β, γ, δ1 and δ2 ENaC were a kind gift from Prof. Dr. Clauss laboratory (University of Giessen) where the inserts were amplified by RT-PCR from human lung RNA and in case of δ1 and δ2 from human bronchiolar epithelial H441 cell line RNA, which express both isoforms (Ji *et al.*, 2006). The purified PCR products were subcloned into pTNT vector (*Promega*) by using restriction enzyme sites (*New England Biolabs*) added to the flanks of the coding sequences (**Tab. II.1**). Inserts were fully sequenced and compared with published sequences in the National Center for Biotechnology Information (*NCBI*) data bank to ensure the absence of mutations. SGK1.1 cloned from mouse brain total RNA and ligated to the pCDNA3.1/V5-His-TOPO (*Invitrogen*) plasmid vector was a kind gift from Dr. Canessa's laboratory (Yale University) (Arteaga *et al.*, 2008).

Plasmid vector maps used in this study are provided in **Fig. II. 1 & 2**.

Tab. II.1 Coding sequences of ENaC subunits and SGK1.1 with the respective plasmid vectors, restriction enzyme sites and NCBI references.

Insert	Plamid vector	Organism	Insert-length [bp]	Restriction site	NCBI reference #
α-ENaC	pTNT	*Homo sapiens*	2010	*Eco*RI	NM_001038
β-ENaC	pTNT	*Homo sapiens*	1923	*Not*I	NM_000336
γ-ENaC	pTNT	*Homo sapiens*	1950	*Eco*RI	NM_001039
δ1-ENaC	pTNT	*Homo sapiens*	1917	*Eco*RI	NR_002978
δ2-ENaC	pTNT	*Homo sapiens*	2115	*Eco*RI	NM_001130413.1
SGK1.1	pcDNA3.1/V5-His-TOPO	*Mus musculus*	60kDa/118bp	*Eco*RI	NM_001161845.2

bp, base pairs
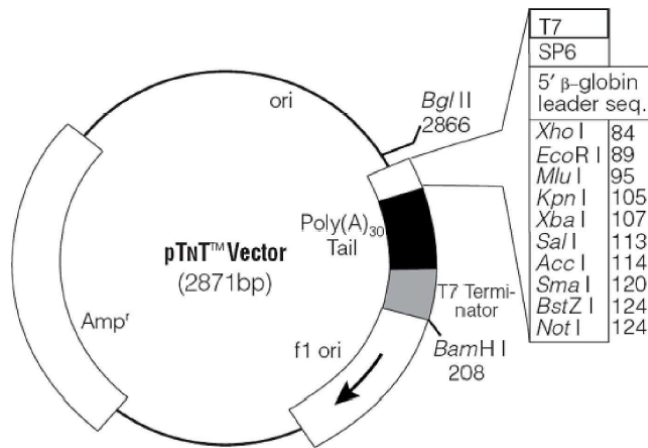
Fig. II.1 Schematic representation of the pTNT plasmid vector. Indicated are the viral promotor sequences of the T7- and the SP6-polymerases, the insertion points for α, β, γ, δ1 and δ2 ENaC in the polylinker region and the poly-A-tail. Upstream the poly-A-tail is the poly-linker region with the restriction sites located, into which the inserts were linked. Downstream the poly-A-tail is the T7 terminator sequence and the restriction site for *Bam*HI for plasmid linearization. Amp', ampicillin resistance. (*Promega*)
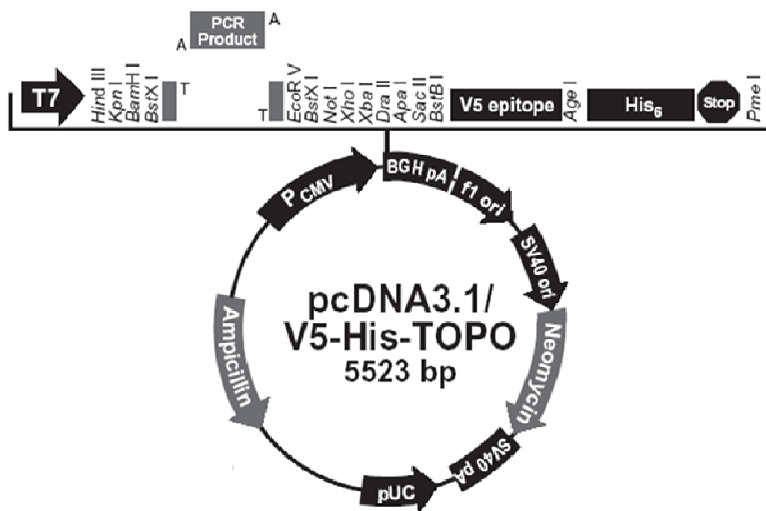
Fig. II.2 Schematic representation of the pcDNA3.1 plasmid vector. Mapped are the polylinker with the insertion site for SGK1.1 as listed in Tab.II.1 and the restriction site for linearization with *Pme*I and the viral promoter sequence for the T7 polymerase. (*Invitrogen*)

II. 1.2 Generation of fluorescently labelled constructs

For the purpose of generating fluorescently labelled δ1 and δ2, cDNAs were amplified by primers listed in **Tab. II.2** using the pTNT expression vectors with the δ1 and δ2 inserts as templates. The products were subcloned into pTNT-YFP previously generated by excising the fluorescent protein coding sequence from peYFP-N1 (*Clontech*, **Fig. II.3**) with *Eco*RI/*Not*I. Inserts were cloned in the *Eco*RI site of pTNT-YFP to obtain an in-frame fusion of the yellow fluorescent protein (YFP) coding sequence at the C-terminus of each construct. ENaC subunits are not affected in their functionality by tagging with YFP (Giraldez *et al.*, 2007). Afterwards the δYFP-fusions were subcloned into pTNT for expression in *Xenopus* oocytes.

SGK1.1 was fluorescently labelled by amplifying the cDNA with PCR using the inserts in vector pcDNA3.1 as templates and the primers listed in **Tab. II.2**. SGK1.1 was then subcloned into *Eco*RI/*Bam*HI sites of peCFP-N1 (*Clontech*, **Fig. II.3**) to produce an in-frame fusion to the cyan fluorescent protein (CFP) at the SGK1.1 C-terminus, which was described to be fully functional (Arteaga *et al.*, 2008). Finally, SGK1.1 CFP was subcloned into pGEMHE (**Fig. II.4**) using *Eco*RI/*Not*I.

The generation of the human large-conductance Ca^{2+}-gated K^+ channel (BK) tagged with YFP has been described previously (Giraldez *et al.*, 2005).

Tab. II.2 Amplification primer pairs of δ1, δ2 and SGK1.1.

Constructs	forward primer	reverse primer
δ1	5' – GAGAATTCGCCACCATGGCTGAGCACCGAACGAAGCA	5' – CAGAATTCGGGTGTCCAGAGTCTCAAGGGGCTG –
δ2	5' – GACTGAATTCGCCACCATGGCTTTCCTCTCCAGGACG	5' – CAGAATTCGGGTGTCCAGAGTCTCAAGGGGCTG –
SGK1.1	5' – CGGAATTCGCCACCATGGTAAACAAAGACATGAATGG	5' – GCGGATCCCGGAGGAAGGAATCCACAGGAGGTG –

*, the reverse primer is common to both isoforms 3'
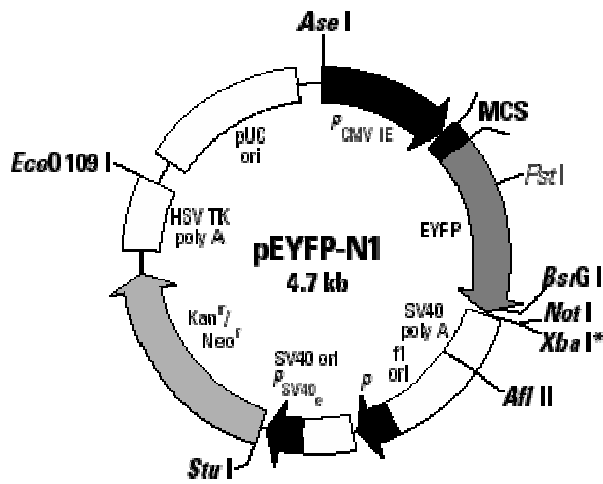
Fig. II.3 Vector map of peYFP-N1 (peCFP-N1).
Shown are the YFP insert with points for insertion of α, δ1, δ2, SGK1.1 in the polylinker region. Kan', kanamycin resistance (*Clontech*)
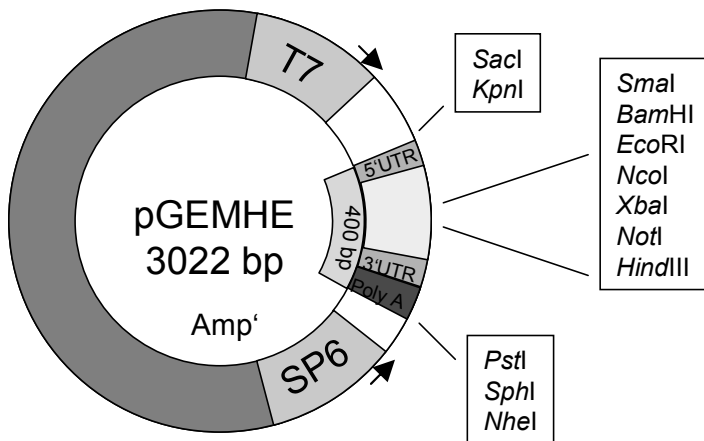
Fig. II.4 Vector map of pGEMHE.
Shown are the polylinker region with points for insertion of SGK1.1, the promotor sequences for in vitro transcription T7 (5' – 3') and SP6 (3' – 5') and the poly A sequence suited for RNA synthesis and direct heterologous expression in *X. laevis* oocytes. Amp', ampicillin resistance (Liman *et al.*, 1992)

II. 1.3 Mutagenesis

To reveal the function of certain sites in the proteins it was necessary to mutate specifically a variety of amino acids or to delete them. To that end the Quickchange Lightning Site-directed

Mutagenesis Kit (*Agilent Technologies*) was used according to the manufacturer's protocol. Briefly, primer pairs were designed with each primer containing the desired mutation and similar melting temperatures (Tm). Primers were between 25 and 45 bp long, with a Tm of ≥75 °C. Tm was calculated with:

$$Tm = 81.5 + 0.41 \ (\%GC) - 675/N$$

N is the number of bases, value for % GC is a whole number

Ideally, the minimum GC content of a primer was ~40% and it terminated with one or more C or G bases at its 3'-end. Primers also included silent mutations to introduce new restriction enzyme sites for rapid screening of clones.

After the mutant strand synthesis reaction (a typical PCR in a thermal cycler) the amplification products were treated with *Dpn*I to digest the parental non-mutated dsDNA. Then *Dpn*I-treated DNA was transformed into XL10-Gold ultracompetent cells (*Stratagene*). The transformation reaction was plated on an appropriate antibiotic-containing agar plate and incubated overnight. For each reaction six or more colonies were picked and subjected to plasmid preparation with the Illustra MiniPrep Kit (*GE Healthcare*) for control restriction enzyme digestion and sequencing.

II. 1.3.1 Mutations in SGK1.1

SGK1.1 is a serine/threonine kinase and its catalytic active centre is necessary to regulate the expression of ASIC1 (Arteaga *et al.*, 2008). Furthermore, in the same work was reported that SGK1.1 is bound to the membrane via PIP2 and that membrane localization of SGK1.1 is important for the modulation of ASIC1. To explore the possibility, that SGK1.1 also exerts its effect on δ-ENaC dependent on its kinase activity and its membrane localization, SGK1.1 was mutated accordingly. Primers for the mutants SGK1.1-K220A and SGK1.1-KKR (K21N/K22N/R23G) and the respective restriction sites for mutant screening are listed in **Tab. II.3**.

Tab. II.3 Primer sequences for SGK1.1 mutants.

Construct	forward primer	reverse primer	Restriction site
SGK1.1-K220A	5'– CTATGCAGTCgcAGTTcTgCAGAAGAAAGC	5'– CTTCTTCAGGATGGCTTTCTTCTGcAgAA	PstI
SGK1.1-KKR	5'– GCTCAGCGTTCCAATTTTTTAAcAAcgGGG ...TGCAGGcTGGATC –3'	5'– GATCCATCTgCcACCCcgTTgTTAAAAAA TTGGAACGCTGAGC –3'	FspI

Mutant bases are shown in lower cases.

II. 1.3.2 Mutations in the δ2-ENaC subunit

Since the δ2 isoform differs from δ1 in its longer N-terminus, it was searched for possible target sites to unveil the underlying cause for the differential membrane abundance of these isoforms. The canonical αβγ-ENaC is known to be ubiquitinated at its lysine sites by the E3 ubiquitine ligase Nedd4-2 (Kamynina & Staub, 2002). Therefore, the possibility was explored, whether al-

tered ubiquitination of δ2 was the cause for its reduced activity when compared to δ1, and each of the additional lysine sites in the δ2 N-terminus that are absent in δ1 was mutated to arginines by mutagenesis with the Quickchange lightning Kit. The double mutant δ2 K47/71R was generated sequentially. The primer pairs for each point mutation are listed in **Tab. II.4.**

Further, the δ2 N-terminus was truncated and deleted in the area that is not present in the other isoform (δ1) to find out possible sequences that underlie the reduced δ2 activity level. Truncations of the δ2 N-terminus were generated by PCR amplification and cloning into the *Eco*RI site of the pTNT vector. Deletions were obtained by mutagenesis with the Quickchange lightning Kit. The double deletion δ2 2xΔ was generated by sequential deletion. The primer pairs to obtain the mutations are listed in **Tab. II.4**.

Tab. II.4 Primer sequences for point mutations, truncations and deletions in the δ2 N-terminus.

Construct	forward primer	reverse primer
δ2 K47R	5'– GGACGGGAGAATGGaagCAGCCACACG –3'	5'– CGTGTGGCTGcttCCATTCTCCC-GTCC –3'
δ2 K71R	5'– CCTGCCACCTGaagGGATGGCAGCAC –3'	5'– GTGCTGCCATCCcttCAGGTGG-CAGG –3'
δ2 K85R	5'– CAACGCTGCCTGCaaaCAGGGCCAG –3'	5'– CTGGCCCTGtttGCAGGCAGCGTTG –3'
δ2 Δ23	5'– GAGAATTCGCCACCATGGCTA-TCCTGCTTCAGAGCTGCCAG –3'	5' – CAGAATTCGGGTGTCCAGAGTC-TCAAGGGGCTG – 3'*
δ2 Δ63	5'–GAGAATTCGCCACCATGGCTC-CCCAGAGGCCCTGCCAC –3'	5' – CAGAATTCGGGTGTCCAGAGTCT-CAAGGGGCTG – 3'*
δ2 Δ86	5'– GAGAATTCGCCACCATGGCT-CAGGCTGCAGCCCAGACGCCC –3'	5' – CAGAATTCGGGTGTCCAGAGTCT-CAAGGGGCTG – 3'*
δ2 Δ25-45	5'– GCCAGAGGCTCCTGGAAGCAGCCAC –3'	5'– GTGGCTGCTTCCAGGAGCCTCTGGC –3'
δ2 Δ25-65	5'– GCCAGAGGCTCCAGGCCCTGCCACC –3'	5'– GGTGGCAGGGCCTGGAGCCTCTGGC–3'
δ2 Δ25-85	5'– GCCAGAGGCTCCCAGGGCCAGGCTG –3'	5'– CAGCCTGGCCCTGGGAGCCTCTGGC –3'
δ2 Δ66-85	5'– TGTGGCTCCCCAGCAGGGCCAGGCT –3'	5'– AGCCTGGCCCTGCTGGGGAGCCACA –3'

Mutant bases are shown in lower cases. Underlined is the *Eco*RI site, grey letters show the Kozak sequence, italic are sequences not present in the original and bold are the to the deletion adjacent amino acids. * is the common δ reverse primer, also used for sequencing.

II. 1.3.3 Sequencing and control of the constructs

Unless otherwise stated, all generated mutation constructs were sent to an in-house sequencing service of the University of La Laguna. Mutations were confirmed using the 4peaks software (*mekentosj*) and the BLAST tool at *NCBI*.

II. 1.4 *in vitro* transcription

To synthesize cRNA the plasmids were linearized with the appropriate restriction enzyme according to the manufacturer's protocol. The restriction site for digestion of each ENaC subunit was *Bam*HI. The restriction enzyme for SGK1.1 in pcDNA3.1/V5-HisTOPO was *Not*I. Constructs cloned in pGEMHE (SGK1.1 and BK) were linearized with *Nhe*I. After linearization each construct served as template for *in vitro* transcription with the mMessage mMachine Kit (*Ambion*). Each reaction was prepared referring to the manufacturer's instructions.

The plasmid vectors contained viral promotor sequences for the DNA-dependent RNA-polymerases SP6 and T7. Based on the linearized plasmid DNA, a complementary RNA (cRNA) was synthesized with the polymerases SP6 and T7 (according to the promoter sequence in each vector).

cRNA synthesis was controlled with denaturing agarose gel-electrophoresis, which contained formaldehyde (Sambrook *et al.*, 1989). After *in vitro* transcription, for each entry appeared a prominent band in the gel at corresponding size (**Fig. II.5**).
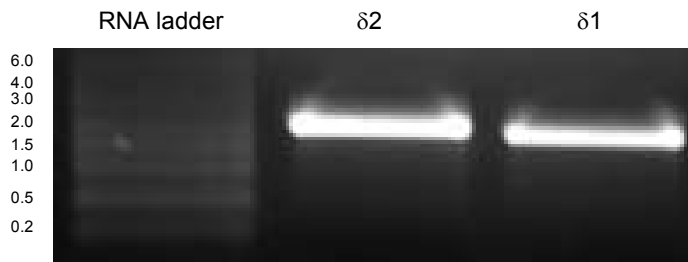
Fig. II.5 Ethidium bromide fluorescence of an agarose gel for trancsription check.
The transcribed cRNAs of δ1 and δ2 ware unequivocally detectable as single bands in the gel (1 %). The sizes of the RNA ladder (*Novagen*) bands are indicated to the left in kb.

II. 2   Heterologous expression of ENaC and electrophysiology

All electrophysiological experiments were performed in Faraday cages (*Newport*) and on anti-vibration tables (*Newport*), to avoid environmental noise, which could disturb the recording. In this study, oocytes of adult female clawed frog *Xenopus laevis* served as test objects that are established as heterologous expression system for TEVC (Wagner *et al.*, 2000). In certain patch clamp experiments, heterologous expression in human embryo kidney cells (HEK293) was used.

II. 2.1 *Xenopus laevis* oocytes and heterologous expression

Advantages of the *Xenopus* oocytes as an heterologous expression system are that they express exogenic membrane proteins by virtue of their huge content of ribosomes and thus their immense translational capacity. Oocytes express extrinsic RNA with correct posttranslational processing of the proteins. Thanks to the few endogenous transport system (Wagner *et al.*, 2000), it is possible to investigate exogenously added transport systems. Furthermore, oocytes are huge cells of ~1 – 1.3 mm at their mature stages V and VI (Dumont, 1972), relatively modest in maintenance and highly abundant. Drawbacks of the oocytes as heterologous expression system are the biological variety intra and inter donor and their seasonal variance (Rossier, 1998; Weber, 1999).

The African clawed frog *Xenopus laevis* is classified as follows (Hilken *et al.*, 1997):

Phylum:	Chordata
Class:	Amphibia
Order:	Anura
Family:	Pipidae
Genus:	*Xenopus*
Species:	*Xenopus laevis*

X. Laevis derives its name from the three short claws on each hind foot. Since *X. laevis* is euryoecious, hence not tightly depending on a certain environment and extremely adaptable, it requires a relatively easy keeping in laboratories and is therefore a favoured subject.

For experimental purposes female clawed frogs were purchased from the *African Xenopus facility C. C.* (Knysna, South Africa) and maintained according to the University of La Laguna Research Ethics Committee in agreement with the Spanish legislation.

To obtain oocytes for the experiments, animals were anesthetized by immersion in tap water containing 1.7 g/L tricaine. The abdomen was opened ventrally and the subjacent myolayer removed for ovariectomy. The ovary was kept in oocyte ringer 2 without calcium (OR2 w/o Ca^{2+}). Its composition is listed in **Tab. II.5**.

To isolate the oocytes from the ovary they were dispersed in collagenase IA solution (1.75 mg/ml OR2 w/o Ca^{2+}) and incubated in agitation for 1 h. The oocytes were then washed and maintained in OR2 until use. For experiments oocytes at stages V and VI were selected. At these stages useful oocytes are ball-shaped, ~1 – 1.3 mm big, and have a polarized organization. The dark animal pole is markedly separated from the vegetative hemisphere by its melanine granula. Mature oocytes feature a bright equatorial belt (**Fig. II.6**).

Tab. II.5 Solutions for oocyte isolation and maintenance.

Substance	OR2 [mM]	OR2 w/o Ca^{2+} [mM]	post-injection saline
NaCl	82.5	82.5	10
KCl	2	2	1
CaCl$_2$	2	2	-
MgCl$_2$	2	2	-
Na$_2$HPO$_4$	1	1	-
HEPES	10	10	5
Na$^+$-Pyruvat	-	-	2.5
Penicillin G	-	-	0.02*
Streptomycin sulfate	-	-	0.025*
NMDG	-	-	80

pH 7.4 adjusted with 2 N NaOH and/or 25% HCl. HEPES, N-(2-hydroxyethyl)piperazin-N'-(2-ethansulfonic acid); NMDG, N-methyl-D-glucamine; *, g/l
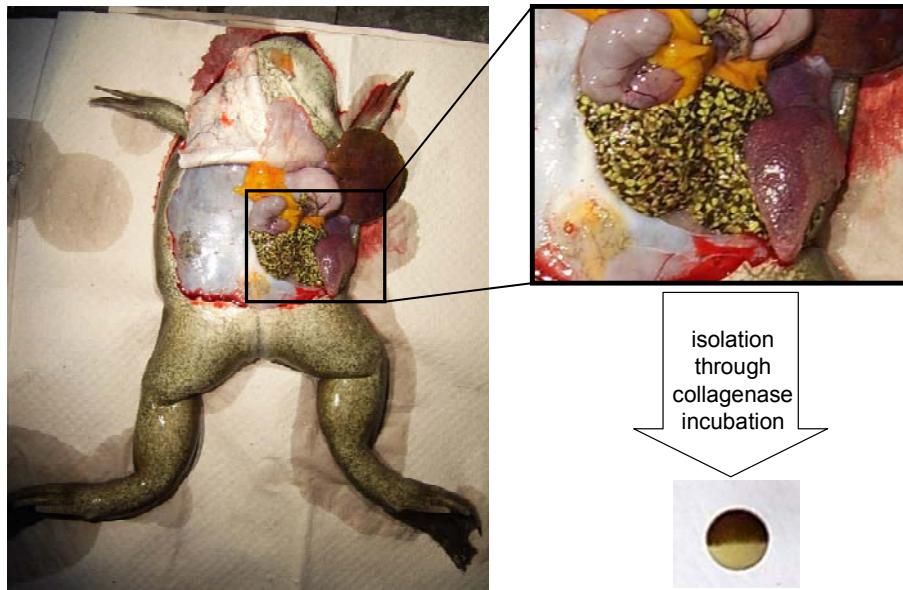
Fig. II.6 Preparation of *Xenopus* oocytes.
Ovaryectomy in female *Xenopus* upon tricaine anesthesia. Oocytes were then isolated with collagenase. (The photograph was taken from a sacrificed animal at the University of Giessen for the purpose of illustration.)

For heterologous expression of ENaC and other proteins, the oocytes were injected with a defined amount of appropriate cRNA. The ENaC subunits, whether as wild type or mutated, were concentrated at 100 ng/µL and co-injected in equal amounts – 1:1:1 for δ:β:γ. SGK1.1 or its respective mutants were at 500 ng/µL and co-injected five times more (e.g. 1:1:1:5 for δ:β:γ:SGK1.1). After injection the oocytes were incubated at 17 °C overnight or 48 h in post-injection saline (composition listed in **Tab. II.5**). After incubation, the oocytes were ready for experimental use.

II. 2.2 Two-Electrode-Voltage-Clamp (TEVC)

The discovery that a constant voltage can be hold over a membrane through electric back coupling, contributed crucially to the understanding of signal processing on membranes. This method, called voltage-clamp, was firstly applied in 1949 on the giant axon of the squid by K. COLE (Eckert *et al.*, 2002).

To determine the conductance (g) of a membrane, the voltage (U) at constant current (I, current clamp) or the current at constant voltage can be measured according to:

$$g = I / U$$

(conductance g [S], current I [A], voltage U [V])

To follow a change in the conductance of a membrane voltage-clamp techniques are preferred, because the whole membrane current (I_M) is composed by capacitive (I_C) and ion current (I_i). Capacitive currents only occur by changes of the membrane potential. With constantly held potential it is possible to separate ion currents from capacitive currents. Further, many channels display a

voltage dependent open probability. For example, if all-or-nothing responding channels are present in the membrane (e.g. voltage dependent sodium channels), under current clamp can appear regenerative all-or-nothing potential changes (e.g. by current injection). In the voltage range, where all-or-nothing responds happen, current clamp does not provide any information about the underlying changes in conductance.

Ohm's law facilitates the calculation of the resistance (R) of a system, in this case the membrane resistance:

$$R = U / I$$

(resistance R [Ω], voltage U [V], current I [A])

Fig. II. 7 shows the basic arrangement of the two electrode voltage clamp, which is explained below.
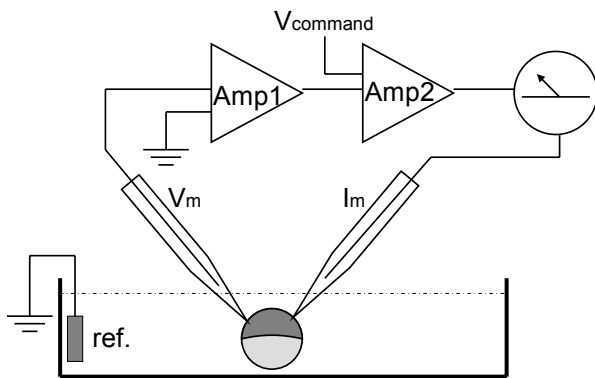
Fig. II.7 TEVC arrangement.
$V_{command}$, holding potential; V_m, membrane potential; I_m, membrane e current, Ref., reference electrode, Amp, amplifier.

The two-electrode voltage clamp (TEVC) is suited for current recordings over the whole cell membrane of huge cells with a high current density, like oocytes. TEVC allows the recording of the total current (transmembrane current, I_M) of all electrogenic transport systems in the membrane in the *whole-cell* mode (Wagner *et al.*, 2000). TEVC is based on the principle described above, where the potential over the membrane is held to a certain value. Differences between intracellular potential and holding potential are compensated by means of current administration from the amplifier, in this study the Oocyte Clamp OC-725C (*Warner Instrument Corp.*).

Two glass micro-electrodes are impaled into the cell, whereas one electrode registers the membrane potential V_m and the other is used for current injection Im. The current, which is applied to compensate the difference between membrane and command potential $V_{command}$, is to equalize with the ion current over the membrane.

The micro-electrodes were silver-chloride wires inserted in filamentous borosilicate glass capillaries KwikFil[TM] (*World Precision Instruments*), which were pulled before with a horizontal-puller (*Sutter instruments*) and filled with 1 M KCl solution, to enable current flow from the solution to the silver wires. For registration, only electrodes with a resistance of 0.3 – 2 MΩ were used. Reference electrodes, also called bath electrodes, were silver-chloride wires, which lay directly in the bath solution.

The experimental setup was constituted according to **Fig. II. 7**. Further, the setup included a peristaltic pump Minipuls3 (*Gilson*) driven perfusion system, which permanently supplied the oocyte in its measuring chamber with fresh bath solution (composition listed in **Tab. II.6**) at a constant volume level. The throughput rate was 25 s, so that after perfusion change the bath solution was completely replaced after 25 s.

In each experiment one oocyte was placed in the measuring chamber and impaled with the micro electrodes. At the beginning no current was applied (0 current) and the membrane potential of the oocyte was measured over the potential electrode. The membrane potential of a native oocyte is about -30 to -70 mV (Weber, 1999). The command potential of -70 mV was then applied. The necessary compensation current (holding current) was mediated by the current electrode. This current is to equalize with the ion current over the membrane and its signal is recordable with the Axon Digidata (*Axon instruments*). Once the current stabilized, the experiments began. Current and potential were recorded with the clampex software (*Axon instruments*).

Tab. II.6 TEVC bath solution for ENaC (TES).

Substance	TEVC ENaC solution [mM]
Na$^+$ gluconate	150
KCl	4
CaCl$_2$	1.8
MgCl$_2$	2
BaCl$_2$	5
HEPES	5

pH 7.4 adjusted w/ith 2 N NaOH. pH 4 adjusted with 25 % HCl. HEPES, N-(2-hydroxyethyl)piperazin-N'-(2-ethansulfonic acid)

Per conventionem, negative current (or negativity of the current) in TEVC means that positive charge enters the cell (cation influx) or that negative charges leaves the cell (anion efflux). *Vice versa*, a positive current (or positivity) is defined as entry of negative charges into the cell (anion influx) or that positive charges leave the cell (cation efflux) (Eckert *et al.*, 2002).

II. 2.2.1 Experimental procedures

In this study the potential was preset at -70 mV by a voltage clamp amplifier and currents were recorded at 1 kHz. I/V curves were generated by increasing the holding potential from -70 to +40 mV in sequential 10 mV steps of 100 ms duration. Stimulation and data acquisition were controlled using the pClamp 10.0 software (*Axon instruments*). Each set of experiments was confirmed by at least three independent batches of oocytes.

Oocytes were clamped in TEVC ENaC solution (TES, **Tab. II.6**) at -70 mV and the *I/V* curve protocol was applied. Then the perfusion was changed to 100 µM amiloride containing TEVC ENaC solution, which was prepared by adding amiloride 1:1000 from a 100 mM stock solution in DMSO to the TEVC ENaC solution. Again, the *I/V* curve protocol was applied. Since amiloride specifi-

cally inhibits ENaC, ENaC specific currents could be calculated as the difference before and after the addition of amiloride.

Perfusion scheme II. 1 Succession of the experimental procedures for ENaC recording with TEVC.

TES → *I/V* curve (before) → TES + 100 µM amiloride → *I/V* curve (after)

When necessary, a time course protocol at a given potential was applied, which is indicated accordingly in the corresponding figures.

Endocytosis rates were revealed by incubating the oocytes in injection saline containing 5 µM brefeldin A (BFA), which blocks forward trafficking of vesicles from the trans-Golgi network (TGN) (Klausner *et al.*, 1992), and recording the amiloride sensitive current in the same oocytes consecutively at times 0, 1.5 and 4 h.

To investigate channel insertion, the oocytes were incubated in 80 µM Dynasore, a blocker of dynamin-dependent endocytosis (Cholon *et al.*, 2010; Macia *et al.*, 2006), and amiloride sensitive currents were recorded in the same oocytes consecutively at time points 0, 1.5, 4 and 24 h.

In the case of BK currents, recording was performed in OR2 by application of voltage pulses to +100 mV from a holding potential of -70 mV.

II. 2.3 Single channel recordings with the patch clamp technique

Single channel recordings of δβγ-ENaC expressing oocytes were performed in collaboration with Prof. Clauss' laboratory in the Institute of Animal Physiology at the University of Giessen. Dr. Mike Althaus conducted the studies according to previously described protocols, which are summarized briefly in the following: Oocytes were injected with cRNA encoding αβγ, δ1βγ or δ2βγ ENaC (0.5 ng per subunit). Single channel recordings were performed in the cell-attached configuration 1-2 days after RNA injection. ENaC expressing-oocytes were devittelinized prior to placement into the recording chamber. A potassium-rich bath solution was employed to keep the endogenous membrane potentials of the oocytes close to 0 mV. The Bath solution contained (in mM) 145 KCl, 1.8 $CaCl_2$, 2 $MgCl_2$, 5.5 glucose, 10 HEPES, pH 7.4. Borosilicate glass capillaries (outer diameter: 1.6 mm; Hilgenberg, Germany) were pulled to patch electrodes of 4-10 MΩ resistance, fire polished and filled with pipette solution. Pipette solution contained (in mM) 145 NaCl, 1.8 $CaCl_2$, 2 $MgCl_2$, 5.5 glucose, 10 HEPES, pH 7.4. Single channel currents were amplified with a LM/PC amplifier (List, Germany), low pass filtered at 100 Hz and acquired with 2 kHz using an Axon interface (1200 series; Axon instruments, USA) together with the Axon Clampex software (Axon instruments, USA). The holding potential was clamped to -100 mV, and single channel amplitudes were measured from at least three channel events for each experiment, to calculate the single-channel conductance. Other single channel parameters like open probability, relative open probability, mean open and closed times – all at -100 mV holding potential – were determined as described (Althaus *et al.*, 2007).

II. 2.4 Cell culture of human embryonic kidney (HEK293) cells and heterologous expression

Not only *Xenopus* oocytes are useful heterologous expression tools, but also cell culture lines, which require sterile handling and can be stably or transiently transfected with cDNAs.

In this study human embryonic kidney 293 cells (HEK293, purchased from the *American Type Culture Collection* #CRL-1573) were maintained in culture medium, which consisted of Dulbecco's modified Eagle's medium (DMEM) supplemented with 100 U/ml penicillin, 1.1 mg/ml streptomycin and 10% fetal bovine serum (FBS), at 37 °C in an incubator (*Thermo Scientific*) with humidified atmosphere of 95 % air and 5 % CO_2. Cells were passaged when a confluence of ≥80 % was reached using trpysin (0.1 %, *Lonza*) to detach the cells from the culture surface. After passage the cells could be maintained for growing again plated at 1:5 dilution, or could be transiently transfected in 35-mm diameter tissue culture plastic dishes on sterile poly l-lysine (0.01 %) coated cover slips plated at 40 % density. ENaC transfection was performed after 24 h as previously described (Staruschenko *et al.*, 2006). According to the manufacturer's protocol the transfection mixture contained the plasmid vectors pcDNA3.1 with the inserts of δ1-, δ2-, β- or γ-ENaC and peGFP-N3 codifying green fluorescent protein (eGFP) as a marker for transfection (δ1 or δ2:β:γ:eGFP at 0.3:0.3:0.3:0.5 µg, 1.4 µg of total DNA) and 3 µL of the vehicle lipofectamine 2000 (*Invitrogen*) and was incubated in a serum-free medium (OPTI-MEM, *GIBCO*) for 20 min before adding it to the cells in serum-containing medium. Chemical transfection with lipofectamine is highly efficient and involves the inclusion of the DNA to be transfected in liposomes, i.e. small, membranous bodies that are in some ways similar to the structure of a cell and can actually fuse with the cell membrane, releasing the DNA into the cell. After 2 h the ENaC-specific blocker benzamil (10 µM) (Waldmann *et al.*, 1995) was added to the medium to avoid cell death due to Na^+ overloading. Cells were incubated for another 24 – 48 h prior to electrophysiological recordings.

II. 2.5 Perforated patch clamp experiments on HEK cells expressing ENaC

The patch clamp technique allows the study of single or multiple ion channels in cells. Patch clamp is a refinement of the voltage clamp and was developed by E. NEHER and B. SAKMANN, who for the first time were able to record single ion channel currents, thus proving their involvement in fundamental cell processes such as action potential conduction. Patch clamp recording uses a glass micropipette as an electrode that has an open tip diameter in the micrometer range. This is a size, which encloses a relatively small membrane surface area or patch that contains just one or a few ion channel molecules. The interior of the pipette is filled with a solution matching the ionic composition of the bath solution, as in the case of cell-attached recording, or the cytoplasm for whole-cell recording. A chlorided silver wire is placed in contact with this solution and conducts electric current to the amplifier. The pipette solution can be varied by adding drugs to study the ion channels under different conditions. The micropipette is pressed against a cell membrane and suction is applied to assist in the formation of a high resistance seal (gigaseal)

between the glass and the cell membrane, which allows registration of very small currents through a single channel molecule. In the on-cell or cell-attached configuration (**Fig. II.8 a**), the cell regulation of channel activity can be assessed for example under hormonal influence. After the formation of a gigaseal withdrawing the micropipette from the cell leads to an inside-out patch (**Fig. II.8 c**), where not only the pipette solution on the outside but also the bath solution on the inside can be experimentally controlled. To investigate currents through multiple channels over the entire cell, the membrane within the patch can be removed through suction, called whole-cell mode (**Fig. II.8 b**). This allows access to the cell inside, e.g. to exchange the cytosol with pipette solution. After withdrawing the pipette in this configuration the membrane reforms in the outside-out mode (**Fig. II.8 d**), where the cytoplasmic inside turns towards the pipette solution and the outside faces the bath solution. This configuration is used for testing of exogenous influences on the channels, e.g. effects of toxins.

Unlike traditional TEVC recordings, patch clamp recording uses a single electrode to record currents. Therefore, many patch clamp amplifiers do not use true voltage clamp circuitry but instead are differential amplifiers that use the bath electrode to set the zero current level. This enables keeping the voltage constant while observing changes in current.

Fig. II.8 Patch clamp configurations.
Depicted are the configurations, in which patch clamp experiments can be performed: cell-attached (a), whole-cell (b), inside-out (c) and outside-out (d). (Numberger & Draguhn, 1996)

The variation perforated patch of whole-cell recording, is achieved after forming of the GΩ seal, by perforating the patch membrane with an antibiotic instead of suction to rupture the patch membrane. The electrode solution contains small amounts of e.g. amphothericin-B, nystatin or gramicidin. As the antibiotic molecules diffuse into the membrane patch, they cause small perforations in the membrane, providing electrical access to the cell interior. Its major advantage is reducing the dialysis of the cell that occurs in whole-cell recordings, for which it was chosen in this study. Disadvantages of the perforated patch include: 1) higher access resistance accompanied by decreased current resolution, 2) a significant amount of time for perforation (10 – 30 minutes), and 3) membrane weakness, which can rupture leading to antibiotic contaminating the inside of the cell.

Ionic current recordings in HEK293 cells were performed at RT in the perforated patch configuration of the patch-clamp technique as described previously (Miranda *et al.*, 2005). Patch pipettes with tip resistances of 3 – 5 MΩ were pulled from Kimax disposable micropipettes (*Kimble glass Inc.*). The standard extracellular saline contained (in mM): 137 NaCl, 4 KCl, 1.8 CaCl$_2$, 1 MgCl$_2$, 10 glucose, and 10 HEPES (pH 7.4 with NaOH). Internal pipette solution contained (in mM): 65

KCl, 30 K_2SO_4, 10 NaCl, 1 $MgCl_2$, 50 sucrose and 10 Hepes (pH 7.4 with KOH). The tip of the pipette was initially filled with nystatin-free solution and the remainder of the pipette was back-filled with the same solution containing 250 µg/mL nystatin, added from a stock of 50 mg/mL nystatin freshly dissolved in dimethylsulphoxide (DMSO), which were sonicated just before use. The course of perforation was followed by monitoring the progress of capacitive transients under voltage-clamp mode, setting the pipette voltage at a value of −70 mV. Access resistance, as estimated from the capacitive compensation circuitry on the amplifier, reached 10 – 30 MΩ within 5 – 20 min after the seal was made. During this time until perforation, benzamil was washed out of the medium allowing the detection of the δβγ-ENaC current immediately after accessing the currents in whole cell mode. Solution junction potentials were resetted before seal formation. An axopatch 700A patch-clamp amplifier (*Axon Instruments*) was used to record membrane currents. Stimulation and data acquisition were controlled with the Clampex software (*Axon*). Data analysis was performed with Igor-Pro (*WaveMetrics Inc.*).

Currents through ENaC were elicited by voltage ramping from +60 mV down to -100 mV over a 500 ms period and calculated by subtraction of the currents before and after adding benzamil (10µM) to the extracellular bath solution. The benzamil-sensitive current at -100mV was divided by the cell membrane capacitance to obtain the benzamil-sensitive current density, which was compared between cells expressing δ1βγ and δ2βγ.

II. 3   Protein detection by Western blot, fluorometry and confocal microscopy

Western blot was applied for δ-ENaC-specific protein detection in the whole oocytes whilst fluorometry was used to detect YFP-specific fluorescence in whole oocyte extracts. To specifically detect proteins in the membrane, it was necessary to label them with fluorescent marker proteins, which can be detected under the confocal microscope.

II. 3.1 Western blot

The Western blot method allows detecting specific proteins, to determine their molecular weight and to measure relative amounts of the protein present in different samples. G. STARK developed this method in 1979 at Stanford University. A brief description of how western blots are performed is given below.

Before the virtual western blot, a protein mixture is separated into bands by sodium-dodecyl-sulfate polyacryl-amide gel-electrophoresis (SDS-PAGE). The proteins migrate according to their size and charge to the positive pole, because SDS denatures the proteins by disrupting their quaternary and tertiary structure and confers them with negative charges. A vertical electric field drives the negatively charged proteins from the gel (on the – side) onto a membrane (on the + side). Mostly nitrocellulose or polyvinylidenfluorid (PVDF) membranes are used for the electro-

phoretic transfer, which resembles a sandwich (pictured in **Fig. II.9**). The proteins adhere to the membrane surface due to hydrophobic interactions and preserve the separation pattern. SDS is washed and the proteins renature incompletely into their tertiary structure. Now the proteins are accessible for antibody binding. With the aid of specific mono- or polyclonal antibodies, the band of the protein in question can be identified. Unspecifically bound antibodies are washed with detergent containing buffers, and are thus removed for specific immune visualization. Coomassie marks unspecifically all proteins and thus permits detection of them all. The immune detection is based on the principle of antigen-antibody binding: an antigen-specific primary antibody binds to its epitope on a certain protein. A conjugated secondary antibody binds the primary antibody, and thus marks indirectly the protein of interest. Detection occurs via the secondary antibody by its conjugation to a visualization marker, in this study horseradish peroxidase (HRP). HRP catalyses a chemiluminiscent reaction: the conversion of luminol and its derivatives into its oxidized form. One of the major advantages of this two-step detection is the signal amplification through multiple binding of several conjugated secondary antibodies to one primary antibody. The secondary antibody is of wider specifity, so that all primary antibodies of one species can be discerned, therefore it is universally applicable, and secondary antibody conjugates are available commercially.
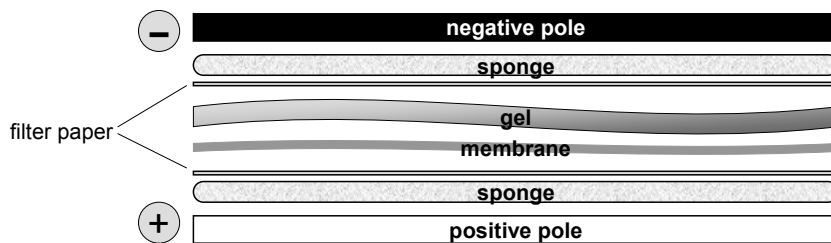
Fig. II.9 Western blot transfer sandwich.
Compounds of a Western blot electrophoretic transfer sandwich. Proteins migrate from the negative pole to the positive pole.

Oocytes expressing either $\delta1_{YFP}\beta\gamma$ alone or in combination with SGK1.1 or the mutant SGK1.1-K220A, or for another set of experiments $\delta1\beta\gamma$ or $\delta2\beta\gamma$, were lysed in buffer (compounds listed in **Tab.II.7**) containing a protease inhibitor cocktail (*Roche*) to obtain a total protein extract of the whole cell. After clearing the lysates by centrifugation (12.000 x g during10 min at RT), Laemmli buffer was added to the supernatant and the lysates were heated to 90 °C for 5 min. Equal amounts of protein were resolved by SDS-PAGE and transferred to Immobilon PVDF membranes (*Millipore*). The membranes were blocked with 5% dry milk (Carnation, *Nestle*), and YFP- or CFP-tagged protein expression was detected with anti-green fluorescent protein (anti-GFP) monoclonal antibody (*Clontech*) followed by incubation with goat anti-mouse secondary antibody conjugated to HRP (*GE Healthcare*). For detection of δ-ENaC without YFP a polyclonal serum was raised against the C-terminus of the δ subunit by injecting rabbits repeatedly with a fusion protein between fragment R563-T638 (numbers refer to the δ1. sequence) and glutathione-S-transferase (GST) purified from *E.coli*. As a secondary antibody a goat anti-rabbit antibody conjugated to HRP (*Bio-Rad*) was applied. Chemiluminiscence evolved with Immun-Star WesternC kit (*Bio-Rad*), and signals were detected with a Versadoc 4000 MP imaging system (*Bio-Rad*).

Tab. II.7 Composition of the lysis buffer for oocytes.

Substance	Lysis buffer [mM]
Tris-HCl, pH 7.5	50
EDTA	5
NaCl	150
Triton X-100	1%
25x Protease inhibitor cocktail	1:25

Tris, tris(hydroxymethyl)aminomethane; EDTA, ethylenediaminetetracetic acid

II. 3.2 Fluorometry

Fluorometry or fluorescence spectroscopy is a type of electromagnetic spectroscopy which analyzes fluorescence from a sample. It involves a beam of light of a certain wavelength, that excites the electrons in molecules of fluorescing compounds and causes them to emit light of a lower energy (= greater wavelength, known as Stokes' rule) as illustrated in a simplified Jablonski diagram (**Fig. II.10**).
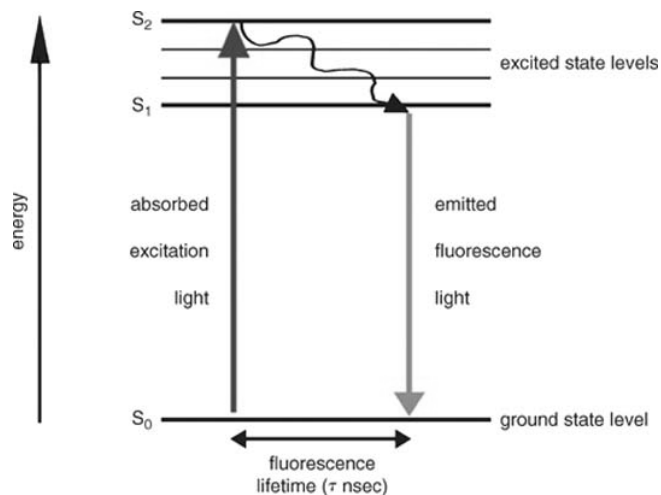
Fig. II.10 Jablonski diagram.
In fluorochromes with delocalized electrons fluorescence happens after an electron changes from the ground state (S_0) to an excited state (S_2) by photon-excitation and when during transmission of the electron into the S_0 the nascent energy emits as fluorescent light (photon). A transmission from the S_2 to the S_1 does not require the emission of a photon (inner transmission). A Jablonski diagram shows the energy levels of the electron transmission during absorption and emission of light (photons), each happening very fast within 10^{-15} seconds.

In this study a filter fluorometer Victor^{TM} X5 (*Perkin-Elmer*) was used, which produced amongst others the specific excitation (480 nm filter) and emission (535 nm filter) wavelengths for YFP by using optical filters. The light passes through the YFP-containing sample, and a certain wavelength is absorbed while a longer wavelength is emitted, which was detected with a photomultiplier and recorded by the Perkin-Elmer software according to its intensity as relative fluorescence units (RFU).

The samples were total protein extracts (**II. 3.1**, **Tab. II.7**) of oocytes expressing $\delta1_{YFP}\beta\gamma$ or $\delta2_{YFP}\beta\gamma$ or non-injected oocytes, which served as controls to ensure that basal fluorescence of the oocytes was significantly lower than that of YFP-expressing oocytes. RFU values of each sample were determined and compared between each condition.

II. 3.3 Confocal microscopy

To further characterize cell surface expression of ENaC and SGK1.1, fluorescence detection by confocal microscopy was employed. Therefore, the proteins of interest were tagged with fluorescent proteins as described in **II.1.2** and expressed in *Xenopus* oocytes. A confocal microscope allows focusing with high resolution on a specific area of a specimen, particularly in the sample depth direction, as a result of point illumination and pinhole-limited light detection. The spatial filtering eliminates out-of-focus light or glare in specimens, whose thickness exceeds the immediate focal plane and would perturb the image, as is the case in the traditional wide-field fluorescence microscopes. However, since much of the light from sample fluorescence is blocked at the pinhole, the increased resolution is at cost of decreased signal intensity. Long exposure times are often required. The achievable thickness of the focal plane is defined mostly by the wavelength of the used light divided by the numerical aperture of objective lens, but also by the optical properties of the specimen. The basic concept of confocal microscopy (**Fig. II.11**) was patented in 1957 by M. MINSKY, who aimed to visualize biological events as they occur in living systems (Claxton *et al.*, 2006).
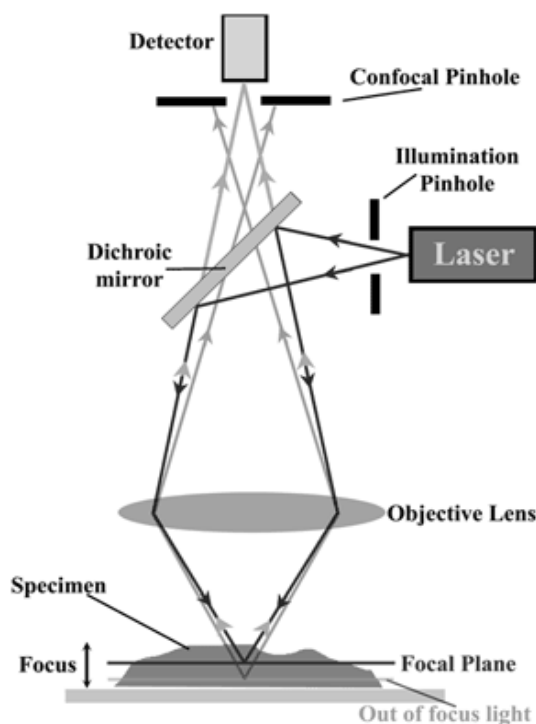
Fig. II.11 Diagramm of the confocal principle in Fluorescence laser scanning microscopy.

Coherent light emitted by the laser system (excitation source) passes through a pinhole aperture that is situated in a conjugate plane (confocal) with a scanning point on the specimen and a second pinhole aperture positioned in front of the detector (a photomultiplier tube). As the laser is reflected by a dichromatic mirror and scanned across the specimen in a defined focal plane, secondary fluorescence emitted from points on the specimen (in the same focal plane) pass back through the dichromatic mirror and are focused as a confocal point at the detector pinhole aperture. The significant amount of fluorescence emission that occurs above and below the objective focal plane is not confocal with the pinhole (termed Out of focus light rays) and is not detected. Refocusing the objective in a confocal microscope shifts the excitation and emission points on a specimen to a new plane that becomes confocal with the pinhole apertures of the light source and detector. (Fellers & Davidson, 2009; John Innes Centre, 2011)

The oocyte's opaque cytosol is an advantage to detect proteins was abundant at the cell surface, since it obscures fluorescence detection not present in the focused membrane plane. Only fluorescent proteins in the membrane or just beneath it can be detected with this method. In this study, membrane staining was verified by applying AlexaFluor 568 conjugated transferrin (tf-AF568, *Molecular Probes, Invitrogen*) to stain the transferrin receptor (tfr), which is a membrane marker (Macdonald & Pike, 2005) in *Xenopus* oocytes (Lund *et al.*, 1990). To avoid endocytosis of the tfr, staining with tf-AF568 (200 µg/ml) was performed on ice during 30 min. Then the oocytes were thoroughly washed with ice-cold OR2 and immediately subjected to fluorescence detection as previously described (Barroso-Gonzalez *et al.*, 2009).

Tab. II.8 Excitation and emission wavelengths of fluorescent proteins. (Fluorescence Spectra Viewer, *Invitrogen*)

Fluorescence	Excitation [nm]	Emission [nm]
CFP	395, 475	509
YFP	488	527
AlexaFluor 568	543	603

In this study, the fluorescently tagged proteins of oocytes expressing $\delta_{YFP}\beta\gamma$, $\alpha_{YFP}\beta\gamma$ or SGK1.1-CFP were excited at the wavelengths indicated in **Tab. II.8**. Fluorescence detection took place at wavelengths chosen to specifically detect each protein as listed in **Tab. II.8**. The equipment consisted of a laser-scanning confocal fluorescence microscope, Fluoview™ FV1000 (*Olympus*). It contained multiple laser excitation sources, a scan head with optical and electronic components, an electronic photomultiplier detector and a computer for acquisition, processing, analysis and display of images with the manufacturer's software. Fluorescence emission that passed through the pinhole aperture is converted into an analog electrical signal by the photomultiplier. Analog image data collected by the photomultiplier is digitized by an analog-to-digital (A/D) converter in the electronic cabinet and the image information is displayed on the monitor. The confocal image of a specimen is a point by point reconstruction of emitted photon signals. Analysis was conducted with the Olympus FV 1.6 software and quantitative measurements were achieved by maintaining the parameters of laser-intensity, gain and offset constant.

II. 3.2.1 Fluorescence recovery after photo-bleaching (FRAP)

The method of Fluorescence recovery after photo bleaching (FRAP) utilizes the phenomenon of photo bleaching of fluorescent probes (in this study YFP) to measure parameters related to molecule mobility. The phenomenon of photo bleaching occurs when a fluorophore permanently loses its ability to fluoresce due to photon-induced chemical damage and covalent modification. In FRAP experiments, a region of interest is selectively photo bleached by high power laser pulses (**Fig. II.12**). Subsequently the kinetics of fluorescence recovery are recorded in a time-course (**Fig. II.13**), by sampling images at regular time intervals with the same laser at lower detection power. This provides quantitative information about the mobility of a fluorescent molecule in a defined compartment, here the plasma membrane. Two parameters can be deduced from FRAP: the mobile fraction of fluorescent molecules (Fm) and the rate of mobility (т).
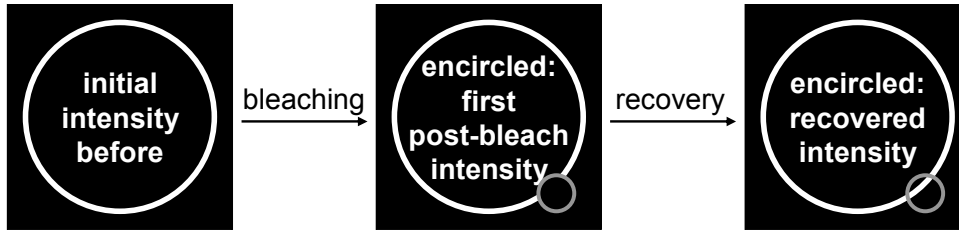
Fig. II.12 Schematic representation of a FRAP experiment on an oocyte membrane.
First, the fluorescent cell surface of the oocyte is monitored (white big circle). Then intensive laser pulses are applied at a certain area (encircled), where fluorescence is bleached and disappears. After a individual protein-specific recovery time, fluorescence reappears in the area, where photo bleaching occurred before (Neijssen *et al.*, 2005). The influence of lateral movement was avoided by only considering the central part of the bleached region (Pochynyuk *et al.*, 2007).

The experimental setup for the FRAP experiments consisted of a laser-scanning confocal microscope as described before with oocytes expressing $\delta_{YFP}\beta\gamma$ or $\alpha_{YFP}\beta\gamma$. Initial plasma membrane fluorescence (I_I) was recorded by exciting at 488 nm and detecting emission at 529 nm. For bleaching the laser at 488 nm was used at its most intense power and focused on a region of interest in the cell surface. Afterwards the remaining first post-bleach fluorescence intensity (I_0) was measured. Images were then sampled at a frequency of 15 seconds during a recovery time of 30 minutes. Recovery is completed when the FRAP recovery curve reaches a plateau (I_E). At this stage all fluorescent mobile molecules replaced the bleached mobile ones, represented by the fraction (Fm) below the plateau from I_0 to I_E. The fraction between I_E and I_I represents the immobile molecules (Fi), which are bleached and stay in the region of interest.

For comparison of the fluorescence recovery between αYFP and δYFP, the initial fluorescence of each was normalized to 1 (I_I=1). Then the curve parameters could be further analysed.
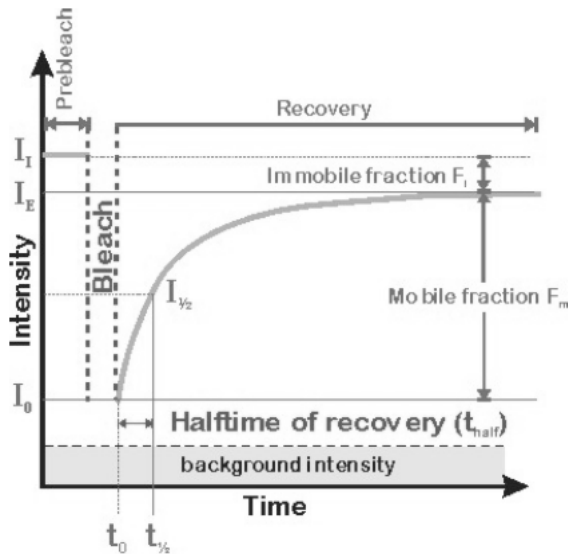
Fig. II.13 Idealized plot of a FRAP recovery curve.
I_I, initial intensity; I_0, intensity at time point t_0 (first post-bleach intensity); $I_{1/2}$, half intensity ($I_{1/2} = (I_E - I_0) / 2$); I_E, endvalue of the recovered intensity, t_0, first post-bleach time-point; $t_{1/2}$, halftime of recovery corresponding to $I1/2$; mobile fraction Fm = ($I_E - I_0$) / ($I_I - I_0$); immobile fraction Fi = 1 – Fm. (Reits & Neefjes, 2001)

To determine the recovery dynamics, in this case to compare differences between αYFP and δYFP, the recovery speed is indexed as the time it takes to reach 50% of the end plateau value, called half-life $t_{1/2}$.

Data analysis was performed with Prism5.0 (*GraphPad*) by fitting the normalized FRAP curve I(t) to the exponential equation:

$$I(t) = A (1 - e^{-\tau t})$$

(time t [s], mobile fraction (Fm) value A, recovery constant τ [s^{-1}])

Once the time constant of recovery τ is assessed, the $t_{1/2}$ can be calculated with:

$$t_{1/2} = ln\ 0.5\ /\ \text{-}τ$$
(time t [s], recovery constant τ [s^{-1}])

Generally photo bleaching happens while recording, because it is necessary to excite the fluorophore before obtaining a fluorescence signal. With this process the fluorescence fades every time an image is taken. Therefore, the FRAP values had to be extrapolated according to values acquired from areas in the same oocyte, where no selective photo bleaching took place.

II. 4 RNA detection by ISH and qPCR

II. 4.1 *in situ* hybridization (ISH)

To qualitatively determine whether δ-ENaC or SGK1.1 were expressed in neurons *in situ* hybridization (ISH) histochemistry were performed in colaboartion with Tomás González' laboratory at the University of La Laguna, Tenerife, with their established protocols as described previously (Wesch *et al.*, 2010): The expression of δ1-, δ1-ENaC and SGK1.1 was studied in monkey (*Macaca fascicularis*) and human cerebral cortex. Monkey samples were provided by Dr. J. L. Lanciego (CIMA, University of Navarra, Pamplona, Spain). The experimental protocol was approved by the Ethical Committee of the University of Navarra (reference 001/006) and was in accordance with the European Communities Council Directive of 24 November 1986 (86/609/EEC) regarding the care and use of animals for experimental procedures. Human brains were provided by the Brain Bank of Navarra (Dr. T. Tuñón, Hospital de Navarra, Servicio Navarro de Salud, CIMA, Pamplona, Spain). They came from five patients with an average age of 61.2 ± 5.3 yr and died without history of drug abuse, neurological or psychiatric illness. Brains were removed after a postmortem period of 10.1 ± 2.4 h. In each case, the absence of degenerative or vascular disease was confirmed by pathological examination. Blocks containing the frontal and temporal cortices were briefly washed in 0.1 mol/L phosphate-buffered saline (PBS) at pH 7.4, and immediately immersed in 4% paraformaldehyde in PBS for 72 h at 4 °C. Four adult male monkeys (5–8 yr old, 3.5– 4.8 kg) were administered an overdose of pentobarbital sodium and were transcardially perfused with heparinised ice-cold 0.9 % saline followed by 3–4 L of 4 % paraformaldehyde in PBS. Brains were removed, cut into blocks, and immersed in fixation solution overnight. Human and monkey samples were cryoprotected by consecutive immersion in 10 %, 20 %, and 30 % sucrose in PBS (24 h each), frozen, and cut into 40 μm-thick sections perpendicular to the long axis of the cortical gyri in human cortex and in the coronal axis in monkeys, with a freezing microtome.

ISH probes for δ1- and δ2-isoforms consisted of sense and antisense biotin-labeled 40-mer oligonucleotide probes and have been previously described (Giraldez *et al.*, 2007). Sense oligonucleotides were used as control for nonspecific binding. A 511-bp fragment of human SGK1.1 (-295 to +216 relative to the start of the coding sequence) was amplified by PCR from human brain cortex cDNA using the following oligonucleotides: gagattggccgtatcccaccgtcc (forward) and gcatgttcacccaggcatgtttgac (reverse). This sequence does not overlap to the other known SGK1 isoforms (Arteaga *et al.*, 2008). The PCR product was purified and cloned in pCR4-TOPO (*Invitrogen*). Insert identity and orientation were verified by DNA sequencing. Sense and antisense digoxigenin (DIG)-labeled cRNA probes for ISH were made by in vitro transcription using T7 or T3 RNA polymerases and the DIG RNA labeling kit (*Roche*). Labeling efficiency was determined by direct detection of the probes in a spot test.

SGK1.1 detection by single ISH labeling was performed as previously described (Giraldez *et al.*, 2007). Briefly, sections were prehybridized at 45 °C for 2 h in hybridization solution (50 % formamide, 5x sodium chloride and sodium citrate solution (SSC), and 40 µg/mL denatured salmon DNA). Probes were added to the hybridization mix at 400 ng/mL, and sections were incubated at 45 °C for 16 h. Posthybridization washes included 2x SSC at 22 °C for 10 min, 2x SSC at 55 °C for 15 min, and 0.1x SSC at 55 °C for 15 min. The slides were then equilibrated for 5 min in TN buffer (TNB, 100 mmol/L Tris·HCl and 150 mmol/L NaCl, pH 7.5) and incubated for 2 h at 22°C with alkaline-phosphatase-conjugated anti-DIG monoclonal antibody (1:2500 final dilution in TNB with 0.5 % blocking reagent; *Roche*). After washes, the slides were equilibrated for 5 min in TNM buffer (100 mmol/L Tris·HCl, 100 mmol/L NaCl, and 50 mmol/L MgCl2, pH 9.5) and incubated in substrate solution (Nitro-Blue tetrazolium chloride and 5-bromo-4-chloro-3=-indolyphosphate *p*-toluidine salt in TNM buffer; *Roche*). Staining was stopped in TE (10 mmol/L Tris·HCl and 1 mmol/L EDTA, pH 8.0), and the slides were dehydrated and mounted in Entellan (*Merck*). Further, co-localization of δ-ENaC and SGK1.1 was ascertained by double ISH labelling, where biotin- and DIG-labeled probes were simultaneously added to the hybridization mix. The combination of probes that gave optimal results was biotin-δ1 or -δ2 and DIG-SGK1.1. The fluorescent visualization of the biotin-labeled probe was carried out first. After the final wash in 0.1x SSC, sections were equilibrated in TNB for 30 min and were then incubated with streptavidin-HRP (1:150, *Perkin-Elmer*) in TNB buffer for 30 min at RT. After several washes with TNT (Tris-NaCl-Tween 20) buffer, the sections were incubated for 10 min in biotinyl tyramide (1:75 in amplification diluent; *Perkin-Elmer*). Fluorescence was developed using Cy2-conjugated streptavidin (*GE Healthcare*). The second transcript was detected with a DIG-labeled riboprobe that was visualized after the biotin-labeled probe. The sections were briefly rinsed with TNB and incubated for 90 min at room temperature with a sheep anti-DIG antibody conjugated to alkaline phosphatase (1:500; *Roche*). After several rinses in TNT buffer, sections were washed twice for 10 min with TNM buffer at room temperature and transcripts were visualized using the HNPP fluorescence detection kit (*Roche*). To eliminate autofluorescence arising from lipofusin deposition, sections were incubated in 5 mM CuSO4 and 50 mM ammonium acetate pH 5.0 for 10 min. Thereafter, they

were mounted on glass slides, air-dried at RT in darkness, rapidly dehydrated in toluene, and coverslipped with DPX (*BDH Chemicals*). Images were obtained under a Leica DMR photomicroscope (*Leica Microsystems*) or a FluoView 1000 confocal microscope (*Olympus*) and compiled using Adobe Illustrator software (*Adobe Systems*) (Gonzalez *et al.*, 2004).

II. 4.2 Quantitative real-time PCR (qPCR)

To quantitatively study the amount of δ-ENaC expressed in native tissue we performed quantitative real-time PCR (qPCR) on human cerebral cortex.

qPCR is an amplification method for DNA sequences that is based on the principle of conventional PCR and which additionally enables the simultaneous quantification of the amplified products in different samples. The quantification is mediated through fluorescent measurements, which are performed during every PCR cycle. The fluorescence signal increases proportionally to the amount of amplified products, so that at the end of the PCR run the quantification can be determined by the fluorescent signal intensity. Only within the exponential phase of the PCR it is possible to correctly quantify the products, because only in this phase the reaction conditions are optimal for doubled DNA after each round. The Ct value is determined at the cycle, in which the fluorescence signal is firstly exponential and exceeds background fluorescence.

In this study, qPCR was performed with the iQ SYBR Green supermix (*Bio-Rad*) on a Bio-Rad Mini Opticon Real-time PCR thermal cycler system. The samples were prepared as triplicates in a master mix containing the DNA polymerase according to the manufacturer's protocol. SYBR Green (excitation 497 nm, emission 520 nm) increases the fluorescence signal upon intercalating with dsDNA. As negative controls served samples that contained sterile H_2O instead of template DNA. Primer sequences used to analyze total δ and δ2 expression are available in **Tab. II.9**. The efficiency of both primer pairs was quantified and determined with the QPCR Standard Curve Slope to Efficiency Calculator (*Agilent technologies*) to be ~100% (**Fig. II.14**). Data acquisition and analysis was performed with CFX Manager™ software. A quantitative comparison between δ1 and δ2 mRNA was achieved subtracting δ2 threshold cycle (Ct) value from the $δ_{total}$ Ct value.

Tab. II.9 Primer sequences for qPCR.

Product	forward primer	reverse primer
$δ_{total}$	5'– CAGGAGCTCAACTACCGCTCAGTG –3'	5'– GCAGCTCCAGGAGCTCCAGGAGG –3'
δ2	5'– CCCAGAGGCCCTGCCACCTG –3'	5'– GAGGCGGGCAGCTCCACCAGC –3'
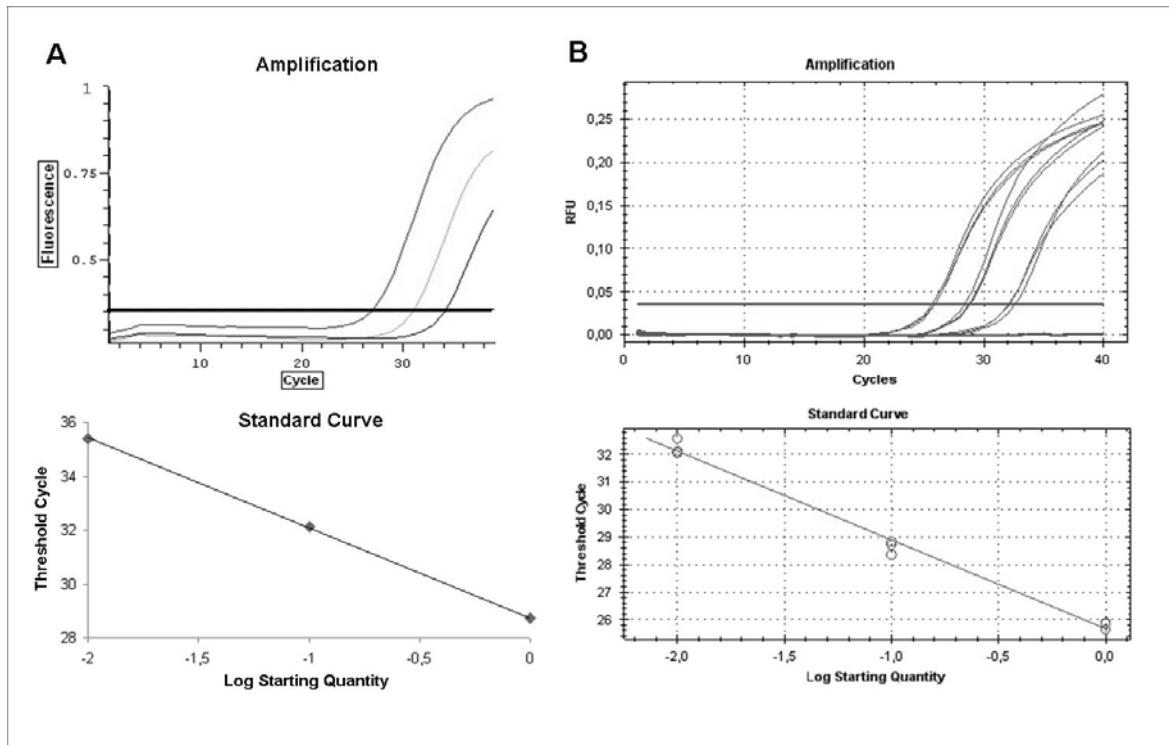
Fig. II.14 Primer efficiency.
A: Efficiency of the primer pair δ_{total} was determined by dilution of the initial cDNA (1, 1^{-1} and 1^{-2}) and maintaining amplification (above) parameters, resulting in C(t) values (threshold lined where exponential phase starts) for a standard curve (below) from which could be calculated its slope = -3.345 with R^2 = 0.999 and thus the efficiency with the formula Efficiency = -1 + $10^{(-1/slope)}$ = 99 %. B: Efficiency of the primer pair $\delta 2$ was determined like δ_{total}, but in triplicates. Slope = -3.230, R^2 = 0.990, Efficiency = 103 %.

Brain samples were obtained from three healthy donors that died without history of drug abuse or neurodegenerative disease, which was confirmed by pathological examination, and provided by the Department of Pathology of the University Hospital of the Canary Islands. Written consent was available and the study was approved by the Human Ethics Committee of the Hospital (reference 277/2010). Brains were removed after a post-mortem period of 7.3 ± 2.4 hours. Total RNA was purified with the Illustra RNAspin Mini Kit (*GE Healthcare*) and cDNA was derived from total RNA by synthesis with the MonsterScript 1st strand cDNA Synthesis Kit (*Epicentre Biotechnologies*) following the manufacturer's instructions.

II. 5 Statistical analysis

Analysis of TEVC and fluorescence data was performed using Excel (*MICROSOFT OFFICE 2003*) and Prism 5.0 software (*Graphpad*). In **III.** the results are represented as arithmetic averages ± standard error of the mean (SE). "n" is the number of experiments, in some cases it is equal to the number of oocytes, while "N" is the number of donors (batches). For comparison of two groups Student's T-test or non-parametric two-tailed Mann-Whitney test was applied. When more than two groups were compared, non-parametric Kluskal-Wallis test or repeated measures ANOVA, followed by Dunn's or Bonferroni multiple-comparison test, respectively, were used.

Significant differences of the average values are marked with an asterisk "*". The significance level was p ≤ 0,05. "n.s." indicates not significant.

For graphic representation of the results in this study, the software FreeHand MX (*MACROMEDIA*), Metamorph (*Universal Imaging Corp.*) and Prism 5.0 (*Graphpad*) was employed. The manuscript of the present dissertation was written with the text processing programme Word (*MICROSOFT OFFICE 2003*).

III.   Results

III. 1. Differential N-termini in ENaC δ subunit isoforms modulate channel trafficking

Based on the fact that δ1- and δ2-ENaC show a low co-localization level, which suggests that the isoform expression is under a strict regulation, it was hypothesized that they may feature specific functional roles. Therefore, the focus of interest turned to investigate in more detail how δ1 functionality may differ from that of δ2. As a unique difference in the primary structure, δ2 comprises a longer N-terminus than δ1. Therefore, it was hypothesized that differential N-termini would account for different functionality of the isoforms.

III. 1.1 δ-ENaC isoforms show different current levels when heterologously expressed

Whether δ1 and δ2 ENaC show different functionality was assessed by co-expression of the subunits δ1βγ or δ2βγ in *Xenopus laevis* oocytes. This elicited amiloride-sensitive currents indicating the formation of functional ENaC channels. We consistently observed that the macroscopic whole cell currents in oocytes expressing δ1βγ were higher than the currents in the oocytes expressing δ2βγ (**Fig. III.1 A**). This difference could be seen all along the whole voltage range (-70 mV to +40 mV) measured (**Fig. III.1 B**). The average δ1βγ current was approximately 2.5 fold of the average δ2βγ current (**Fig. III.1 C**).

Since ENaC is constitutively active and despite keeping oocytes in post-injection saline, which contained low Na^+, they were overloaded with Na^+ and thus the reversal potential was shifted to more negative values with higher ENaC activity. A larger shift was observed with δ1βγ (**Fig. III.1 B**).
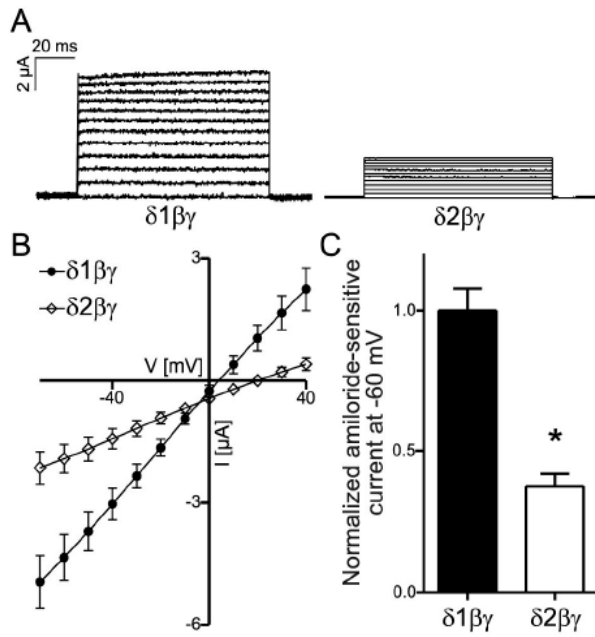
Fig. III.1 δ1βγ-ENaC produces higher macroscopic currents than δ2βγ.
A: representative amiloride-sensitive currents elicited by co-injection of δ1βγ or δ2βγ ENaC cRNAs into *Xenopus* oocytes. Currents were obtained by increasing membrane voltage from -70 mV to +40 mV in sequential 10-mV steps. B: representative current-voltage (*I-V*) curves obtained from oocytes injected with δ1βγ and δ2βγ cRNAs. Data points represent average values ± SE (n≥150). C: normalized amiloride-sensitive current magnitude averages at a holding potential of -60 mV obtained from oocytes injected with δ1βγ or δ2βγ. Error bars represent SE (*n*≥150 for each condition). *, *P* < 0.05, Kruskal-Wallis nonparametric test followed by a Dunn's multicomparison test.

Further, HEK293 cells were co-transfected with δ1βγ or δ2βγ ENaC cDNAs and subjected to perforated patch clamp experiments in the whole cell mode. Formation of functional channels was verified by currents sensitive to benzamil (**Fig. III.2 A**), another specific ENaC blocker (Waldmann *et al.*, 1995). Also in this cell line it was consistently observed that the whole cell current density was higher for δ1βγ-expressing cells than in the δ2βγ-expressing cells (**Fig. III.2 A & B**). This difference could be seen all along the whole voltage range (**Fig. III.2 A**) measured. The average δ1βγ current was approximately 2.3 fold of the average δ2βγ current (δ1βγ: 232.4±19.39 pA/pF and δ2βγ: 99.72±12.22 pA/pF, **Fig. III.2 B**). No benzamil-sensitive current was observed in untransfected cells (data not shown).
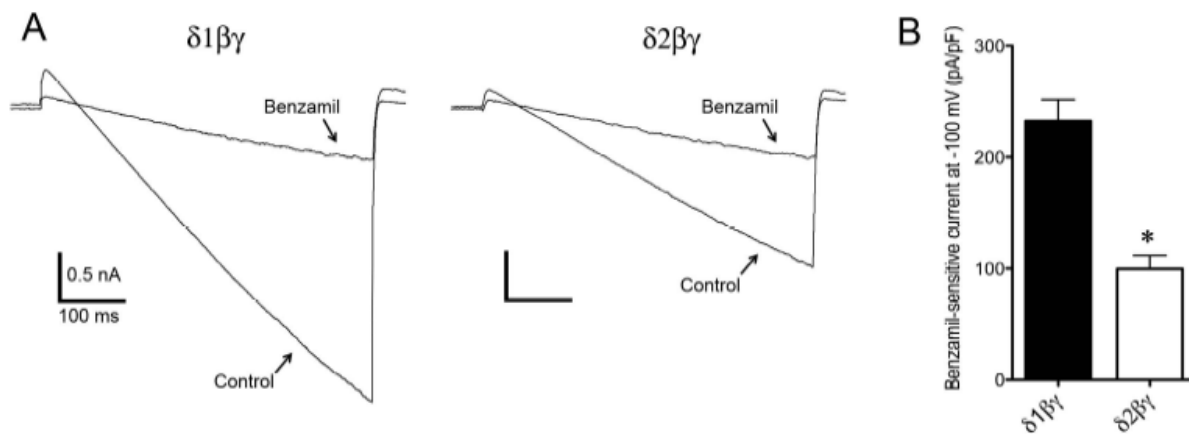
Fig. III.2 δ1βγ ENaC whole cell currents are higher than that of δ2βγ in HEK293 cells.
A: representative overlay of currents in a voltage-clamped HEK cell elicited by co-transfection of δ1βγ or δ2βγ ENaC cDNAs before and after addition of benzamil (10 µM) to the bath solution. Currents were obtained by a ramping protocol from +60 down to -100 mV over a 500 ms period. B: benzamil-sensitive current density averages at a holding potential of -100 mV obtained from HEK293 cells transfected with δ1βγ or δ2βγ. Error bars represent SE (*n*≥6 for each condition). *, *P* < 0.05, unpaired t-test. (results from work performed by Dr. P. Miranda)

III. 1.2 Single channel properties of δ1 and δ2 do not account for the difference in macroscopic currents

The macroscopic current of a channel depends on three factors: its open probability (Po), conductance (g) and the number of channels (N). To investigate whether the difference of the macroscopic currents between the isoforms δ1 and δ2 could be due to varied single channel characteristics, patch clamp experiments were performed in the cell-attached mode with oocytes expressing either δ1βγ or δ2βγ (**Fig. III.3 A**). Channel events were counted during ~5 minutes and the Po was determined to be equal for both isoforms δ1 and δ2 (**Fig. III.3 B**). Further, δ1 and δ2 did not display differences in single channel conductance as determined by measuring the single channel amplitudes (**Fig. III.3 C**). Also the mean open and closed time of both isoforms did not vary significantly (data not shown).
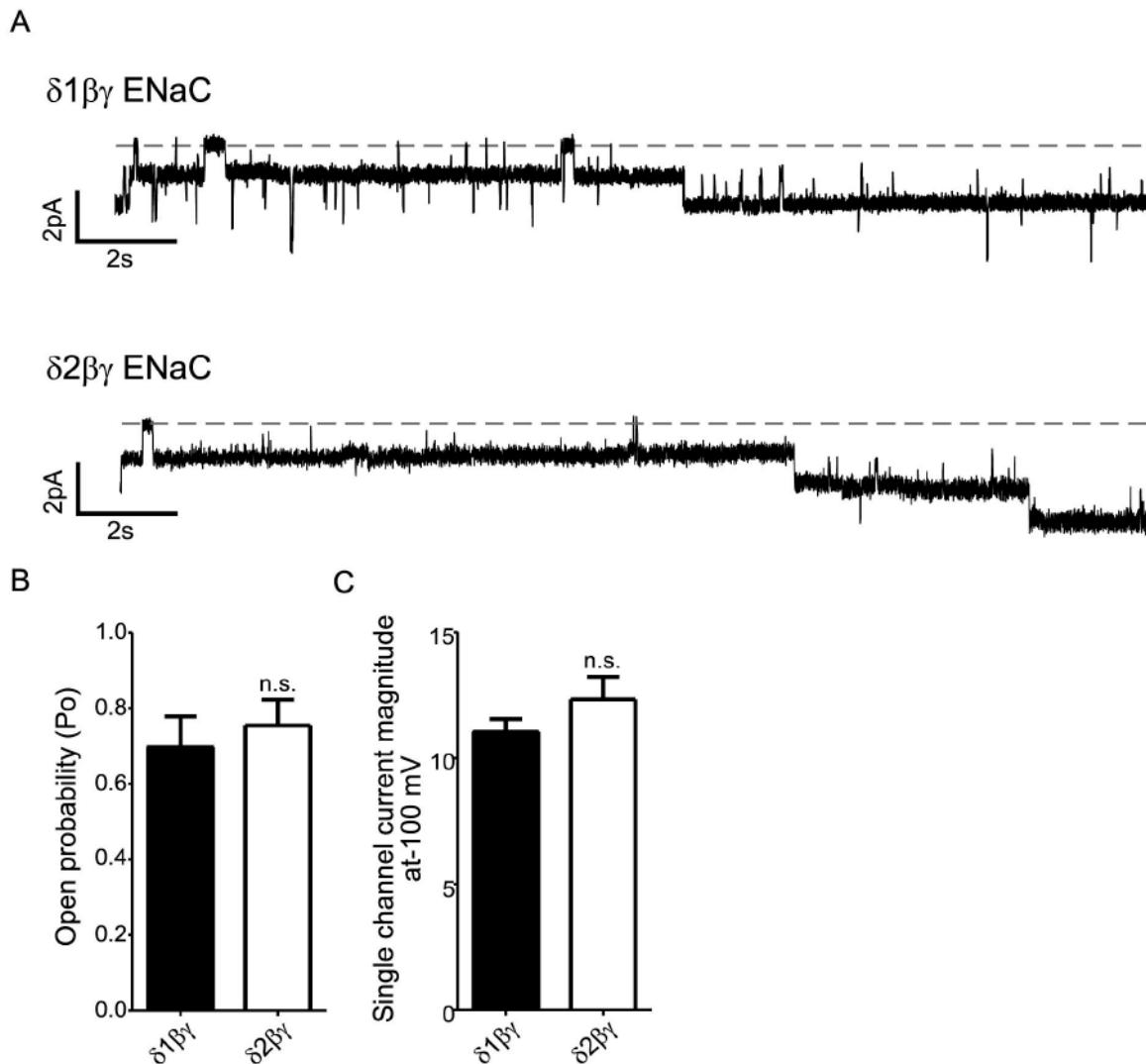
Fig. III.3 Single channel properties of δ1βγ and δ2βγ ENaC.
A: representative cell-attached recordings of δ1βγ and δ2βγ injected oocytes. Single channel currents were recorded at -100 mV. B: the apparent open probability (NPo) was determined for δ1βγ and δ2βγ. Error bars represent SE (n≥6) C: single channel amplitudes were measured from at least three channel events for each experiment, to calculate the single-channel conductance. Errors bars represent SE (n≥6). n.s., not significant, unpaired Student's t-test. (results from work performed by Dr. M. Althaus at the laboratory of Prof. W. Clauss, University of Giessen)

III. 1.3 A decrease in extracellular pH equally potentiates δ1 and δ2 currents

Since δ-ENaC Po is enhanced by extracellular acidic pH, acting on its degenerin sites (Ji & Benos, 2004), it was questioned whether δ1 and δ2 respond similarly to a drop in pH. Therefore oocytes expressing either δ1βγ or δ2βγ were subjected to a time course TEVC experiment, where the amiloride-sensitive currents were measured under physiological pH (7.4) and acidic pH (4.0, **Fig. III.4 A**). δ1βγ and δ2βγ showed a significant enhancement of the amiloride-sensitive current by a drop in pH (2.7±0.4 fold for δ1 and 3.1±0.9 fold for δ2), which was equal in both isoforms (**Fig. III.4 B**).
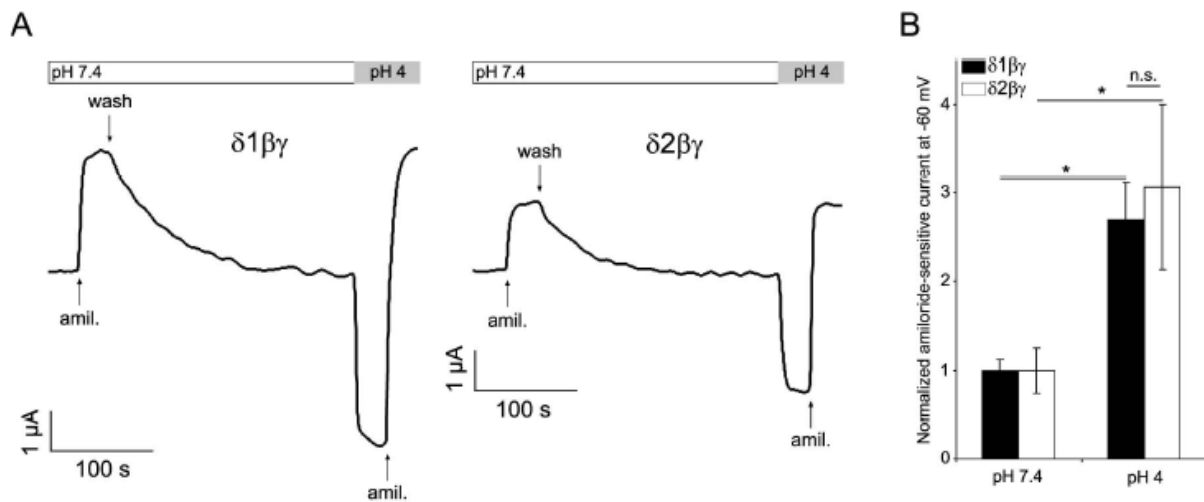
Fig. III.4 δ1βγ and δ1βγ currents are similarly enhanced by pH 4.
A: representative traces of δ1βγ or δ2βγ currents, clamped at -60 mV. amil., amiloride. B: normalized amiloride-sensitive current magnitude averages at a holding potential of -60 mV at pH 7.4 and pH 4. Error bars represent SE ($n≥7$ for each condition). *, $P < 0.05$; n.s., not significant; Student's t-test

III. 1.4 Differential plasma membrane abundance accounts for the difference in δ-ENaC isoforms channel activity

Since Po and g of δ1βγ and δ2βγ were estimated to be very similar, the single channel kinetics were excluded to be responsible for the difference seen in the macroscopic current. In order to monitor if it is N that varies in oocytes expressing δ1βγ or δ2βγ, we investigated channel abundance in the membrane with confocal microscopy. To visualize the channel abundance at the surface of the oocyte membrane we tagged δ1 and δ2 with YFP. Surface staining was verified with tf-AF568 (**Fig. III.5 A**) that bound to the tfr, which is a known membrane protein (Macdonald & Pike, 2005). Oocytes co-expressing δ1$_{YFP}$βγ or δ2$_{YFP}$βγ displayed a yellow fluorescent membrane as could be observed under the confocal microscope (**Fig. III.5 A & B**). The average fluorescence intensity was ~2 fold higher in δ1βγ expressing oocytes than in oocytes expressing δ2βγ, indicating that the δ2 isoform is significantly less abundant in the membrane than δ1 (**Fig. III.5 D**). To exclude that this higher channel abundance of δ1 in the membrane resulted from higher δ1 protein expression in the whole cell, we performed fluorometry and western blot experiments of total protein extracts from oocytes expressing either δ1$_{(YFP)}$βγ or δ2$_{(YFP)}$βγ. As a pri-

mary antibody we used a polyclonal antibody raised against the C-terminus of the δ subunit, which is common in both isoforms δ1 and δ2. These fluorometry and western blot experiments revealed that total protein expression of $δ1_{(YFP)}$ and $δ2_{(YFP)}$ were not significantly different (**Fig. III.5 C & D**). Hence, the differential abundance of δ1 and δ2 in the membrane cannot be explained by different total protein expression of δ1 and δ2.
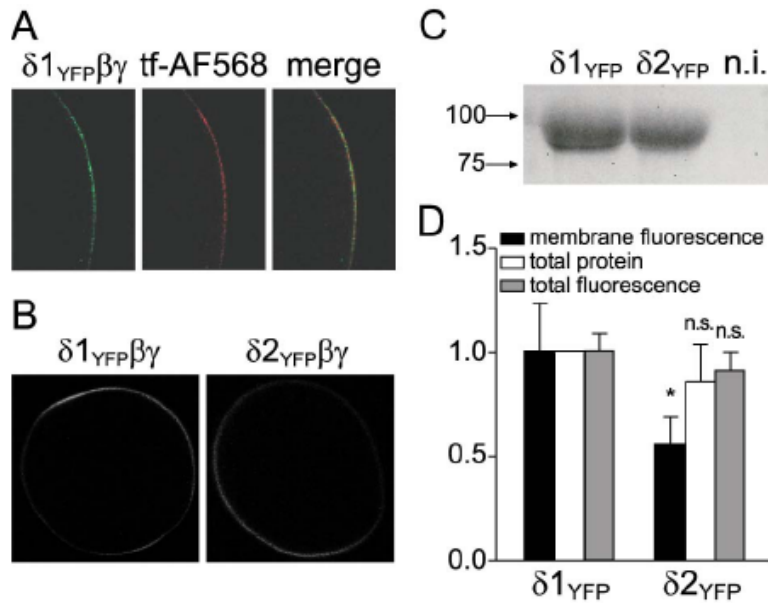
Fig. III.5 Membrane abundance and total protein expression of δ1 and δ2.
A: representative confocal images showing cell surface expression of fluorescently labeled δ-ENaC in *Xenopus* oocytes expressing $δ1_{YFP}βγ$ and tf-AF568 staining of the transferrin receptor on the cell surface of the same oocyte. YFP, yellow fluorescent protein; tf-AF568, AlexaFluor568 conjugated transferrin. B: representative confocal images showing cell surface expression of fluorescently labeled δ-ENaC in *Xenopus* oocytes expressing either $δ1_{YFP}βγ$ or $δ2_{YFP}βγ$. C: Western blot analysis of $δ_{YFP}$-expression in *Xenopus* oocytes expressing $δ1_{YFP}βγ$ or $δ2_{YFP}βγ$ ENaC. Molecular mass (in kDa) marker migration is shown with arrows to the left. n.i., noninjected oocytes. D: black bars represent the average fluorescence intensity of the membrane monitored in oocytes expressing $δ1_{YFP}βγ$ or $δ2_{YFP}βγ$ (n≥15). White bars represent average total protein abundance quantified by Western blot analysis of six independent batches of oocytes expressing δ1βγ or δ2βγ. Grey bars represent the average relative fluorescence of total protein extracts from oocytes $δ1_{YFP}βγ$ or $δ2_{YFP}βγ$ (n≥16). Error bars represent SE. *, $P≤0.05$; n.s., not significant, Kruskal-Wallis nonparametric test followed by a Dunn's multicomparison test.

III. 1.5 Endocytosis rates are similar in δ1 and δ2 and do not account for their differential membrane abundance

The following results demonstrate that the differential membrane abundance of the isoforms cannot be explained by altered endocytosis rates.

III. 1.5.1 The differential membrane abundance of δ-ENaC isoforms is independent of accessory subunits and the presence of PY motifs

TEVC recordings of oocytes expressing either δ1 or δ2 alone displayed a significantly different current, although in a much smaller range (nA) than with β and γ. The δ2 isoform led to an average current of around 0.3 fold of the average δ1 current (**Fig. III.6**). This indicates that the difference observed in δ1 and δ2 macroscopic currents is independent of the accessory subunits β and γ. Further, the δ subunit does not contain a PY motif, in contrast to α, β and γ (Staub *et al.*, 1996; Goulet *et al.*, 1998). In the canonical ENaC composed by α, β and γ, the PY motif was described as a docking site for the E3 ubiquitine ligase Nedd4-2, which ubiquitinates ENaC and

promotes endocytosis. Hence, the difference of δ1 and δ2 does not involve the PY motif or PY motif-dependent altered endocytosis.
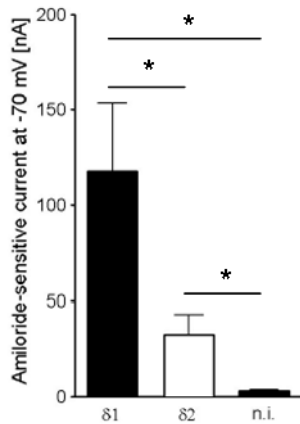
Fig. III.6 Differential δ1 and δ2 currents are independent of β and γ sub-units and thus independent of PY-motifs.
Average currents obtained at -70 mv from oocytes injected with δ1 or δ2 alone (n≥12). Error bars represent SE. *, $P \leq 0.05$, Kruskal-Wallis nonparametric test followed by a Dunn's multicomparison test. (results from work performed by Dr. P. Miranda)

III. 1.5.2 Mutation of lysines in the δ2 N-terminus does not recover δ1 activity levels

Although the difference between δ1 and δ2 is independent of the presence of PY motifs, it was conceivable that altered ubiquitination by a Nedd4-2 independent mechanism could underlie altered channel abundance in the membrane. The δ2 isoform comprises three more lysines at its N-terminus than δ1 (**Fig. III.7 A**), all of them potential targets for ubiquitination. Single and double point mutations were generated, in which the lysines were substituted by arginines (δ2K47R, δ2K71R, δ2K85R and δ2K47/71R). Co-expressing the δ2 mutants with β and γ led to amiloride sensitive currents in TEVC experiments (**Fig. III.7 B**), which were at all ranges of voltage similar to the ones of δ2 (**Fig. III.7 C & D**). Thus the differential membrane abundance of δ1 and δ2 is independent of the additional lysine sites in the δ2 N-terminus. A triple mutant (δ2K47/71/85R) was not generated, because after observing that in some batches the mutants δ2K85R and δ2K47/71R were not functional it was likely that such a mutation would also abrogate channel functionality.

That differential membrane abundance of δ1 and δ2 is independent of the additional lysine sites in the δ2 N-terminus indicates that not altered ubiquitylation-dependent endocytosis is the underlying mechanism for the differential membrane abundance of the isoforms.
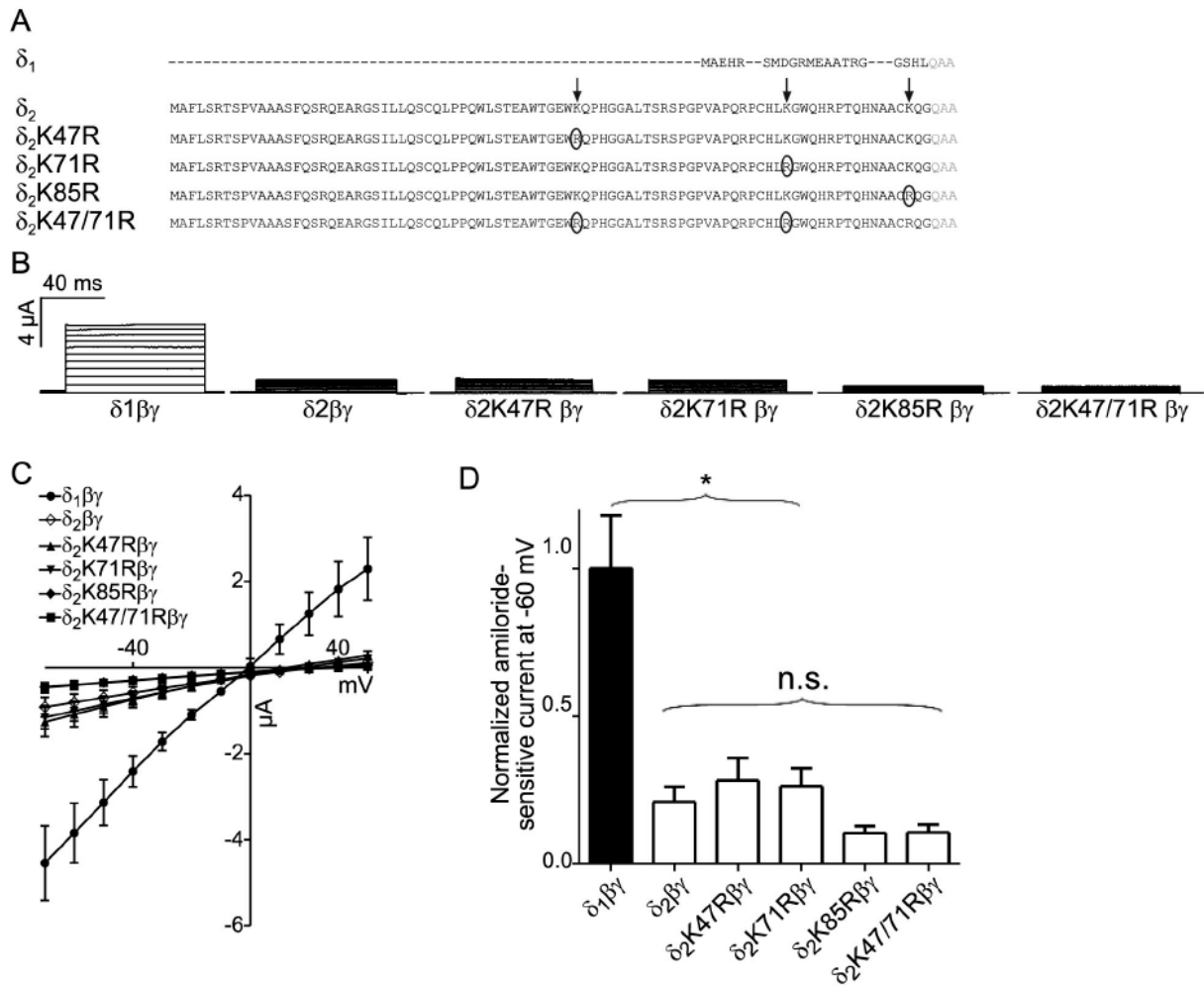
Fig. III.7 Eliminating the additional lysines in the δ2 N-terminus does not affect current levels.
A: schematic representation of the divergent N-terminal region of δ isoforms. Additional lysines present in δ2 and mutated in this experiment are indicated. B: representative amiloride-sensitive current traces of TEVC recordings of oocytes injected with either δ1βγ, δ2βγ or lysine mutated δ2βγ cRNAs, obtained by increasing voltage from -70 mV to -40 mV in sequential 10-mV steps. C: representative current-voltage (*I-V*) curves obtained from oocytes injected with δ1βγ, δ2βγ or lysine mutated δ2βγ cRNAs. Data points represent current average ± SE (n≥18). D: amiloride-sensitive current magnitude averages at a holding potential of -60 mV obtained from oocytes injected with δ1βγ, δ2βγ or lysine mutated δ2βγ cRNAs. Error bars represent SE (*n*≥18 for each condition). *, *P*<0.05; n.s., not significant, Kruskal-Wallis nonparametric test followed by a Dunn's multicomparison test.

Beside ubiquitylation, also other covalent bindings that are implicated in channel trafficking, such as sumoylation, which is described to stabilize proteins in the membrane (Wilkinson & Henley, 2010), could be affected, once the lysines were mutated. Since the δ2 N-terminal lysine mutations revealed no changes, when compared to the δ2 wildtype, any possible lysine based trafficking alteration could be excluded for explanation of the isoform difference.

III. 1.5.3 δ1βγ and δ2βγ show similar endocytosis rates

To test whether the differential channel abundance in the membrane could be due to any other, not ubiquitylation-dependent, altered endocytosis of the channels from the membrane, the insertion pathway of newly synthesized channels from the TGN into the membrane was blocked with brefeldin A (BFA) (Shimkets *et al.*, 1997; Alvarez de la Rosa *et al.*, 1999), so that endocytosis could be tracked without interference by insertion of new channels. Oocytes expressing either

δ1βγ or δ2βγ were incubated in 5 μM BFA and the levels of amiloride sensitive currents were followed with TEVC over a period of 4 hours. As expected, in the presence of BFA, amiloride sensitive currents of δ1βγ or δ2βγ expressing oocytes significantly decreased (~0.5-fold, **Fig. III.8**), resulting from stopped insertion of new channels and simultaneous channel retrieval from the membrane. Currents decreased at a similar rate in oocytes expressing either δ1βγ or δ2βγ, suggesting that endocytosis is similar in both isoforms. In the absence of treatment the currents of δ1βγ or δ2βγ remained unchanged.

Since endocytosis rates are the same for both isoforms, the observed difference in membrane abundance is consistent with a distinctly processed channel insertion.
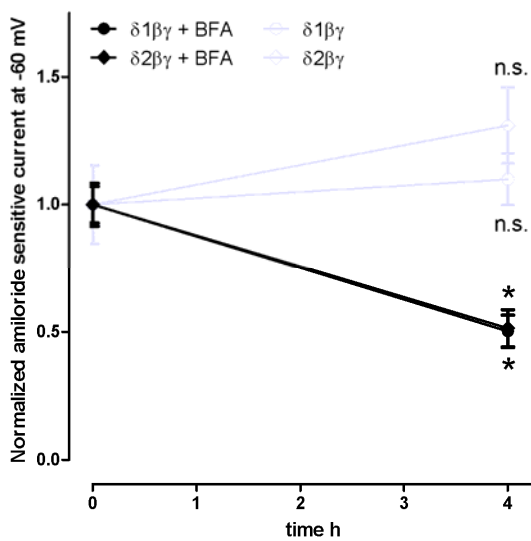
Fig. III.8 Rate of retrieval of channels from the plasma membrane.
Time course of amiloride sensitive current levels of oocytes injected with δ1βγ or δ2βγ during incubation with 5 μM brefeldin A (BFA). Whole cell amiloride-sensitive currents were measured with TEVC in the same oocytes at times 0 h, and 4 h after addition of BFA. Data points represent average values ± SE (n≥6 for δ1βγ/δ2βγ, n≥16 for δ1βγ/δ2βγ+BFA). Data points at 4 h without and with BFA were compared for each subunit combination. *P≤0.05; n.s., not significant, Student's t-test.

III. 1.6 The first 25 amino acids in the δ2-N-terminus are essential for channel activity

Based on the primary protein sequence, the only difference between δ1 and δ2 is the longer δ2 N-terminus. Thus we generated progressive truncations of the δ2 N-terminus, drawing δ2 nearer to δ1, to investigate whether this would increase δ2 currents to δ1 levels (**Fig. III.9 A**). Co-injection of truncations δ2Δ23, δ2Δ63 and δ2Δ86 with β and γ in oocytes did not produce amiloride-sensitive current (**Fig. III.9 B**). Thus, the first 25 amino acids, which were absent in all mutants, include elements necessary for the channel to function.
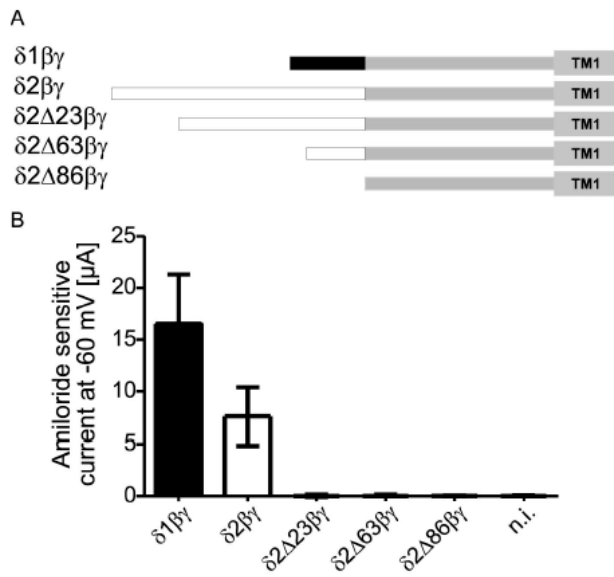
Fig. III.9 Truncation of the first 25 aminoacids of δ2 leads to non-functional channels.
A: schematic representation of the N-termini of δ-ENaC isoforms and truncated δ2 constructs. TM1, transmembrane domain 1. B: amiloride-sensitive current magnitude averages at a holding potential of -60 mV obtained from oocytes injected with δ1βγ, δ2βγ or truncated δ2βγ cRNAs. n.i., non injected. Error bars represent SE (*n*=10) for each condition.

III. 1.7 Simultaneous deletion of positions Δ25-45 and Δ66-85 in δ2 recovers δ1 current levels

Since the first 25 aminoacids of δ2 are indispensable for channel functionality, we generated internal deletion mutants δ2Δ25-45, δ2Δ25-65 and δ2Δ25-85 (**Fig. III.10 A**) and co-expressed them with β and γ in oocytes for TEVC experiments. The deletions δ2Δ25-45 and δ2Δ25-65 produced amiloride sensitive currents similar to the δ2 wild type, while the deletion δ2Δ25-85 produced amiloride sensitive currents similar to δ1 wild type (**Fig. III.10 B & C**). We also confirmed that the membrane abundance of δ2Δ25-85$_{YFP}$ was the same as seen with δ1$_{YFP}$, and thus significantly higher than δ2$_{YFP}$ (**Fig. III.10 D**).

The next approach was to determine whether the fragment of amino acids 66-85 is responsible for the lower δ2 current. Deletion of amino acids 66-85 (δ2Δ66-86) produced δ2 current levels (**Fig. III.10 B & C**).

To respond whether it was the length of the deletion or the sequences between amino acids 25-45 and amino acids 66-85 that reduced δ1 activity to δ2 levels, we decided to simultaneously delete these sequences, to rule out one of the possibilities. Concurrent deletion of the fragments 25-45 and 66-85 (δ2 2xΔ) produced current levels equal to δ1 (**Fig. III.10 B & C**), suggesting that these two regions of the δ2 N-terminus are responsible for reduced channel activity, because once they are deleted δ2 recovers δ1 channel activity.
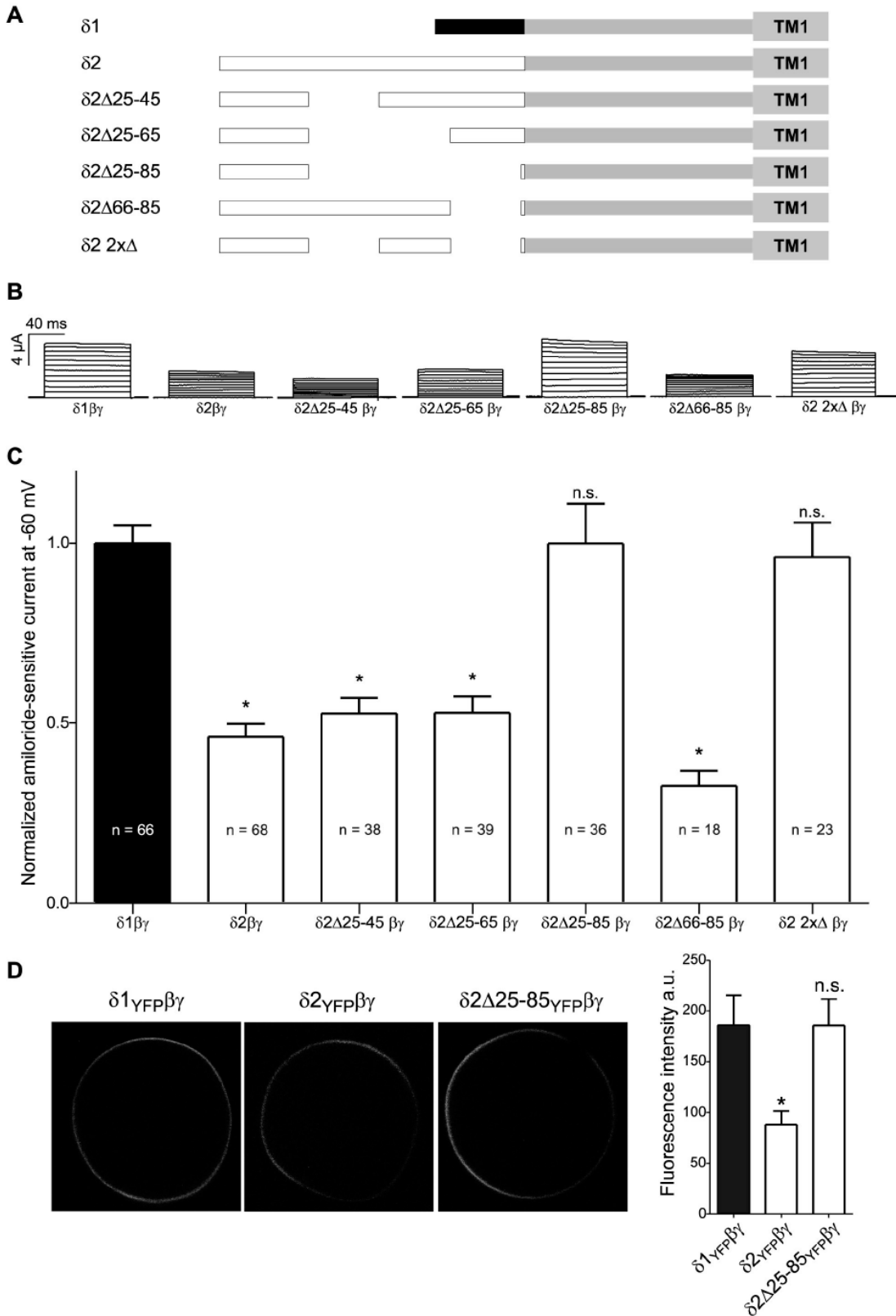
Fig. III.10 δ2 N-terminal deletions recover δ1 activity levels.
A: schematic representation of the N-termini of δ-ENaC isoforms and δ2 deletion constructs. B: representative amiloride-sensitive current traces of TEVC recordings of oocytes injected with either δ1βγ, δ2βγ or deleted δ2βγ cRNAs, obtained by increasing voltage from -70 mV to -40 mV in sequential 10-mV steps. C: amiloride-sensitive current magnitude averages at a holding potential of -60 mV obtained from oocytes injected with δ1βγ and δ2βγ or deleted δ2βγ cRNAs. Error bars represent SE ($n \geq 18$ for each condition). *, $P \leq 0.05$; n.s., not significant, Kruskal-Wallis nonparametric test followed by a Dunn's multicomparison test. D: representative confocal images showing cell surface expression of δ1$_{YFP}$βγ, δ2$_{YFP}$βγ or δ2Δ25-85$_{YFP}$βγ in *Xenopus* oocytes and corresponding average fluorescence intensity ($n \geq 10$ for each condition). Error bars represent SE. *, $P \leq 0.05$; n.s., not significant, Mann-Whitney nonparametric test.

III. 1.8 qRT PCR and cell counting of ISH stained human cerebral cortex reveal higher expression of δ1 than δ2

δ1 and δ2 are widely expressed in pyramidal neurons of the primate brain cortex, with few cells co-expressing both isoforms (Giraldez *et al.*, 2007). The amount of cells expressing either δ1 or δ2 was counted and determined to be approximately 60 % and 30 %, respectively, with 9 % expressing both isoforms (**Fig. III.11 A & B**). qRT-PCR was performed with a primer pair generating a PCR product common to both isoforms (δ_{total}) and another primer pair generating a PCR product specific for δ2. After ensuring that the primer efficiency was equal for both primer pairs, the Ct of the qPCRs was compared to calculate the fold difference in the expression of total δ as opposed to the expression of only δ2 as described in **II.4**. The results show an average difference of 3.5 fold (**Fig. III.11 C**), indicating that δ1 RNA was 2.5 times more abundant than δ2 (**Fig. III.11 C**).
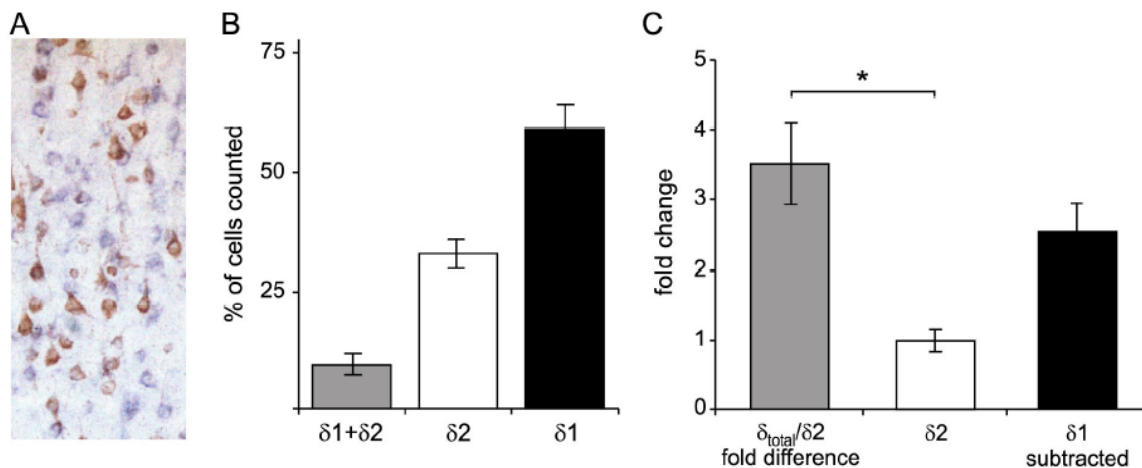
Fig. III.11 δ1 mRNA is more abundant than δ2 mRNA in human brain cortex.
A: *in situ* hybridization for δ1 mRNA (blue) and δ2 mRNA (brown) showing stained pyramidal cells in the human frontal cortex. Black bar, 60 μm. B: count of δ1-, δ2- and δ1+δ2- expressing cells in the human cerebral cortex. C: qPCRs of total δ and δ2 alone were performed on three different human brain cortex samples. Bars represent delta total abundance and the subtracted δ1 values normalized to δ2. Error bars represent SE. *, P<0.05, Student's t-test.

III. 2. α-ENaC turnover is distinct from that of δ-ENaC

While investigating the trafficking of the δ-ENaC isoforms, control experiments were performed on α-ENaC. This revealed that the behaviour of the canonical αβγ-ENaC stands in contrast to that of δβγ-ENaC. The underlying mechanisms of αβγ-ENaC regulation are investigated into detail and widely accepted (Rotin & Staub, 2010). Therefore, revealing differences between α-ENaC trafficking and δ-ENaC trafficking could shed light into the underlying mechanisms for δ-ENaC trafficking.

III. 2.1 The endocytosis turnover of α-ENaC is faster than of δ-ENaC

Experiments with BFA in **III. 1.5.3** showed that insertion of newly synthesized ENaC could be blocked, revealing the endocytosis rates for comparison between different ENaC subunit combinations. To test whether blocking of the insertion resulted in a varied response of αβγ and δβγ ENaC this experiments were performed with oocytes expressing either αβγ or δβγ. The levels of amiloride sensitive currents were followed with TEVC over a period of 4 hours. As expected, in the presence of BFA, amiloride sensitive currents of αβγ expressing oocytes significantly decreased (**Fig. III.12**). Also in oocytes expressing δβγ-ENaC a significant decrease of amiloride sensitive currents was observed, although to a lesser extent than in oocytes expressing αβγ-ENaC (~0.25-fold for αβγ vs. 0.5-fold for δβγ, **Fig. III.12**), indicating a faster endocytosis rate for αβγ than for δβγ. Taking into account that in the absence of treatment αβγ current increased ~4-fold after 4h, while δβγ were unchanged, these findings indicate that the effect of BFA upon αβγ is even more enhanced than upon δβγ. This points towards a faster insertion for α-ENaC than for δ-ENaC and leads to the hypothesis that α-ENaC displays a faster turnover than δ-ENaC.
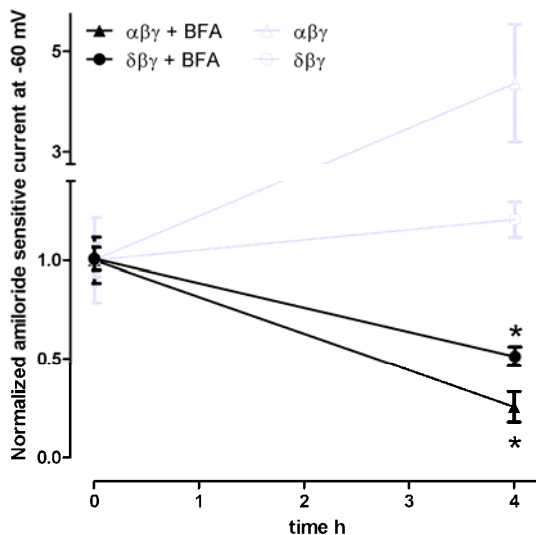
Fig. III.12 αβγ-ENaC endocytosis is faster than that of δβγ-ENaC.
Rate of retrieval of channels from the plasma membrane. Time course of amiloride sensitive current levels of oocytes injected with αβγ or δβγ during incubation with 5 μM brefeldin A (BFA). Whole cell amiloride-sensitive currents were measured with TEVC in the same oocytes at times 0 h, and 4 h after addition of BFA. Data points represent average values ± SE (n≥6 for αβγ/δβγ, n≥16 for αβγ/δβγ+BFA). Data points at 4 h without and with BFA were compared for each subunit combination. *, $P \leq 0.05$; Student's t-test.

III. 2.2 The insertion rate of α-ENaC is faster than of δ-ENaC

Fluorescence recovery after photo-bleaching (FRAP) experiments were conducted on a confocal microscope with αYFPβγ- and δYFPβγ-ENaC expressing oocytes to reveal the kinetics of newly inserted channels into the plasma membrane. **Fig. III.13 (A – F)** shows representative images of oocytes bleached at a small region in the plasma membrane, where the fluorescence of the YFP-tagged channels disappears and recovers after 30 minutes.
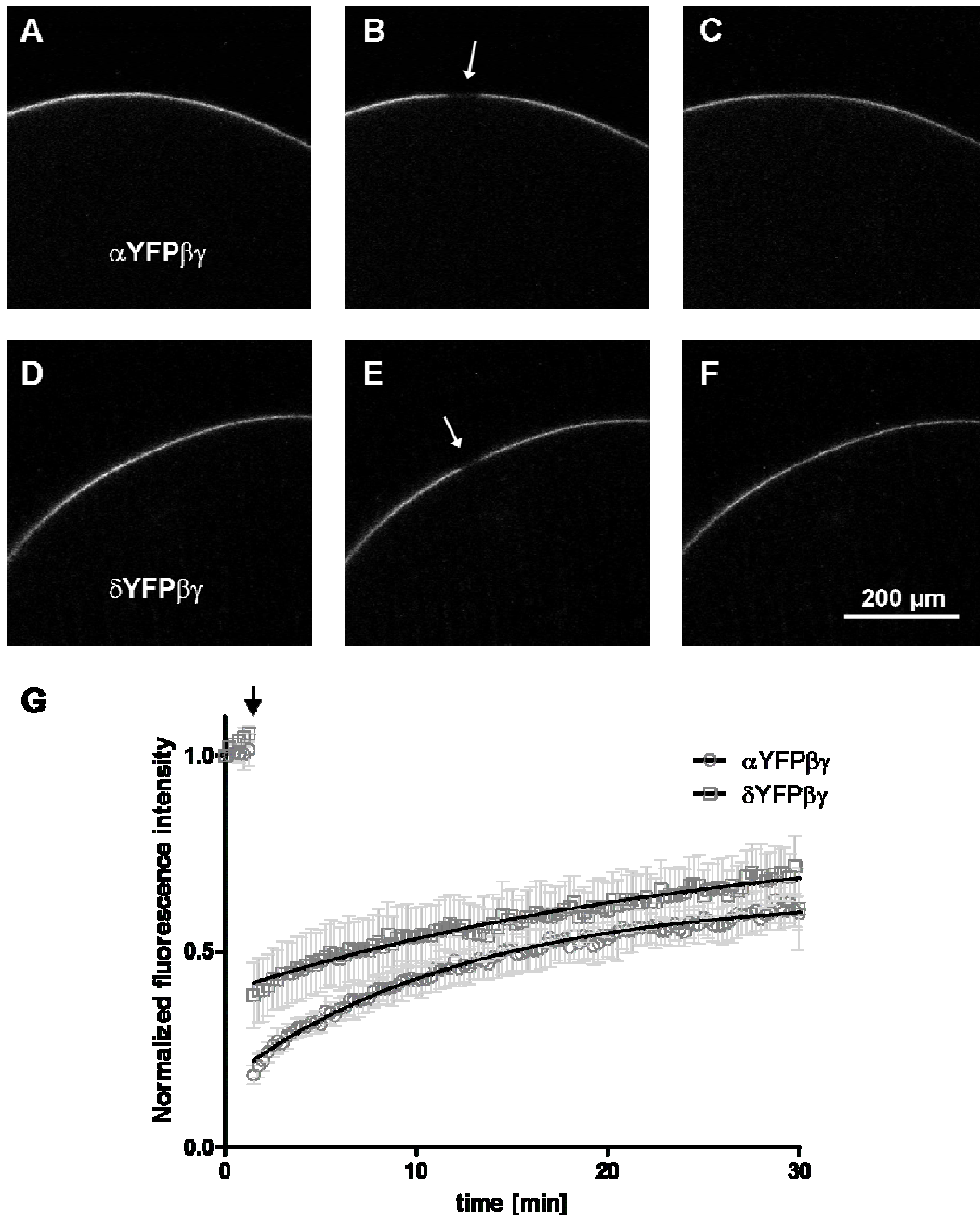
Fig. III.13 αβγ-ENaC insertion is faster than that of δβγ-ENaC.
A-F: Confocal images of oocyte membranes with YFP-tagged channels und FRAP of αYFPβγ expressing oocytes (A-C) and δYFPβγ expressing oocytes (D-F). A, D: representative images of initial fluorescence intensity before bleaching. B, E: first post-bleach image. The bleached region is indicated with an arrow. C, F: fluorescence image after recovery at time point 30 min. G: FRAP recovery curve of αYFPβγ or δYFPβγ expressing oocytes. Plotted is the normalized fluorescence intensity versus time in minutes. Photo bleaching is indicated with an arrow. The fitted curve is drawn in bold. Data points represent average values ± SE (n=4 for αYFPβγ, n=6 for δYFPβγ).

The corresponding FRAP recovery curves are plotted in **Fig. III.13 G,** with the fitted curves according to **II. 3.2.1**. After normalization, the mobile fraction Fm and τ were determined as described in **II. 3.2.1**. A comparison of important parameters made in **Tab. III.1** shows that the recovery curves of αYFPβγ is different from that of δYFPβγ. The halflife of αYFPβγ is significantly less than that of δYFPβγ ($t_{1/2}$ 10 min and $t_{1/2}$ 18 min, respectively), indicating that the velocity of recovery for αYFPβγ is faster than for δYFPβγ. The $t_{1/2}$ of 10 min for αYFPβγ is consistent with previous studies reporting that the $t_{1/2}$ of endogenous αβγ-ENaC was 12 – 17 min at the apical

membrane of A6 cells (Alvarez de la Rosa *et al.*, 2002a). The calculated I_E and Fm with 0.67 and 0.59 for αYFPβγ, respectively, and 0.81 and 0.73 for δYFPβγ, respectively, make reference to-wards a similar mobility. These results indicate that αβγ insertion is faster than δβγ insertion and corroborate the hypothesis that αβγ turnover is faster than that of δβγ, which was concluded from the former result in **III. 2.2** where αβγ was displaying a faster endocytosis than δβγ.

Tab. III.1 Comparison of FRAP parameters between αYFPβγ and δYFPβγ.

parameter	αYFPβγ	δYFPβγ
I_E **(plateau)**	0.67 ± 0.05	0.81 ± 0.07
Fm	0.59 ± 0.05	0.73 ± 0.12
halflife [min]	10.06 ± 2.39	18.13 ± 3.47 *
τ [min⁻¹]	0.079 ± 0.014	0.045 ± 2.39 *

*P≤0.05; I_E, calculated endvalue of fluorescence intensity; Fm, calculated mobile fraction, τ, recovery constant.

III. 2.3 Unlike α-ENaC, the δ-ENaC endocytosis is dynamin-independent

The canonical αβγ-ENaC is known to undergo clathrin-mediated endocytosis (Shimkets *et al.*, 1997), which requires dynamin (Schmid & Frolov, 2011), and thus should be blocked by Dynasore, a known dynamin blocker (Macia *et al.*, 2006), resulting in an increase of channel abundance in the membrane and thus increased current levels. Indeed, incubation of αβγ-ENaC expressing oocytes in 80 µM Dynasore increased the amiloride sensitive currents ~16-fold (**Fig. III.14**), due to constant insertion of new channels during interrupted retrieval. Surprisingly, none of the δ-ENaC isoforms was affected by Dynasore after 4h of incubation (**Fig. III.14**) or at other time-points (1.5h, and 24h, data not shown). Without treatment, the αβγ currents already increased to ~4-fold after 4 hours, while δβγ currents remained the same when compared to the initial value. This observation confirms the conclusion that was drawn from the results **III. 2.1** & **III. 2.2** that the turnover rate of α-ENaC trafficking is faster than for δ-ENaC.

Hence, we conclude that δβγ channels undergo an endocytosis mechanism not only quantitatively different, but also qualitatively different from the classically described dynamin-dependent, clathrin-mediated endocytosis of αβγ.
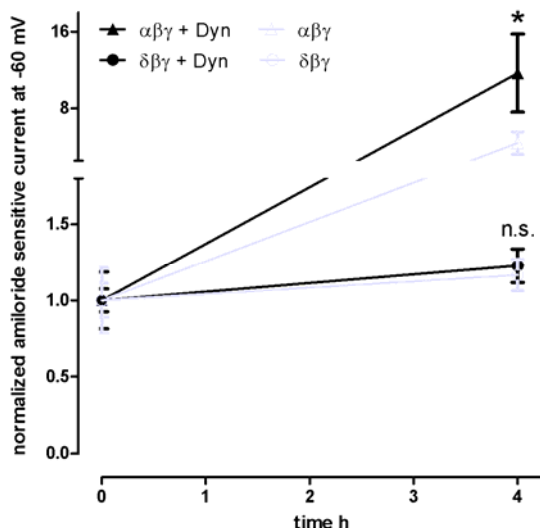
Fig. III.14 δβγ -ENaC undergoes dynamin-independent endocytosis.
Effect of the dynamin blocker Dynasore (Dyn) on αβγ or δβγ. Time course of amiloride sensitive current levels of αβγ or δβγ at times 0h and 4h of incubation in 80 µM Dynasore. Data points represent average values ± SE (n=6 for αβγ /δβγ, n≥10 for αβγ/δβγ +Dynasore). Values at 4 h with and without Dynasore were compared for each subunit combination. *, $P \leq 0.05$; n.s., not significant, Student's t-test.

III. 3. SGK1.1 regulates δ-ENaC independently of PY motifs and couples it to PLC signalling

Since δβγ-ENaC showed trafficking rates not only quantitatively different but also qualitatively different from αβγ-ENaC, the question rose whether δβγ-ENaC could be regulated by a kinase like αβγ-ENaC by the serum- and glucocorticoid-induced kinase 1 (SGK1, referred in **I. 3**). SGK1.1 is a neuronal splice isoform of SGK1 that down-regulates ASIC1, another member of the ENaC/degenerin family and is therefore hypothesized to be a counterpart for regulation of the neuronally expressed δ-ENaC.

III. 3.1 δ-ENaC and SGK1.1 are co-expressed in pyramidal neurons of the human and monkey brain cortex

SGK1.1 mRNA and protein are expressed in the CNS, although its localization in specific cell types has not been described (Arteaga *et al.*, 2008). Whether SGK1.1 colocalizes with δ-ENaC isoforms, was assessed by generating a DIG-labeled cRNA probe specific for SGK1.1 and ISH in sections obtained from human and monkey (*M. fascicularis*) cerebral cortex (**Fig. III.15**). Staining was observed in many neurons with pyramidal morphology through layers II to VI and the under-lying white matter of the frontal and temporal cortices (compare Nissl staining in **Fig. III.15 A** with positive antisense staining in **Fig. III.15 B** and negative sense staining in **Fig. III.15 C**). This expression pattern resembles that of δ1- and δ2-ENaC (**Fig. III.15 D–E**), which in the brain is exclusively neuronal as previously described (Giraldez *et al.*, 2007), suggesting that δ-ENaC and SGK1.1 could be co-expressed in the same neurons. To test this hypothesis, a double fluorescent ISH with a DIG-labelled probe specific for SGK1.1 and biotin-labelled oligonucleotides specific for δ1- or δ2-ENaC. The results showed a co-localization of δ-ENaC isoforms and SGK1.1

mRNAs in 91% of monkey (**Fig. III.15 F–H**) and human (**Fig. III.15 I–N**) pyramidal cells. Less than 10% of pyramidal cells, most of them small in size present in layer IV and in the deep region of layer III, express δ-ENaC isoforms, but not SGK1.1. No SGK1.1 positive cell without δ-ENaC was detected, which hints towards restricted neuronal expression as is the case for δ-ENaC. These results suggested that in pyramidal neurons of primate brain cortex, where both proteins were found to be co-expressed, SGK1.1 could influence the regulation of δ-ENaC.
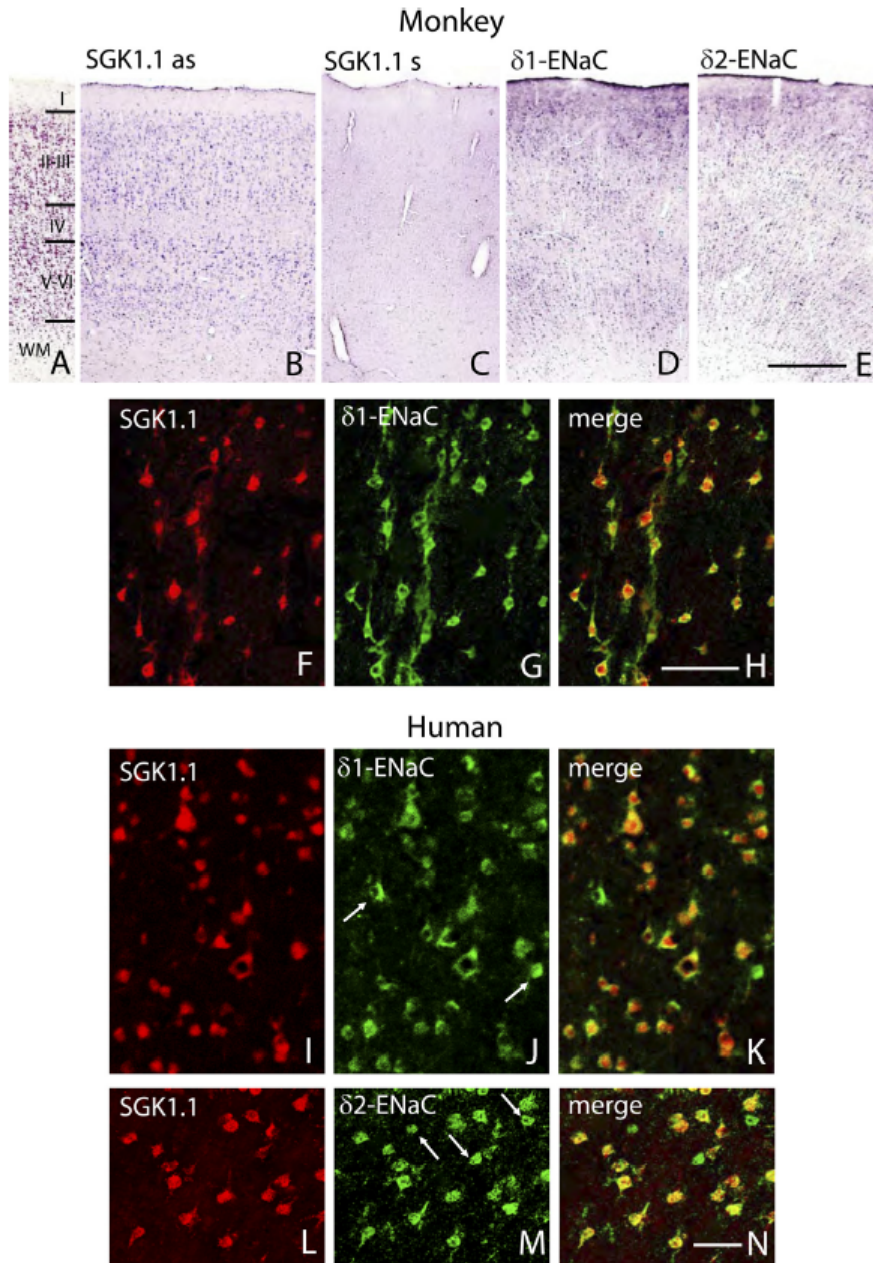
Fig. III.15 Co-expression of δ-ENaC and SGK1.1 in pyramidal neurons of primates.
A: Nissl staining of the layers in the monkey temporal cortex (MTC). WM, white matter. B-E: single colorimetric *in situ* hybridization (ISH) for SGK1.1 antisense (as, B) and sense (s, C) riboprobes, and for δ1 (D) and δ2 (E) in the MTC. F-H: double fluorescent ISH for SGK1.1 and δ1 in layer II of the MTC. I-K: double fluorescent ISH for SGK1.1 and δ1 in layers II-III of the human frontal cortex. L-N: double fluorescent ISH for SGK1.1 and δ2 in layer III of the human temporal cortex. Arrows in J and M indicate neurons expressing δ-ENaC but not SGK1.1. Bar in E (for A-E), 750 μm; in H (for F-H), 100 μm; in N (for I-N), 50 μm. (results obtained from work performed by Prof. Dr. T. González-Hernandez)

III. 3.2 SGK1.1 increases δβγ-ENaC activity in *Xenopus* oocytes

To investigate whether SGK1.1 modulates δ-ENaC, heterologous expression in *Xenopus* oocytes was used, where δ-ENaC subunits form functional channels with β and γ as shown in **III. 1** and previous work (Waldmann *et al.*, 1995; Giraldez *et al.*, 2007). *I/V* curves of δβγ-ENaC with or without SGK1.1 expressing oocytes were generated between -70 mV and +40 mV. ENaC activity was assessed as amiloride-sensitive membrane currents in TEVC experiments, which was calculated by subtracting the current in the presence of 100 µM amiloride from the current in the absence of amiloride at -60 mV. When SGK1.1 was co-expressed with δ1βγ-ENaC, a twofold increase of amiloride-sensitive current was observed at the whole voltage range tested (**Fig. III.16 A-C**). The SGK1.1 mediated increase of δ2βγ was approximately threefold (**Fig. III.16 C**).

To test whether this effect is dependent on the kinase activity of SGK1.1, a mutant with a lysine-to-alanine substitution in the ATP-binding cassette of the protein (K220A) was generated, which lost its kinase activity (Park *et al.*, 1999). SGK1.1-K220A did not enhance channel activity of δ1βγ and δ2βγ (**Fig. III.16 B & C**).

Due to Na$^+$ overloading of the oocytes the reversal potential was shifted to more negative values the more channels were expressed, as is the case when SGK1.1 was co-expressed (**Fig. III.16 B**).
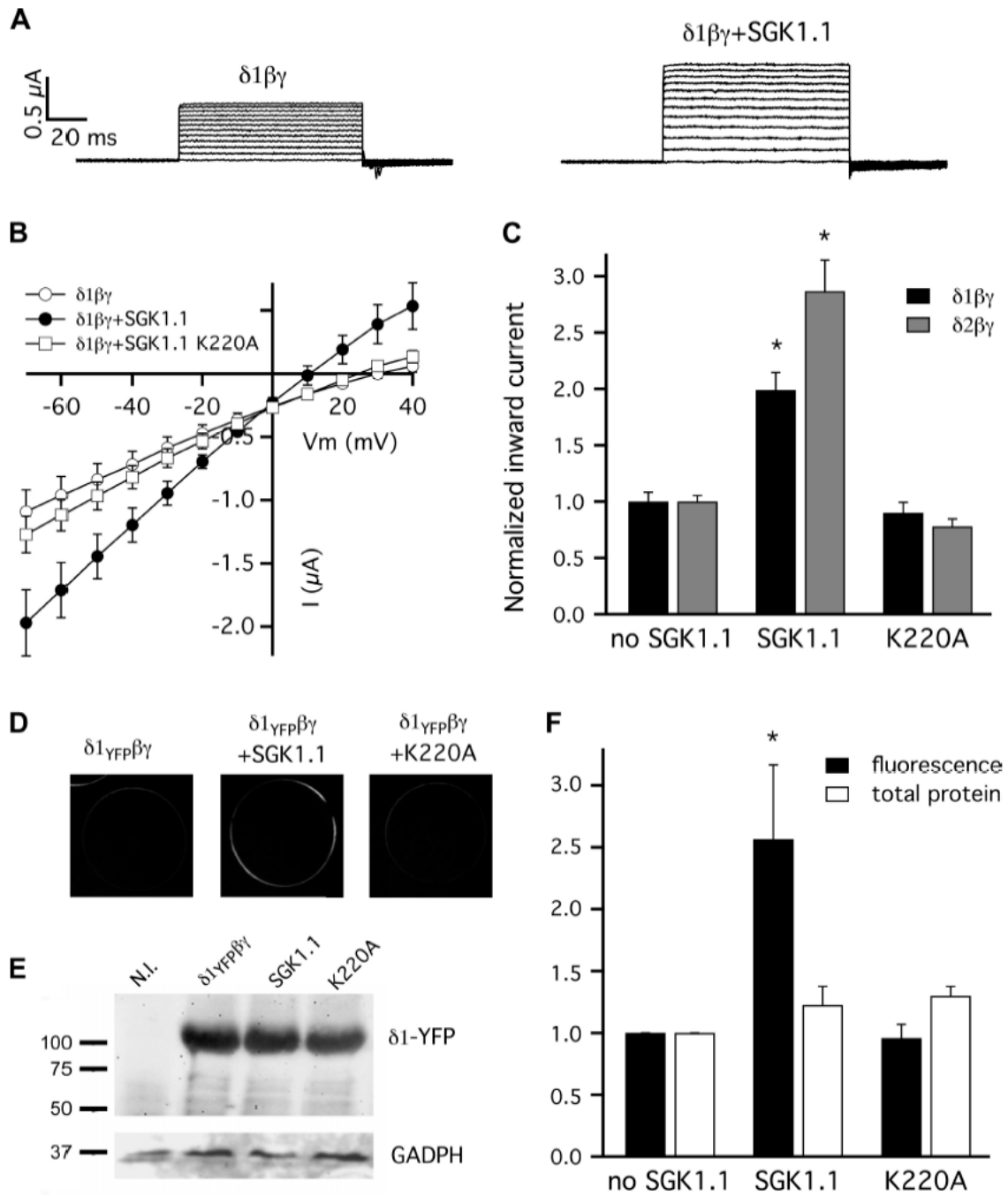
Fig. III.16 SGK1.1 increases δβγ-ENaC currents by increasing channel abundance in the membrane.
A: currents elicited by co-injection of δ1βγ with or without SGK1.1 cRNAs. Shown are representative amiloride-sensitive currents obtained by increasing voltage from -70 mV to 40 mV in sequential 10 mV steps. B: representative *I/V*-curves obtained from one batch of oocytes injected with δ1βγ alone, in combination with SGK1.1, or with SGK1.1-K220A. Data points represent current average ± SE (n=6). Vm, membrane potential. C: normalized amiloride-sensitive current magnitude averages at a holding potential of -60 mV obtained from 3-4 batches of oocytes co-injected with δ1βγ (black) or δ2βγ (grey) subunits, with or without SGK1.1, or SGK1.1-K220A. Error bars represent SE (n>60 for each condition). *P<0.05, Kruskal-Wallis non-parametric test followed by a Dunn's multicomparison test. D: representative confocal images showing cell surface expression of fluorescently labelled δ-ENaC in Xenopus oocytes w/o SGK1.1, w/ SGK1.1 or w/ SGK1.1-K220A. YFP, yellow fluorescent protein. E: Western blot analysis δYFP-expression in Xenopus oocytes expressing δ1YFP alone or in combination with SGK1.1 or SGK1.1-K220A. Molecular mass (in kDa) marker migration is indicated to the left. N.I. non-injected oocytes. F: black bars represent quantified average fluorescence intensity monitored in oocytes expressing δ1YFPβγ w/o SGK1.1 (n=15), with SGK1.1 (n=8), and w/ SGK1.1-K220A (n=10). White bars represent average total protein abundance quantified by western blot analysis of four independent batches of oocytes. Error bars represent SE. *P<0.05, Kruskal-Wallis non-parametric test followed by a Dunn's multicomparison test.

Whether the increased current resulted from an increase of the channel abundance in the plasma

membrane, was determined by the use of fluorescently labelled δ subunits by tagging YFP to the

C-terminus. Oocytes expressing δ1YFPβγ -ENaC and SGK1.1 showed a 2.5-fold increase in cell surface expression of the labelled subunit compared with those expressing either δ1βγ-ENaC alone or with the inactive SGK1.1-K220A (**Fig. III.16 D & F**).

Western blot analysis of the same oocytes revealed that the effects of SGK1.1 cannot be explained by changes in total protein abundance of δ1 (**Fig. III.16 E & F**), indicating that the increase in plasma membrane expression is due to a change in channel trafficking.

Taken together, these results indicate that SGK1.1 increases expression of δβγ-ENaC at the plasma membrane, thereby increasing Na$^+$ current, through a mechanism that requires the kinase activity of SGK1.1.

III. 3.3 SGK1.1 increases the activity of δ-ENaC alone in Xenopus oocytes

An increase of channel density within the membrane could be due to SGK1.1-mediated stabilization through interrupting the Nedd4-2 interaction with ENaC, leading to a decrease of ubiquitylation and thus diminished channel retrieval as is the case for αβγ-ENaC and SGK1. The δ subunit differs from α and lacks a PY motif in the C-terminus (**Fig. III.17 A**), but the effect of SGK1.1 could be mediated by β and γ. Therefore, the focus of interest turned towards the subunits β and γ: is the presence of β and γ necessary for the effect of SGK1.1 on δ-ENaC?
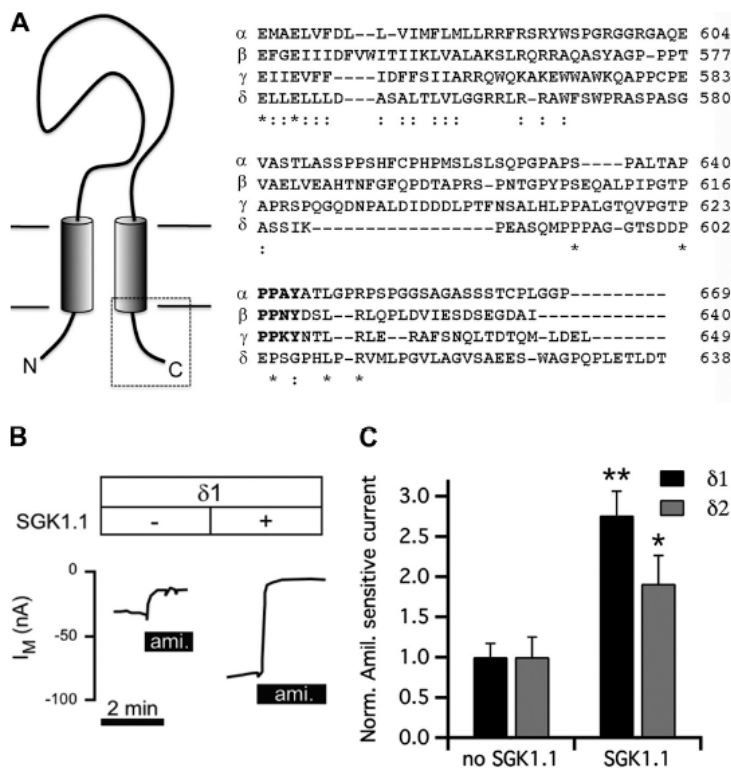
Fig. III.17 SGK1.1 up-regulates ENaC formed by the δ subunit independently of a PY-motif.

A: schematic representation of ENaC subunit topology and its C-terminal (box) sequence alignment of the human α-, β-, γ- and δ-subunits. Sequence analysis was performed with Kalign 2.0 from the European Bioinformatics Institute (Lassmann & Sonnhammer, 2006). Numbering of the δ-subunit sequence refers to the δ1-isoform. PY motifs (PPxY) in α, β and γ are marked in bold. *, identical residues; :, conserved substitutions. B: representative current traces of oocytes injected with δ1 alone or in combination with SGK1.1 and held at -60 mV in the absence or presence of 100 μM amiloride (Ami). C: normalized amiloride (Norm. Amil.) -sensitive current magnitude averages at a holding potential of -60 mV obtained from 3 batches of oocytes injected with δ1- (black) or δ2- (gray) subunits, with or without SGK1.1 (n>10 for each condition). Error bars represent SE. *P<0.05; **P<0.01, two-tailed Mann-Whitney test. (results from work performed by Dr. M. Althaus at Prof. W. Clauss laboratory, University of Giessen)

Expression of the δ-subunit alone produced amiloride sensitive currents in *Xenopus* oocytes (**Fig. III.17 B**), although at a much lower level than that elicited by the combination δβγ, which is consistent with previous observations (Waldmann *et al.*, 1995; Haerteis *et al.*, 2009). Independent of

the basal current level, co-expression of SGK1.1 increased δ1- or δ2-ENaC currents by approximately 2- to 2.5-fold (**Fig. III.17 B & C**), indicating that the presence of a PY motif is not required for the regulation of δ-ENaC by SGK1.1.

III. 3.4 The effect of SGK1.1 on δ-ENaC does not reflect a general trafficking change of membrane proteins

To ensure that the increased δ-ENaC membrane expression is not a consequence of a general effect of SGK1.1 on cellular membrane trafficking, the effect of SGK1.1 on other ion channel currents in the oocyte was assessed. Coexpression of SGK1.1 with a human BK channel tagged with YFP did not induce any variation in K^+ current or membrane expression levels of the channel (**Fig. III.18 A & B**). SGK1.1 did not produce significant changes in endogenous currents of the oocytes (**Fig. III.18 C**). These results are supported by previous studies, where SGK1.1 did not affect endogenous voltage-activated Na^+ currents in neurons (Arteaga *et al.*, 2008).
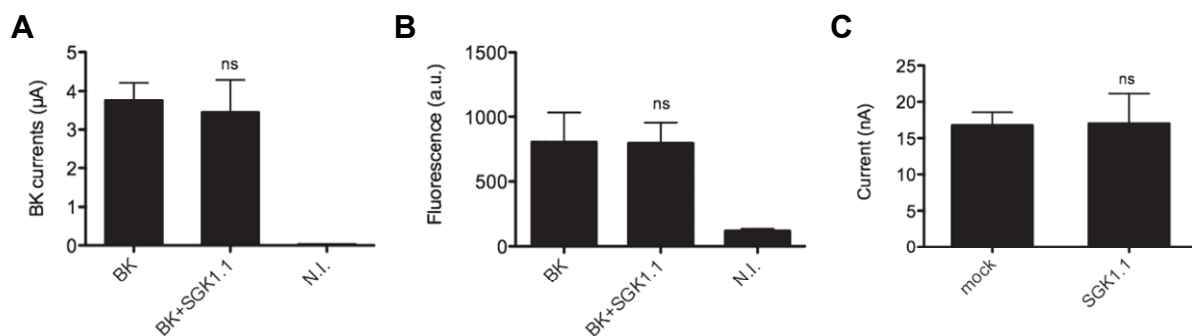
Fig. III.18 SGK1.1 does not increase the expression of other ion channels at the plasma membrane.
A: large-conductance Ca^{2+}-gated K^+ (BK) current magnitude averages at test voltage pulses (+100 mV from a holding of -70 mV) obtained from oocytes expressing BK-YFP channels alone (n=10) or in combination with SGK1.1 (n=10). a.u., arbitrary units. B: average fluorescence intensity monitored by confocal microscopy in the same oocytes used for recording BK-YFP channel activity in A. C: endogenous current magnitude averages at a holding potential of 0 mV obtained from oocytes injected with H2O, with or without SGK1.1 cRNA (n≥12 for each condition). Error bars represent SE. ns, not significant , two-tailed Mann-Whitney test. (results obtained from work performed by Dr. P. Miranda)

III. 3.5 δβγ-ENaC regulation requires basic residues in the N-terminus of SGK1.1

In other cell types, SGK1.1 was found to reside at the plasma membrane by binding to phosphatitylinositol(4,5)-bisphosphate (PIP2) (Arteaga *et al.*, 2008). When the fluorescently labelled SGK1.1-CFP was expressed in *Xenopus* oocytes, a clear plasma membrane localization was observed (**Fig. III.19 A**), demonstrating that this process is conserved in the oocyte expression system. PIP2 binding by SGK1.1 depends on a N-terminal polybasic motif including the residues K21, K22, and R23 (Arteaga *et al.*, 2008). In *Xenopus* oocytes this also seems to be the case, because mutating those residues for neutral ones (K21N/K22N/R23G, SGK1.1-CFP-KKR) reduced membrane fluorescence to levels slightly above those of non-injected oocytes (**Fig. III.19 A & B**). This difference in cell surface expression is not due to a generally diminished protein ex-

pression, as shown by Western blot analysis (**Fig. III.19 B**). Therefore, SGK1.1 follows the same subcellular localization pattern in *Xenopus* oocytes and mammalian cells.

Co-expression of SGK1.1-CFP-KKR with ENaC δ1βγ channels did not significantly increase the amiloride-sensitive current as opposed to the effect of the wild type kinase (**Fig. III.19 D & E**). Thus, these three residues are not only needed for the kinase to be bound to the membrane, but also to regulate δ1βγ function.
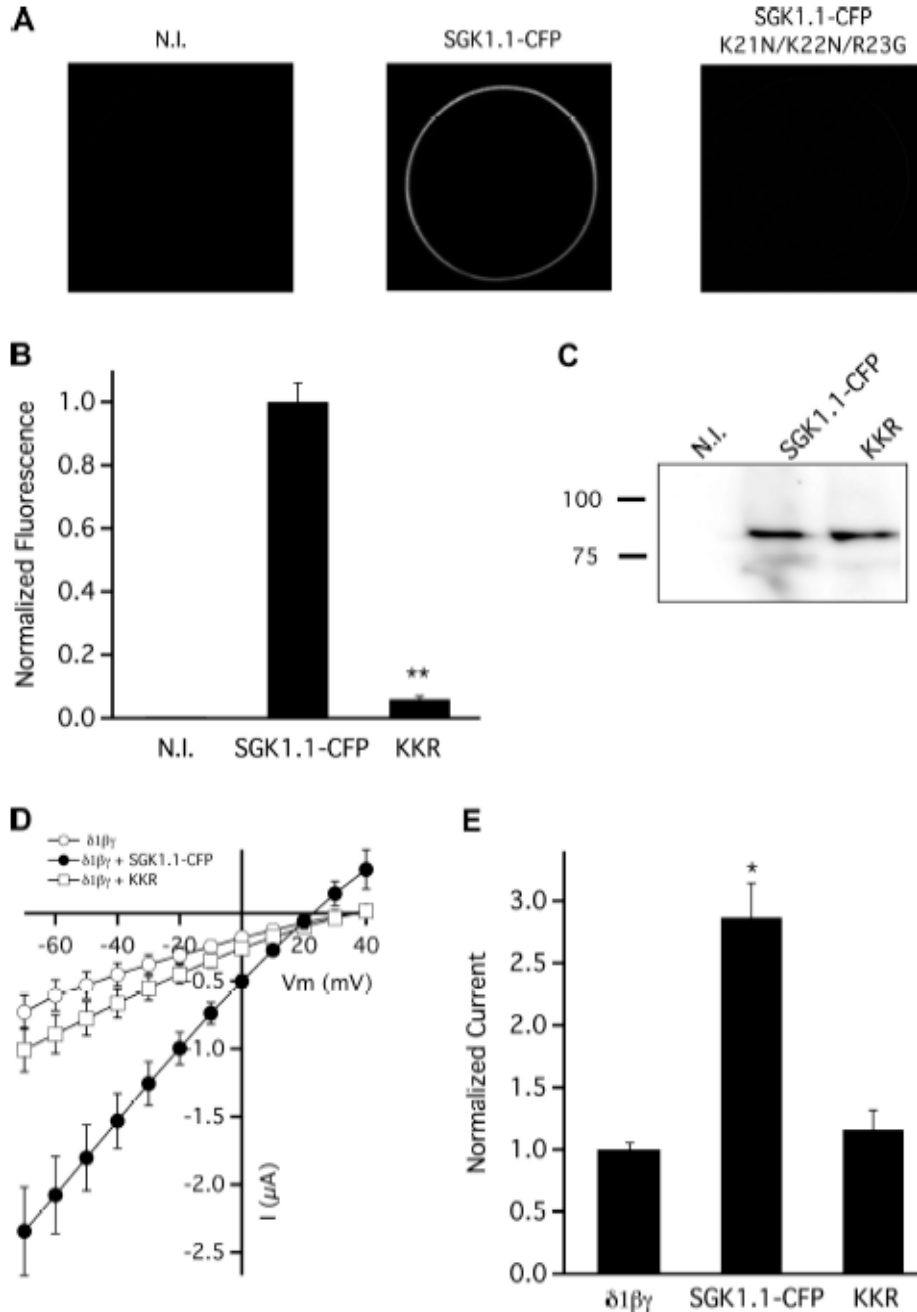
Fig. III.19 Basic residues in the SGK1.1 N-terminus are required for membrane localization and δβγ-ENaC regulation.
A: representative confocal images showing cell surface expression of SGK1.1-CFP and SGK1.1-CFP-KKR mutant in *Xenopus* oocytes. B: SGK1.1 protein expression analysis by Western Blot from non-injected oocytes (N.I.), or oocytes injected with SGK1.1-CFP or SGK11.1-CFP-KKR. Migration of 100 kDa and 75 kDa molecular weight standards is shown to the left. C: quantitative representation of average fluorescence intensity monitored in non-injected oocytes (N.I.) and oocytes expressing SGK1.1-CFP and SGK1.1-CFP-KKR. Error bars represent the SE, **P<0.001 (n=20), two-tailed Mann-Whitney test. D: representative *I/V* curves obtained from one batch of oocytes injected with δ1βγ alone, with SGK1.1-CFP or with SGK1.1-CFP-KKR. Data points represent current average ± SE (n=6). E: normalized average amiloride sensitive current magnitudes at a holding potential of -60 mV obtained from 3-4 batches of oocytes injected with δ1βγ, δ1βγ + SGK1.1-CFP and δ1βγ + KKR (n≥25 for each condition). Error bars represent the SE, *P<0.05, two-tailed Mann-Whitney test.

III. 3.6 Activation of PLC removes SGK1.1 from the membrane and abrogates its effects on δβγ-ENaC

Since phospholipase C (PLC) activation transiently reduces PIP2 levels at the plasma membrane (Stryer *et al.*, 2003), the focus of interest turned towards the question, whether the PLC pathway could modulate the effects of SGK1.1 on δ-ENaC currents. The effect of pharmacological activation of PLC with 3M3FBS (Horowitz *et al.*, 2005) on SGK1.1-CFP plasma membrane localization was monitored in living oocytes using confocal microscopy. Within 20 s after the activator was added, a rapid decrease in fluorescence was observed, which peaked at 25 % of the baseline, indicating that SGK1.1 was being retrieved from the membrane (**Fig. III.20 A & B**). The same effect was observed when the oocytes were pre-incubated with 3M3FBS for 1-2 min, although the average decrease in this case was lower (60 % of the baseline, **Fig. III.20 B & C**), probably because PLC activation had been partially reversed as described in and previous work (Horowitz *et al.*, 2005). The effect of 3M3FBS was not observed in oocytes expressing the SGK1.1-CFP-KKR, which is not bound to the membrane. In this case, addition of the PLC activator did not reduce the membrane fluorescence that was not enhanced by SGK1.1-KKR, indicating that the result with wt SGK1.1 is due to PLC-mediated PIP2 hydrolysis (**Fig. III.20 C**).

Based on the fact that SGK1.1 is required to be tethered on the membrane to exert its effects upon δβγ -ENaC, it was hypothesized that PLC-mediated removal of SGK1.1 from the membrane may also result in reduced δβγ current levels. The approach to answer this question was to measure amiloride sensitive inward currents of oocytes injected with δ1βγ-ENaC or δ1βγ + SGK1.1, before and after 3M3FBS (10 µM) incubation. As expected, without SGK1.1, the current levels of δβγ-ENaC remained equal by incubation of 3M3FBS (**Fig. III.20 D**, left), but with SGK1.1 the amiloride sensitive currents were significantly reduced (**Fig. III.20 D**, right). This suggests that the effect of SGK1.1 on δβγ-ENaC-mediated current decreased upon PLC activation with 3M3FBS.
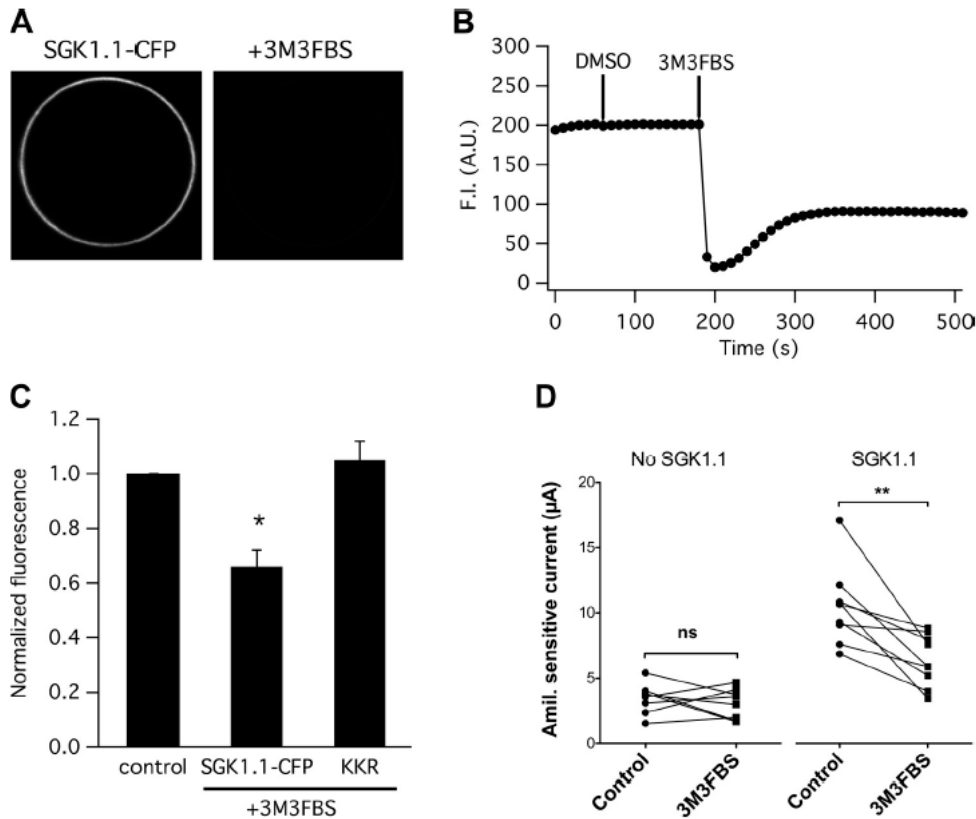
Fig. III.20 Activation of PLC with 3M3FBS removes SGK1.1-CFP from the membrane and partially reverses the effect of SGK1.1 on δβγ -ENaC.
A: representative confocal microscope images of oocytes injected with SGK1.1-CFP in absence and presence of 3M3FBS. B: Representative time-course recording of membrane fluorescence intensity of SGK1.1-CFP injected oocytes. Addition of DMSO and 3M3FBS is shown with arrows on top of the trace. Images were taken every 10 s. C: Quantitative representation of normalized fluorescence intensity obtained from oocytes expressing SGK1.1-CFP or SGK1.1-CFP-KKR before (control) and after 2-3 min incubation with 3M3FBS (n=10 for each condition). Each treatment was normalized to its control. Error bars represent the SE, *P<0.05, Krusal-Wallis non-parametric test followed by a Dunn's multicomparison test. D: quantitative representation of amiloride sensitive currents compared before and after incubation of oocytes with 3M3FBS (10 µM, 30 min), expressing δ1βγ alone (n=6) or δ1βγ with SGK1.1 (n=8). Data is represented as linked-pairs of control and LPA-treated oocytes. **P<0.01, Wilcoxon signed-rank test. (results from work performed by Dr. P. Miranda)

A common physiological situation where activation of PLC occurs is upon the activation of G-protein coupled receptors (GPCR) at the membrane. *Xenopus* oocytes endogenously express lisophosphatidic acid (LPA) receptors, which are GPCRs and thus are coupled to various signalling cascades that involve PLC activation (Van Ham & Oron, 2005). To study if physiological activation of PLC through the activation of LPA receptors could modulate SGK1.1 subcellular localization, the membrane fluorescence of oocytes expressing SGK1.1-CFP was monitored before and after addition of LPA to the medium. As shown in **Fig. III.21 A**, a significant and sustained reduction of SGK1.1 membrane levels to an average of 60% of its initial value was observed.
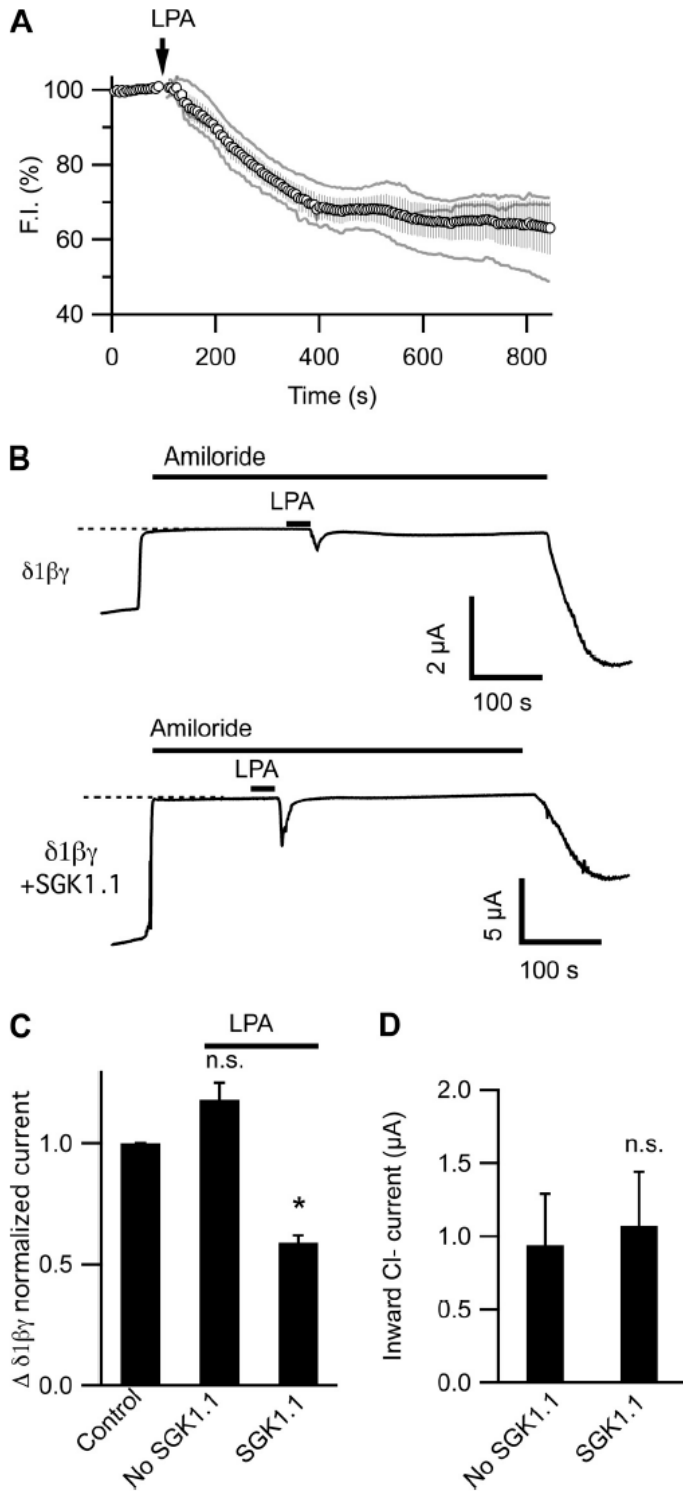
Fig. III.21 Activation of PLC through LPA GPCRs removes SGK1.1 from the membrane and diminishes its effect on δ-ENaC currents.
A: average fluorescence intensity time-course of oocytes expressing SGK1.1-CFP. Addition of LPA 5 mM is indicated with an arrow over the graph. Grey lines correspond to individual oocytes fluorescence time courses. Error bars represent the SEM (n=8). B: representative current recordings of individual oocytes expressing δ1βγ alone (top trace) and δ1βγ with SGK1.1 (bottom trace). Addition of amiloride 100 µM and LPA 5 mM are shown with bars. C: quantitative representation of amiloride sensitive currents compared before and after adding LPA (5mM) to oocytes expressing δ1βγ alone (n=7) or δ1βγ with SGK1.1 (n=6). *P<0.05, Kruskal-Wallis non-parametric test followed by a Dunn's multicomparison test. D: average amount of Ca^{2+}-induced Cl^- currents activated after LPA addition, with or without SGK1.1. n.s., not significant, Wilcoxon signed-rank test.

To test whether the removal of SGK1.1 from the membrane by physiological activation of LPA receptors, would consequently lead to reduced δβγ-ENaC current levels, amiloride sensitive currents before and after LPA addition were measured in oocytes held at -70 mV. Initial ENaC activity was determined by adding 100 µM amiloride and calculated by subtraction of remaining current under amiloride from the current before adding amiloride. LPA was added in the presence of amiloride to avoid Na^+ overloading of the oocytes. Amiloride was washed at the end of the experiment to calculate the remaining ENaC activity under LPA. Representative traces from oocytes injected with δ1βγ alone or in combination with SGK1.1 are shown in **Fig. III.21 B**. Soon after addition of LPA a transient inward current corresponding to Ca^{2+}-dependent activation of Cl^- channels (Weber, 1999) was observed. The results show that LPA did not produce a significant change in the amiloride-sensitive inward current in oocytes expressing only δ1βγ-ENaC (**Fig. III.21 B & C**), although a tendency toward increased current was observed. When SGK1.1 was co-expressed with δ1βγ-ENaC, LPA produced a significant reduction of the amiloride sensitive current to ~40% of the initial value (**Fig. III.21 B & C**).

To verify the specificity of the LPA effect on δβγ-ENaC, the amount of Ca^{2+}-induced Cl^- current from the recordings were quantified and determined to be not significantly different in δβγ-ENaC expressing oocytes with or without SGK1.1 (**Fig. III.21 D**).

These data demonstrate that activation of PLC signalling upon an endogenous GPCR can be linked to the modulation of δβγ-ENaC through SGK1.1, proposing a mechanism for δ-ENaC regulation in neurons.

IV.   Discussion

The work presented in this study, was performed to characterize possible mechanisms underlying δ-ENaC regulation. In this chapter the results are discussed into detail following their sequential arrangement in **III**. A brief summary with future outlooks is provided in **IV.4** and final conclusions are drawn at the end (**V**).

The results are discussed in terms of the following questions:

1) What is the molecular basis for the differential activity of δ-ENaC isoforms? (**IV. 1**)
2) How does δ-ENaC trafficking differ from that of α-ENaC? (**IV. 2**)
3) Does co-expression of SGK1.1 modulate δ-ENaC and what are the underlying mechanisms? (**IV. 3**)
4) What is the physiological impact of δ-ENaC regulation? (**IV. 1.4 & 3.2**)

IV. 1. Differential N-termini of the ENaC subunit isoforms δ1 and δ2 result in varied channel activity

The experiments presented in **III.1** showed that δ1 consistently produced higher macroscopic currents than δ2 when expressed in *Xenopus* oocytes and HEK293 cells. This difference was due to δ1 greater steady state membrane abundance, without changes in single channel conductance or open probability between isoforms. The different isoform abundance in the membrane cannot be explained by altered endocytosis rates and was independent of the presence of PY motifs or additional lysines in the δ2 N-terminus, suggesting that the variation between isoforms is based on altered insertion rates of newly synthesized or recycled channels. Further, two sequences in the δ2 N-terminus independently reduced the channel abundance, but were not additive.
Since the N-termini of each the α, β and γ subunits are ubiquitinated and involved in trafficking of the channel (Ruffieux-Daidie & Staub, 2011), the question arose whether we could get insight into δ-ENaC trafficking, once it is revealed what precisely in the different isoform N-termini alters channel abundance and thus trafficking.

IV. 1.1 Reduced δ2-ENaC abundance in the membrane

It is unclear why a previous report did not find a difference in the macroscopic currents elicited by the δ ENaC isoforms (Yamamura *et al.*, 2006). Methodological differences between this study and the reported one, mainly in the medium and protocol used for electrophysiological recordings

and also in the number of oocytes examined (4-13 per condition vs. ≥ 150 in this study), could account for the divergent results. Remarkably, in this study the difference between δ1 and δ2 was observed very consistently, not only in *Xenopus* oocytes, but also in HEK293 cells. Further, it was apparent in both electrophysiological recordings and by confocal microscopic detection of the channel abundance in the membrane.

The macroscopic current levels of either δ1βγ- or δ2βγ-ENaC assessed by TEVC revealed that δ1βγ activity was ~2.5-fold higher than that of δ2βγ, and in HEK293 cells the whole-cell currents of δ1βγ was determined to be ~2.3-fold higher than that of δ2βγ by perforated patch. This was not due to single channel properties as demonstrated by patch clamp experiments, where the δ-ENaC isoforms displayed similar open probabilities and single channel conductance. A drop in extracellular pH, known to change the Po of δ-ENaC by acting on its degenerin sites (Ji & Benos, 2004), which is common to both isoforms (Giraldez *et al.*, 2007), enhanced the δ1βγ and δ2βγ currents equally. This confirms that the Po determining sites of both isoforms respond in the same manner and thus δ1 and δ2 must display the same Po.

Since the macroscopic current of a channel depends on three factors, its open probability, conductance and the number of channels present in the membrane (Hille, 2001), experiments were performed to examine channel abundance in the plasma membrane. In fact, higher membrane abundance for δ1 than for δ2 was observed, which explained the higher current levels of δ1 when compared to δ2.

Concerning the protein sequence the only difference between δ1 and δ2 is the N-terminal variation, which must therefore be responsible for the differences between the activity levels of the isoforms. The α-ENaC N-terminus has been described to be implicated in channel activity: 1) A membrane-near region within the N-terminus of α-ENaC was reported to play a role in the control of channel gating (Kellenberger & Schild, 2002). In the case of the δ subunit it is possible that the fragment of the N-terminus close to the membrane and common to both isoforms controls channel gating independently of the rest of the region. Regardless of any common gating regulation mechanism, the equal Po and single channel conductance demonstrate that the differences in macroscopic currents between δ isoforms result from differential channel abundance in the membrane. 2) The α subunit contains an N-terminal endocytic motif, which controls channel membrane abundance (Chalfant *et al.*, 1999) and could possibly explain differential channel abundance in the membrane between the isoforms. However, this motif is absent in the δ subunits. The δ2 isoform comprises a 66 amino acids longer N-terminus than δ1 (depicted in **Fig. I.4 & Fig. III.6**). Differential membrane abundance can be explained by differential channel trafficking, and lysines in the N-termini of the subunits in αβγ-ENaC are described to be implicated in PY motif-dependent ubiquitination and thus endocytosis (Kamynina & Staub, 2002). Since δ2 contains within its N-terminus three more lysines than δ1, it was examined whether endocytosis of the isoforms was different. However, the difference in the activity levels of δ1 and δ2-ENaC was not lysine-dependent as shown by experiments where the lysines in the δ2 N-terminus as possible additional ubiquitylation targets were mutated to arginines and exhibited δ2 wild type properties.

IV. 1.2 Differential channel abundance in the membrane of the δ-ENaC isoforms does not result from varied endocytosis rates

A possible explanation for the reduced δ2 activity could be that δ isoform N-termini affect channel trafficking regulated by the Nedd4-2 system. The canonical αβγ-ENaC in tight epithelia is mainly controlled by the E3 ubiquitine ligase Nedd4-2 (Verrey *et al.*, 2008). Ubiquitination of αβγ-ENaC (as explained into detail in **I. 3**) requires the PY motifs in ENaC C-termini as docking sites for Nedd4-2 (Rauh *et al.*, 2006). Nedd4-2 then ubiquitylates several lysine sites, marking the channel for endocytosis (Hallows *et al.*, 2010).

The δ subunit lacks a PY motif in the C-terminus and differential isoform activity was still seen in experiments with oocytes expressing only δ1 or δ2 without the β and γ subunits. Consequently, it is unlikely that endocytosis of δ ENaC is mediated by Nedd4-2, which requires association of its WW binding domain to the PY motif to initiate ubiquitination and thus endocytosis (Staub *et al.*, 1996).

A general mechanism of endocytosis of δ-ENaC mediated by other E3 ubiquitine ligases, as shown in previous studies with the copper metabolism Murr1 domain1 (COMMD1) (Chang *et al.*, 2011), cannot be ruled out. Nevertheless, the differential membrane abundance of the isoforms cannot be explained by a possibly increased ubiquitination of δ2, since mutations of the additional target lysine sites at the δ2 N-terminal do not affect current levels.

More generally, a differential endocytosis rate between isoforms was not observed when insertion of the channel was blocked with BFA. This suggests that altered channel trafficking of δ2 compared to δ1 may reflect a reduced insertion rate into the membrane either of newly synthesized or recycled channels (Butterworth *et al.*, 2009).

The results demonstrate that δ2 accumulates intracellularly but the precise compartment where it is localized remains unknown. In the case of αβγ-ENaC a subapical pool was thought to be important for the rapid replenishment in the plasma membrane upon a determined stimulus (Lu *et al.*, 2007b). In the case of δ-ENaC no such pool has yet been descxribed, but it could be possible that in the oocytes δ2 resides in a submembranous compartment. δ2 channels could be localized in recycling endosomes as described for the canonical αβγ-ENaC (Butterworth *et al.*, 2007; Taruno & Marunaka, 2010; Zhou *et al.*, 2010). This option would not preclude the possibility that also δ1 is also localized within recycling endosomes as previously reported (Chang *et al.*, 2011), but this would be to a lesser extent. Otherwise, the δ2 progress through the biosynthetic pathway could be slower than that of δ1.

IV. 1.3 N-terminal sequence motifs of δ2 are responsible for its reduced channel abundance

Through serial deletion of the δ2 N-terminus two regions were identified that independently reduced δ current levels and abundance in the membrane. Once both of these regions are deleted, the mutants δ2Δ25-85 and δ2 2xΔ recover δ1 levels of both macroscopic currents and channel abundance in the membrane. Since deleting either of these two regions produce current levels equal to δ2 wild type, it is concluded that they are not additive and that they could converge into the same regulation pathway of δ2 trafficking (**Fig. IV.1**). Another possible explanation for this result would be that these regions, amino acids 25-45 and amino acids 65-85, mask an area – common to both δ1 and δ2 – required to be accessible as an unknown structure or for an unidentified factor that enhances δ currents once it is uncovered (**Fig. IV.1**).
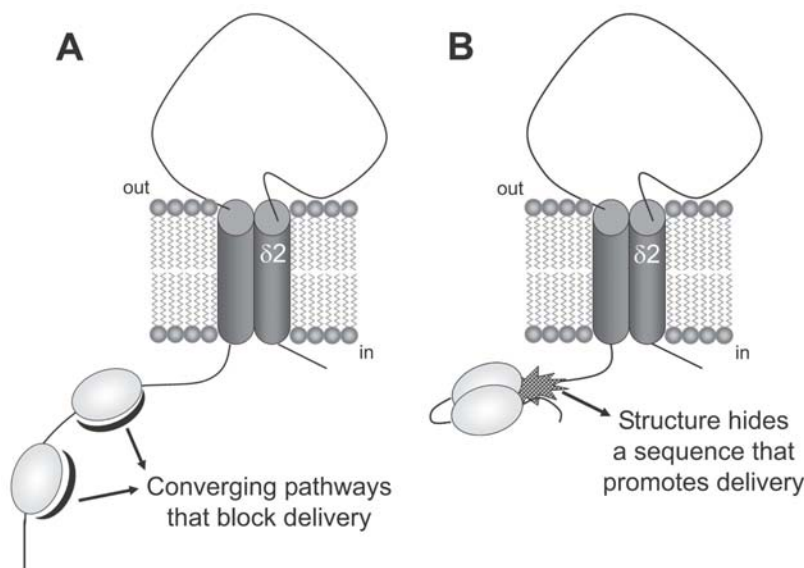
Fig. IV.1 Proposed models for the effect of the two regions in the N-terminus of δ2 on channel abundance in the membrane.
A: Each region forms a structure that interacts with the same or converging pathways that block delivery of channels to the membrane. B: Both regions form structures that hide a motif present in both δ isoforms that promotes delivery of channels to the membrane.

Having a closer look into the deleted sequences of the δ2 N-terminus one could think of possible sequence motifs that are implicated in distinct channel trafficking, such as the dileucine (LL) motif located in the first deletion sequence (LL26/27). Cytoplasmic LL motifs are known to serve as short signals for sorting membrane proteins along the endocytic and secretory pathways as previously reviewed (Pandey, 2009). An example for LL-dependent sorting is the neonatal Fc receptor, which transports immunoglobulin G across intestinal cells in suckling rats (Wu & Simister, 2001). The LL motif present in the N-terminus of the glucose transporter 8 (Glut8) has been suggested to regulate intracellular sequestration in various cell systems, because mutation of the dileucine motif showed increased expression of Glut8 on the cell surface. Coexpression of the dominant-negative mutant of dynamin enhanced the accumulation of Glut8 on the cell surface, and Glut8 constantly recycled between distinct intracellular vesicles and the cell surface via the dynamin-dependent pathway (Lisinski *et al.*, 2001). These results suggested that N-terminal LL motifs in Glut8 constitute a docking site that is responsible for endocytic processes.

In general, the LL residues are preceded by a polar residue and a negatively charged amino acid residue, which may be aspartic acid, glutamic acid, or phosphoserine. In the case of δ2, a serine (S24) is indeed preceding the LL. The LL sequence motif is usually context-dependent and it is characteristically surrounded by polar and/or charged amino acid residues. Also an arginine is found near to the δ2 N-terminal LL (R 22). However, a particular sequence before LL residues is not absolutely required. Although LL motifs with acidic amino acid residues are constitutively active, those LL motifs that contain serine residue are activated by phosphorylation (Geisler *et al.*, 1998). Since the amino acid sequence preceding the LL in the δ2 N-terminus (ARGSILL) contains both a charged/basic (R22) and a phosphorylable amino acid (S24), it is conceivable that such a motif could contribute to δ2 channel sorting. Though, this is still not enough to explain, why a second not-adjacent deletion is required to abolish the reduced δ2 channel activity and regain δ1 activity levels.

Since the LL motif is reported to be involved in dynamin-dependent endocytosis it is unlikely that in the case of the δ1 vs δ2 dissimilarity this was the cause for such a difference, because in **III. 2.3** is shown that δ-ENaC trafficking was not dependent on dynamin. This result will be discussed into more detail in chapter **IV. 2**.

Beside the LL motif, a PPXhydrophobic (PPXW) similar to the PY motif is found within the first N-terminal deletion sequence that may contribute to distinct δ2 trafficking when compared to δ1. In general, proline-rich motifs were found to be required for many protein-protein interactions (Li, 2005). Since δ-ENaC lacks a common PY motif, which was proved to serve as a sorting signal for the canonical αβγ-ENaC (Staruschenko *et al.*, 2005), one could think of a possible role of this alternative proline-rich sequence for being involved in channel trafficking.

Further, additional cytoplasmic cysteines in the δ2 N-terminus could be modified by lipids and so lead to a differential membrane trafficking of δ2. For post-translational processing a variety of covalent modifications on cysteines are described, amongst others these include acylation (mainly s-palmitoylation), s-glutathionylation, and s-nitrosylation, which are necessary for membrane targeting of proteins (Resh, 2004; Shipston, 2011; Dalle-Donne *et al.*, 2009; Daaka, 2011). The transferrin receptor is an example for that acylation at its defined cysteines is underlying enhanced cell surface expression (Alvarez *et al.*, 1990). S-palmitoylation is the thioester linkage of the long-chain fatty acid palmitate to cytoplasmic cysteine residues, which in turn can modulate interactions with other proteins and membranes and therefore regulate protein trafficking and enzyme activity (Salaun *et al.*, 2010).

Mutating these well-known trafficking motifs may shed light into the differential trafficking mechanism between δ1 and δ2. However, not all signal motifs are short peptide sequences. In certain circumstances, the trafficking and sorting determinants seem to be folded structures and the critical amino acid residues are not necessarily linear (Pandey, 2009). The precise mechanism underlying the action of possible new motifs for trafficking lowering the δ2 abundance in the membrane remains to be elucidated, since two not-adjacent sequences are required to be deleted to regain δ1 activity levels.

To explain the results obtained by deleting Δ25-45 and Δ66-85, these two sequences most likely either affect two distinct, but converging trafficking pathways (**Fig. IV.1 A**) – as is shown for LL and tyrosine based signals, which both are involved in clathrin-mediated endocytosis (Pandey, 2009), or form a particular structure necessary for channel trafficking (**Fig. IV.1 B**).

IV. 1.4 Physiological impact of the δ-ENaC isoform differences

The physiological role of δ-ENaC in neurons is still uncertain. Voltage-independent, constitutively active Na^+ channels such as those formed by δ-ENaC could contribute to the resting Na^+ permeability of neurons. Recently, a member of the voltage-gated Na^+ channel family, NALCN, has been shown to form voltage-independent cation channels and encode the background Na^+ conductance in mouse hippocampal neurons (Lu *et al.*, 2007a).

Concerning the possible physiological functions of δ-ENaC isoforms producing different current levels in the central nervous system, it is necessary to take into consideration the relative amounts of neurons expressing one or another isoform and the abundance of each mRNA. Our data show that at least in the human brain cortex there is a higher amount of δ1-containig cells than δ2 or both. When mRNA abundance, analysed by qPCR, is corrected by the number of cells expressing each isoform, one can conclude that the mRNA levels of each isoform are of a similar magnitude. Assuming that the difference in whole-cell current displayed by δ isoforms in *Xenopus* oocytes and transiently transfected HEK293 cells also takes place in neurons, cells expressing δ1 would conduct approximately twice the amount of current mediated by δ-ENaC than cells expressing δ2, and therefore display enhanced basal sodium current. This could in turn modify the membrane resting potential and thus make the cell more excitable than with δ2.

In conclusion, we found that δ1 showed higher macroscopic currents than δ2, which is due to δ1 greater membrane abundance than δ2, but not to single channel conductance or Po. The different membrane abundance of the channels does not result from altered internalization rates, as corroborated by the finding that it is also independent of PY motifs and of the presence of additional lysines in the N-terminus of δ2, hence of altered ubiquitination. At this stage it is not yet defined whether an altered insertion rate of new channels into the membrane or varied channel recycling could explain the differential membrane abundance of δ isoforms. Furthermore, two independent regions in the N-terminus of δ2 underlie its lower membrane abundance in a non-additive manner.

IV. 2   δ subunit trafficking vs α subunit trafficking

In chapter **III. 2** results concerning the trafficking differences between the canonical αβγ-ENaC and the channel formed by the subunits δ, β and γ are presented. The most striking finding was

that δβγ-ENaC was not affected by Dynasore, a pharmacological inhibitor of dynamin. Further, trafficking of δβγ-ENaC is slower than that of αβγ-ENaC, either in the insertion pathway or the internalization pathway as shown in the experiments with BFA or FRAP, respectively.

These results suggest that the mechanism for δβγ-ENaC endocytosis is different from the generally described clathrin-mediated endocytosis of αβγ-channels, which requires dynamin.

IV. 2.1 Endocytosis of δ-ENaC is different from that of α-ENaC

Dynasore, an inhibitor of dynamin and thus clathrin-mediated endocytosis blocker, was used in experiments to reveal the insertion rate of the different ENaC channel. Dynasore had the predicted effect on αβγ ENaC, which has been described to be internalized by means of clathrin (Shimkets *et al.*, 1997; Wang *et al.*, 2006). Unexpectedly, with Dynasore no effect was apparent on either δ1βγ or δ2βγ. Therefore, the results indicate an alternative endocytosis mechanism for δ1βγ and δ2βγ, which is independent of dynamin and thus excludes clathrin-mediated endocytosis and other dynamin-dependent sorting mechanisms, such as the RhoA-regulated mechanisms and caveolar uptake (Mayor & Pagano, 2007; Sandvig *et al.*, 2008). Dynamin-independent endocytosis mechanisms have been described and involve small GTPases such as Cdc42 or Arf6 (Sandvig *et al.*, 2011; Grant & Donaldson, 2009). Hence, it is conceivable that one of the small GTPases could account for δ-ENaC endocytosis instead of the GTP-binding protein dynamin.

The family of rab small GTPases is linked to the canonical ENaC trafficking (Saxena & Kaur, 2006). Overexpression of Rab3 and Rab27a down-regulated αβγ-ENaC activity (Saxena *et al.*, 2005) while Rab4 was found to modulate αβγ-ENaC depending on its GTP-GDP status by effects on the cytosolic ENaC pool, retaining the channels in the cytoplasm while recycling (Saxena *et al.*, 2006). This fact would further corroborate the idea of an enhanced intracellular δ2 channel pool explaining the reduced δ2 abundance in the membrane when compared to δ1, once the δ2 N-terminus could be linked to altered channel trafficking through rabs, or more general, any small GTPases.

Since Rab11a increased αβγ-ENaC (Karpushev *et al.*, 2008), the situation for δ-ENaC could be *vice versa*: the sequences of the δ2 N-terminus deleted in the δ1-like δ2 mutants could be impairing an ENaC-activating rab to exert its enhancing effect on δ-ENaC.

IV. 2.2 The turnover of δ-ENaC is slower than that of α-ENaC

Apart from the qualitatively different endocytosis modes between αβγ and δβγ, the results with BFA show a quantitative difference between αβγ endocytosis and δβγ endocytosis: αβγ endocytosis is ~2-fold faster than that of δβγ. This corroborates the idea of an endocytosis mechanism for δ-ENaC different from the generally described clathrin-mediated endocytosis of αβγ-ENaC.

Besides the endocytosis, a closer look was taken into channel insertion with FRAP experiments. This led to the finding that insertion of new channels was faster for αβγ-ENaC than for δβγ-ENaC.

Physiological implications of a slower turnover of δ-ENaC could be that in neurons a more stable environment for the establishment of the resting potential could be facilitated by δ-ENaC. In contrast, fast turnover rates of apical channels in epithelial cells allow for a rapid regulation of ion transport, which is necessary to adapt the organism to fast changing environmental conditions.

Taken together, these results support further that δβγ-ENaC trafficking is generally slower than that of αβγ, and that it is also qualitatively different from the one described for the canonical αβγ-ENaC.

IV. 3 SGK1.1 up-regulates δ-ENaC

In chapter **III. 3** evidence supporting a role for SGK1.1 in the control of neuronal Na$^+$ channels formed by the δ-ENaC was presented. Both proteins co-localize in pyramidal neurons of the monkey and human brain cortex. When co-expressed in *Xenopus* oocytes, SGK1.1 enhances the activity of both δ-ENaC isoforms, regardless of the presence of β and γ. This effect of SGK1.1 depends on its enzymatic activity and binding to membrane phospholipids. Pharmacological or physiological activation of PLC abrogates the effect of SGK1.1 on δ-ENaC, suggesting that SGK1.1 connects the PLC pathway with the control of δ-ENaC activity.

IV. 3.1 Cellular localization of SGK1.1 in the cerebral cortex of primates

Initial characterization of SGK1.1 expression showed that its mRNA is highly expressed in the mouse and human CNS, although there may be species-specific differences regarding expression in other tissues (Arteaga *et al.*, 2008; Raikwar *et al.*, 2008). Moreover, it was shown that because of increased protein stability, SGK1.1 is the predominant isoform expressed in the mouse brain (Arteaga *et al.*, 2008). However, the precise cellular localization pattern of SGK1.1 in the brain has not been described. Results of **III. 3.1** show a high level of SGK1.1 expression in pyramidal neurons of the human and monkey cerebral cortex, except in layer IV, where its expression is clearly diminished. Double fluorescent ISH experiments demonstrated a high degree of co-localization between SGK1.1 and δ-ENaC isoforms. Pyramidal neurons expressing SGK1.1 but not δ-ENaC were not detected. Previous studies with double staining experiments excluded the expression of δ-ENaC in nonpyramidal neurons or glial cells in the human or monkey cerebral cortex (Giraldez *et al.*, 2007). Therefore, SGK1.1 expression also appears to be restricted to cortical pyramidal neurons. Expression in other cell types was not apparent by ISH, although it cannot be excluded that they express low levels of mRNA that fall under the detection threshold of the applied technique. Most importantly, co-expression of δ-ENaC and SGK1.1 indicates that the functional relationship found in oocytes could be relevant in pyramidal neuron physiology.

IV. 3.2 Mechanisms of δ-ENaC regulation by SGK1.1

It is well established that the ubiquitous kinase SGK1 up-regulates the canonical αβγ-ENaC and participates in the regulation of transepithelial Na^+ transport (Kamynina & Staub, 2002). The effect of SGK1 is primarily based on an increased expression of the channel at the plasma membrane (Alvarez de la Rosa *et al.*, 1999), although it has also been reported that SGK1 increases ENaC Po (Vuagniaux *et al.*, 2002; Alvarez de la Rosa *et al.*, 2004), so that a dual mechanism of ENaC activation by SGK1 has been proposed.

First, as described in **I. 3**, the effects of SGK1 on αβγ trafficking are mediated, at least in part, by phosphorylation and subsequent prevention of Nedd4-2 interaction with ENaC (Debonneville *et al.*, 2001; Snyder *et al.*, 2002). Nedd4-2 as an E3 ubiquitin ligase binds to PY motifs in the C-terminus of ENaC subunits and ubiquitylates the channel, promoting its endocytosis.

It was shown that reversal of Nedd4-2 ubiquitylation of ENaC by the aldosterone-induced DUB Usp2-45 caused significant stimulation of ENaC activity, accompanied by a modest increase of ENaC cell surface expression and a strongly enhanced proteolytic cleavage (Ruffieux-Daidie *et al.*, 2008). Therefore it was suggested a multi-step mechanism for ENaC activation, in which Usp2-45 deubiquitylates ENaC, thereby activating the channel via proteolysis and interfering with its endocytosis, which in turn favours ENaC cleavage. Hence, ENaC ubiquitylation and proteolytic activation are related to each other (Ruffieux-Daidie *et al.*, 2008; Rossier & Stutts, 2009). Moreover, it was proposed by the same group that intracellular ubiquitylation of ENaC controls extracellular proteolytic channel activation via conformational change, in a way that reduced ubiquitylation enhanced channel cleavage (Ruffieux-Daidie & Staub, 2011).

ENaC matures upon proteolytic processing (Hughey *et al.*, 2003) by increasing its Po (Caldwell *et al.*, 2004). Therefore, the second mechanism of ENaC activation by SGK1 involves a variance of Po by proteolytic cleavage (Caldwell *et al.*, 2004) and could be indirect: different pools of ENaC in the plasma membrane have been proposed displaying a varied Po, so that a change of different ENaC Po could be perceptible not because of directly increased Po by SGK1, but by SGK1 stabilizing the high Po channel pool in the membrane through preventing its internalization by SGK1 (Ruffieux-Daidie *et al.*, 2008).

This study concludes that SGK1.1 affects δβγ-ENaC trafficking, stabilizing the channel at the plasma membrane, which in turn can account for the increase in whole-cell current. This conclusion is corroborated by 1) the fact that Po of δβγ is already very high – 0.7 in **Fig. III.3** and nearly 1 in previous work by other authors (Haerteis *et al.*, 2009) – therefore it is unlikely that SGK1.1 increases even more δ-Po. Further, ENaC cleavage, which is demonstrated to enhance its Po, stimulates δβγ less than αβγ (Haerteis *et al.*, 2009). 2) Indeed an increased membrane abundance of δYFPβγ could be detected under the confocal microscope, when co-expressed with SGK1.1 as seen in **Fig. III.16 D**.

The δ subunit lacks PY motifs and would therefore depend on the presence of β and/or γ sub-units for the Nedd4-2-mediated internalization mechanism to take place. The possibility that

SGK1.1, like its counterpart SGK1, acts upon δ-ENaC through the same Nedd4-2 mediated pathway on ENaC is discarded by the finding that SGK1.1 up-regulated ENaC channels formed only by δ-subunits, indicating that the kinase acts through a PY motif-independent pathway. Moreover, other cell-type specific factors may participate, since the combination of αβγ subunits is not affected by SGK1.1 in oocytes (Arteaga et al. 2008) but SGK1.1 does regulate ENaC αβγ channels in Fischer rat thyroid epithelial cells (Raikwar *et al.*, 2008). In addition, SGK1 can also modulate plasma membrane expression of channels and transporters that lack PY motifs, indicating that multiple trafficking pathways are regulated by the kinase (Lang *et al.*, 2006).

Other ion channels regulated by SGK1 besides ENaC are for instance the epithelial Ca^{2+} channel TRPV5 (Embark *et al.*, 2004), the voltage-gated Na^+ channel SCN5A (Boehmer *et al.*, 2003), the K^+ channels ROMK (Yoo *et al.*, 2003), KCNE1/KCNQ1, KCNQ4 (Embark *et al.*, 2003; Seebohm *et al.*, 2005) and Kv1.3 (Henke *et al.*, 2004). Further, carriers and pumps such as the Na^+/H^+ exchanger NHE3 (Musch *et al.*, 2008), the dicarboxylate transporter NaDC-1 (Boehmer *et al.*, 2004), the glutamate transporters EAAT1-5 (Lang *et al.*, 2006), and the Na^+/K^+-ATPase (Zecevic *et al.*, 2004; Alvarez de la Rosa *et al.*, 2006) are regulated by SGK1. Recently, an interaction between the neuronal KCNQ2/3 potassium channels and SGK1.1 was found to enhance channel activity by increasing its abundance in the plasma membrane (Miranda, Alvarez de la Rosa & Giraldez, unpublished data).

SGK1 effects alternatively include a Rab4-dependent facilitation of AMPA receptor recycling to the membrane in cultured cortical neurons (Liu *et al.*, 2010) and an increased insertion of the kainate receptor GluR6 into the membrane (Strutz-Seebohm *et al.*, 2005). Moreover, the neuronal SGK1.1 has been shown to down-regulate another member of the ENaC/Degenerin family, ASIC1, by decreasing its abundance in the plasma membrane (Arteaga et al. 2008). That the effects of SGK1.1 on δ-ENaC or ASIC1 were not a consequence of a general effect of SGK1.1 on cellular membrane trafficking, was verified by co-expression of SGK1.1 with a human BK channel tagged with YFP, which did not induce any variation in K^+ current or membrane expression levels of the channel, and by the result that SGK1.1 did not produce significant changes in endogenous currents of the oocytes. These results are further supported by the fact that SGK1.1 did not affect endogenous voltage-activated Na^+ currents in neurons (Arteaga *et al.*, 2008). Taken together, the information available clearly indicates that the modulation of channel membrane expression by SGK1.1 is specific for the vesicular cargo, and is not a general effect on cellular membrane trafficking.

At this stage it can only be speculated about an as-yet-unidentified substrate targeted by SGK1.1, which modifies the traffic of δ-ENaC from or to the membrane in neurons, as it is the case for the concerted action of αβγ-ENaC and Nedd4-2 regulated by SGK1 in transepithelial Na^+ transport (Kamynina & Staub, 2002). Preceding reports point towards small GTPases, rabs, to be such a connection between SGK1.1 and δ-ENaC. This assumption seems plausible since rabs are implicated in αβγ-ENaC trafficking (Saxena & Kaur, 2006). Moreover, there is evidence that at least

SGK1 is involved in rab dependent AMPA receptor trafficking (Liu *et al.*, 2010). In that study, the stress hormone corticosterone was shown to increase AMPA receptors via SGK mediated regulation of a complex formed by Rab4 and the guanosine nucleotide dissociation inhibitor (GDI). Phosphorylation of GDI by SGK upon its activation by corticosterone led to the formation of a Rab4:GDI complex, which in turn led to enhanced AMPAR recycling to the membrane. SGK1.1 is unlikely to be activated by corticosterone (Arteaga *et al.*, 2008), but since SGK1.1 preserves the enzymatic activity domain of SGK1 it is conceivable that SGK1.1 could also be involved in GDI phosphorylation and thus in rab-dependent recycling pathways. Preliminary data obtained by co-expression of δβγ-ENaC with GDI and SGK1.1 show that GDI abrogates the effect of SGK1.1 on δβγ-ENaC, whereas it does not affect the basal δβγ current. This indicates that GDI participates in the regulation pathway between SGK1.1 and δ-ENaC (Miranda, Alvarez de la Rosa & Giraldez, unpublished data). However, the precise mechanisms underlying the specific effect of SGK1.1 on ENaC remain to be elucidated.

COMMD1, another regulator of δ-ENaC has been described (Biasio *et al.*, 2004), which down-regulated channel abundance in the membrane via ubiquitylation (Chang *et al.*, 2011). Though SGK1.1 exerts its effect upon δ-ENaC in a PY motif-independent manner, it is possible that other ubiquitine ligases than Nedd4-2 could be implicated. The interaction between the COMMD1 pathway and SGK1.1 remains to be explored.

IV. 3.3 Physiological roles of SGK1.1 and the regulation of δ-ENaC in the nervous system

Whereas there is little information available regarding the roles of SGK1.1 in the nervous system, SGK1 has been implicated in a wide variety of physiological, pathological, and pharmacological processes in the brain (Lang *et al.*, 2006). Some of SGK1 effects are mediated by modulation of ion channel or transporter activity. As noted above, SGK1 regulates several glutamate transporters, voltage-dependent K^+ channels (Lang *et al.*, 2006), and AMPA and kainate glutamate receptors (Liu *et al.*, 2010; Strutz-Seebohm *et al.*, 2005) , indicating that the kinase could be involved in the modulation of synaptic transmission, plasticity, and neuronal membrane potential. It is noteworthy that most of the studies addressing the effects of SGK1 on neuronal ion channels or transporters have been performed in heterologous expression systems. Given that SGK1.1 is the predominant isoform in the brain under physiological conditions (Arteaga *et al.*, 2008) and the conservation of the catalytic domain between both isoforms, it would not be surprising if many of the effects attributed to SGK1 in the brain turn out to be conducted by SGK1.1.

It has been proposed that SGK1 mediates the effects of glucocorticoids in the brain (Kaufer *et al.*, 2004). Unlike SGK1, SGK1.1 does not seem to be a target of glucocorticoids but has high constitutive levels of expression in the CNS (Arteaga *et al.*, 2008). However, the kinase still needs to be phosphorylated to become enzymatically active, a process that has been shown to be dependent

on the PI3K pathway for SGK1 (Park *et al.*, 1999). The region conserved between SGK1 and SGK1.1 includes the amino acid residues that are essential for kinase activation. Therefore, it is reasonable to assume that SGK1.1 activation will also depend on PI3K activity. This idea is reinforced by the fact that SGK1.1 effects are enhanced by a phosphomimetic mutation in serine-515 (Arteaga *et al.*, 2008), equivalent to serine-422 in SGK1, which is the primary target of the PI3K activation pathway (Park *et al.*, 1999).

The revised data indicate that although SGK1 and SGK1.1 share many common properties, functional specificity is achieved by differential transcriptional regulation and subcellular localization. However, most of the studies addressing SGK1 transcriptional regulation and its effects on the activity of neuronal channels and transporters do not differentiate between isoforms, and therefore a reevaluation of the relative importance of SGK1 and SGK1.1 in neuronal physiology is needed to ensure the property association of each.

Regulation of leak Na^+ channels is essential for neuronal survival and excitability. If δ-ENaC contribution to the resting Na^+ permeability of specific types of neurons such as the cortical pyramidal cells of the human and monkey cortex would be validated, the role of SGK1.1 could be essential in the maintenance and function of those neurons. Given the putative role of δ-ENaC in the transduction of ischemic signals during tissue inflammation and hypoxia (Ji *et al.*, 2006), it is conceivable that SGK1.1 could also play a role in that signaling cascade.

IV. 3.4 SGK1.1 as an integrator of signaling pathways?

Addition of 3M3FBS, a specific activator of PLC (Horowitz *et al.*, 2005), has been shown to produce translocation of SGK1.1 from the membrane to the cytoplasm, due to PIP2 hydrolysis (Arteaga *et al.*, 2008). The experiments performed with *Xenopus* oocytes demonstrate that the kinase exhibits the same behaviour when endogenous PLC is pharmacologically activated using 3M3FBS and additionally show the time course of SGK1.1 retrieval from the membrane. Moreover, a 3M3FBS-induced decrease in δβγ-ENaC current was observed only when the kinase is present, suggesting that PLC activation is able to trigger a cascade of signaling events that opposes the effects of SGK1.1.

Remarkably, direct regulation of αβγ-ENaC by PIP2 hydrolysis has been previously described (Kunzelmann *et al.*, 2005; Pochynyuk *et al.*, 2008). A change of δβγ-ENaC current after 3M3FBS incubation could not be observed, but a significant current decrease is seen when SGK1.1 is co-expressed. The regulation of ENaC by PIP2 hydrolysis could be specific of certain subunit combinations and/or cell types, and this is an interesting issue that should be pursued in more detail. The validation of the *Xenopus* oocyte model allowed further demonstration that the physiological PLC activation through a GPCR has a similar effect on SGK1.1 subcellular localization. Again, the shift in SGK1.1 localization abrogates its effects on δ-ENaC activity. This effect takes place in

a timeframe of minutes, consistent with a regulation of channel trafficking by the kinase, since it has been demonstrated that ENaC has a remarkably short half-life in the plasma membrane (Alvarez de la Rosa *et al.*, 2004).

The probable need of PI3K activity for SGK1.1 activation, together with its regulation by the PLC pathway, implies that this kinase has the potential to play a role as an integrator of different pathways converging on δ-ENaC activity in neurons. It has been shown that SGK1 serves an analogous role in kidney epithelial cells, integrating different hormonal signals (Alvarez de la Rosa & Canessa, 2003; Pearce, 2003). For instance, the cAMP signaling has been shown to converge in the regulation of SGK1 and thus enhanced ENaC activity (Alvarez de la Rosa & Canessa, 2003; Thomas *et al.*, 2011).

In neurons, signals converging on SGK1.1 and δ-ENaC may include activators of PI3K such as the brain-derived neurotrophic factor (Almeida *et al.*, 2005), which influences, among other processes, neuronal survival and plasticity (Bramham & Messaoudi, 2005). In addition, GPCR signaling through PLC, such as group I metabotropic glutamate receptors (Bird & Lawrence, 2009) or "M1-like" muscarinic receptors (Gulledge *et al.*, 2009), could potentially modulate δ-ENaC activity in coordination with other pathways.
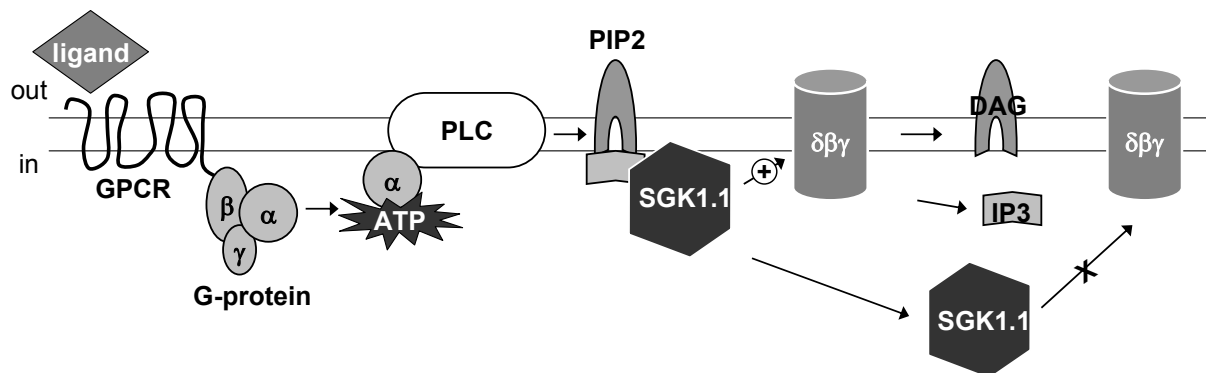
Fig. IV.2 Regulation of δ-ENaC through PLC signalling.
Depicted is the proposed pathway for δ-ENaC regulation. A ligand is received by the GPCR, which in turn activates its G-protein. The activated G-protein activates PLC. This leads to hydrolysis of PIP2 that is normally bound to SGK1.1, which in the bound conformation enhances δ-ENaC activity. Once PIP2 is degraded into IP3 and DAG, SGK1.1 is released from the membrane and its effect on δ-ENac is abrogated.

In summary, the results presented in **III. 3** demonstrate that SGK1.1 provides a new mechanism for δ-ENaC regulation, which may connect channel activity and PLC signalling in neurons.

IV. 4 Summary and future outlook

Beside the similarities between δ- and α-ENaC, channels formed by the δ subunit display several differences to its counterparts α, β and γ, not only in expression but also in functionality. Since δ, unlike α, β and γ, is expressed in neurons and activated by a drop in extracellular pH, δ-ENaC may be involved in signal transduction of noxious stimuli (Ji & Benos, 2004). Its role is not ascertained yet, but in this study a possible neuronal regulation of δ-ENaC was found by SGK1.1 and

through SGK1.1 by the PLC signalling pathway. A further result of this study is that δ-ENaC is regulated in its abundance in the plasma membrane, but neither in its conductance nor in its open probability. In one way this resembles the SGK1 regulation of αβγ-ENaC mediated by Nedd4-2 (Kamynina & Staub, 2002), suggesting that the SGK1.1 effect on δ-ENaC is also indirect and requires a mediator. Approaches to determine, whether SGK1.1 not only co-localizes but interacts with δ-ENaC, or not, would be needed to reject or confirm this hypothesis. Since δ-ENaC lacks a PY motif, the PY motif requiring E3 ubiquitine ligase, Nedd4-2 could be discarded as a mediator of the SGK1.1, yet finding another mediator warrants further investigation. On the other hand, regulation of δ-ENaC is different from αβγ-ENaC, since the canonical ENaC is known to change Po dramatically upon maturation, which involves proteolytic cleavage by extra- and intra-cellular proteases (Diakov *et al.*, 2008). Channels formed by the subunit combination δβγ displayed a Po of nearly 1 even without proteolytic processing and were less activated by proteases. From this finding it was concluded that the near-silent pool of δ-containing channels was smaller than that of αβγ-ENaC (Haerteis *et al.*, 2009).

But δ-ENaC is not only modulated by external factors, it also appears as an N-terminally varied isoform: the subunit called δ2 exhibits a 66 amino acids longer N-terminus than δ1 (Giraldez *et al.*, 2007). One observation of this dissertation was that δ1 activity was higher than δ2 activity. This was due to reduced δ2 channel abundance when compared to δ1. Deletions of two non-adjacent sequences in the δ2 N-terminus (δ2 2xΔ) reversed δ2 activity level to that of δ1. The elements in the δ2 N-terminus necessary for impairment of δ1 activity levels are not yet exactly defined. Since ISH staining revealed that pyramidal neurons either express δ1 or δ2, the expression of one or another isoform could be a tool for the cell to regulate how much δ-ENaC activity is exerted.

Another difference between αβγ-ENaC and δβγ-ENaC found in this study is that the endocytosis of δβγ-ENaC was not only slower that that of αβγ-ENaC, but also qualitatively distinct: unlike the canonical ENaC endocytosis (Shimkets *et al.*, 1997), δβγ-ENaC endocytosis was dynamin-independent, thus was not mediated by clathrin. No involvement of Nedd4-2 and dynamin-independence suggests that δ-ENaC undergoes a yet unknown trafficking mechanism different from the canonical ENaC.

Since the channels formed by the δ subunit alone showed currents about 50 times smaller than coexpressed with β and γ (Waldmann *et al.*, 1995), it is thought that it may form channels with other members within the ENaC/Degenerin family. A possible match for δ-ENaC could be the closely related acid sensing ion channels (ASICs), which comprise several subunits (Alvarez de la Rosa *et al.*, 2000). Besides the proximity within the ENaC/Degenerin family, ASICs display similar features to δ-ENaC: a neuronal expression pattern and pH-sensitivity (Waldmann, 2001; Deval *et al.*, 2010), and therefore a proposed implication in ischemia (Allen & Attwell, 2002; Ji & Benos, 2004; Xiong *et al.*, 2004). Although the response of δ-ENaC towards a drop in pH is sustained (Waldmann *et al.*, 1995) and not rapidly desensitizing as is the case for ASIC (Zhang &

Canessa, 2002). Also both ENaC and ASICs have been reported to interact with CFTR and proteases (Ji *et al.*, 2002; Clark *et al.*, 2010). Therefore, ASIC could be a partner to form functional channels with δ-ENaC. In human glioma cells and rat astrocytes, the ENaC subunits α and γ were found to associate with ASIC1 (Kapoor *et al.*, 2011), which supports the hypothesis. Another indication pointing towards ASIC being a partner for δ-ENaC is that both can be regulated by SGK1.1 as shown by previous reports (Arteaga *et al.*, 2008) and in this study.

Since ENaC and ASIC have a common evolutionary origin and therefore exhibit sequence conservation, they have a similar structure and thus functionality (Alvarez de la Rosa *et al.*, 2000). Therefore, ASIC may be a useful model for δ-ENaC. Up to date, the mechanisms for ASIC endocytosis are unknown, and only ASIC4 was reported to be modified by poly-ubiquitinylation (Donier *et al.*, 2008). Therefore a comparison with δ-ENaC endocytosis cannot be made. On the other hand, conclusions were drawn concerning the stoichiometry of ENaC, once the crystal structure of ASIC was revealed (Jasti *et al.*, 2007; Kashlan & Kleyman, 2011): With ASIC being a trimeric channel (Carnally *et al.*, 2008), ENaC is also thought to be a trimer (Stockand *et al.*, 2008). To determine in which stoichiometry ENaC, especially δ-ENaC, exists will need further investigation.

It is noteworthy to emphasize that δ-ENaC is unlikely to form channels with β and γ in neurons, since these subunits show little or no expression in neurons (Giraldez *et al.*, 2007). This is supported not only by the fact that the effect of the neuronal SGK1.1 on δ-ENaC does not require the subunits β and γ, but also by the fact that the difference between δ1 and δ2 is independent of β and γ. Traffic itineraries between channels formed by δ alone and δβγ-ENaC have to differ since δ-ENaC currents are 50-fold bigger when coexpressed with β and γ and could be explored more into detail for better understanding of δ-ENaC.

Finally, it is postulated that a rab protein could be involved in δ-ENaC regulation. Previous reports of members of the rab family involved in ENaC trafficking (Saxena & Kaur, 2006) point towards implication of a rab small GTPase in δ-ENaC trafficking, since it was revealed in this study that δ-ENaC trafficking did not require dynamin. The fact that SGK was reported to regulate AMPAR insertion via a rab4/GDI complex and the preliminary findings that GDI abrogates the effect of SGK1.1 on δβγ-ENaC indicate towards a possible regulation of δ-ENaC by SGK1.1 via such a complex, rather than via the classical pathway including Nedd4-2 for αβγ-ENaC.

V. Conclusions

Based on the results of this study, the main conclusions are:

1) N-terminal variation of the δ-ENaC isoforms causes differences in δ-ENaC trafficking, which are not based on differential endocytosis, suggesting distinct insertion

2) δ-ENaC endocytosis is not dynamin-dependent, unlike its counterpart α-ENaC

3) δ-ENaC turnover is slower than that of α-ENaC

4) SGK1.1 displays a modulatory effect on δ-ENaC when co-expressed in *Xenopus* oocytes

5) SGK1.1 requires its kinase activity and membrane binding via PIP2, but not the PY-motif to regulate δ-ENaC

6) control of δ-ENaC activity can be linked to PLC signaling via SGK1.1

VI. References

ABI-ANTOUN,T., SHI,S., TOLINO,L.A., KLEYMAN,T.R. & CARATTINO,M.D. 2011. Second transmembrane domain modulates epithelial sodium channel gating in response to shear stress. *Am.J.Physiol Renal Physiol*.

ABRIEL,H., LOFFING,J., REBHUN,J.F., PRATT,J.H., SCHILD,L., HORISBERGER,J.D., ROTIN,D. & STAUB,O. 1999. Defective regulation of the epithelial Na+ channel by Nedd4 in Liddle's syndrome. *J.Clin.Invest* **103,** 667-673.

ALLEN,N.J. & ATTWELL,D. 2002. Modulation of ASIC channels in rat cerebellar Purkinje neurons by ischaemia-related signals. *J.Physiol* **543,** 521-529.

ALMEIDA,R.D., MANADAS,B.J., MELO,C.V., GOMES,J.R., MENDES,C.S., GRAOS,M.M., CARVALHO,R.F., CARVALHO,A.P. & DUARTE,C.B. 2005. Neuroprotection by BDNF against glutamate-induced apoptotic cell death is mediated by ERK and PI3-kinase pathways. *Cell Death.Differ.* **12,** 1329-1343.

ALTHAUS,M., BOGDAN,R., CLAUSS,W.G. & FRONIUS,M. 2007. Mechano-sensitivity of epithelial sodium channels (ENaCs): laminar shear stress increases ion channel open probability. *FASEB J.* **21,** 2389-2399.

ALVAREZ DE LA ROSA,D. & CANESSA,C.M. 2003. Role of SGK in hormonal regulation of epithelial sodium channel in A6 cells. *Am.J.Physiol Cell Physiol* **284,** C404-C414.

ALVAREZ DE LA ROSA,D., CANESSA,C.M., FYFE,G.K. & ZHANG,P. 2000. Structure and regulation of amiloride-sensitive sodium channels. *Annu.Rev.Physiol* **62,** 573-594.

ALVAREZ DE LA ROSA,D., GIMENEZ,I., FORBUSH,B. & CANESSA,C.M. 2006. SGK1 activates Na+-K+-ATPase in amphibian renal epithelial cells. *Am.J.Physiol Cell Physiol* **290,** C492-C498.

ALVAREZ DE LA ROSA,D., LI,H. & CANESSA,C.M. 2002a. Effects of aldosterone on biosynthesis, traffic, and functional expression of epithelial sodium channels in A6 cells. *J.Gen.Physiol* **119,** 427-442.

ALVAREZ DE LA ROSA,D., PAUNESCU,T.G., ELS,W.J., HELMAN,S.I. & CANESSA,C.M. 2004. Mechanisms of regulation of epithelial sodium channel by SGK1 in A6 cells. *J.Gen.Physiol* **124,** 395-407.

ALVAREZ DE LA ROSA,D., ZHANG,P., NARAY-FEJES-TOTH,A., FEJES-TOTH,G. & CANESSA,C.M. 1999. The serum and glucocorticoid kinase sgk increases the abundance of epithelial sodium channels in the plasma membrane of Xenopus oocytes. *J.Biol.Chem.* **274,** 37834-37839.

ALVAREZ DE LA ROSA,D., ZHANG,P., SHAO,D., WHITE,F. & CANESSA,C.M. 2002b. Functional implications of the localization and activity of acid-sensitive channels in rat peripheral nervous system. *Proc.Natl.Acad.Sci.U.S.A* **99,** 2326-2331.

ALVAREZ,E., GIRONES,N. & DAVIS,R.J. 1990. Inhibition of the receptor-mediated endocytosis of diferric transferrin is associated with the covalent modification of the transferrin receptor with palmitic acid. *J.Biol.Chem.* **265,** 16644-16655.

ARIAS,R.L., SUNG,M.L., VASYLYEV,D., ZHANG,M.Y., ALBINSON,K., KUBEK,K., KAGAN,N., BEYER,C., LIN,Q., DWYER,J.M., ZALESKA,M.M., BOWLBY,M.R., DUNLOP,J. & MONAGHAN,M. 2008. Amiloride is neuroprotective in an MPTP model of Parkinson's disease. *Neurobiol.Dis.* **31,** 334-341.

ARTEAGA,M.F., CORIC,T., STRAUB,C. & CANESSA,C.M. 2008. A brain-specific SGK1 splice isoform regulates expression of ASIC1 in neurons. *Proc.Natl.Acad.Sci.U.S.A* **105,** 4459-4464.

BABINI,E., GEISLER,H.S., SIBA,M. & GRUNDER,S. 2003. A new subunit of the epithelial Na+ channel identifies regions involved in Na+ self-inhibition. *J.Biol.Chem.* **278,** 28418-28426.

BARROSO-GONZALEZ,J., MACHADO,J.D., GARCIA-EXPOSITO,L. & VALENZUELA-FERNANDEZ,A. 2009. Moesin regulates the trafficking of nascent clathrin-coated vesicles. *J.Biol.Chem.* **284,** 2419-2434.

BENOS,D.J., FULLER,C.M., SHLYONSKY,V.G., BERDIEV,B.K. & ISMAILOV,I.I. 1997. Amiloride-sensitive Na+ channels: insights and outlooks. *News Physiol.Sci.* **12**.

BERDIEV,B.K., QADRI,Y.J. & BENOS,D.J. 2009. Assessment of the CFTR and ENaC association. *Mol.Biosyst.* **5,** 123-127.

BERGER,S., BLEICH,M., SCHMID,W., GREGER,R. & SCHUTZ,G. 2000. Mineralocorticoid receptor knockout mice: lessons on Na+ metabolism. *Kidney Int.* **57,** 1295-1298.

BHALLA,V., DAIDIE,D., LI,H., PAO,A.C., LAGRANGE,L.P., WANG,J., VANDEWALLE,A., STOCKAND,J.D., STAUB,O. & PEARCE,D. 2005. Serum- and glucocorticoid-regulated kinase 1 regulates ubiquitin ligase neural precursor cell-expressed, developmentally down-regulated protein 4-2 by inducing interaction with 14-3-3. *Mol.Endocrinol.* **19,** 3073-3084.

BHALLA,V., SOUNDARARAJAN,R., PAO,A.C., LI,H. & PEARCE,D. 2006. Disinhibitory pathways for control of sodium transport: regulation of ENaC by SGK1 and GILZ. *Am.J.Physiol Renal Physiol* **291,** F714-F721.

BIASIO,W., CHANG,T., MCINTOSH,C.J. & MCDONALD,F.J. 2004. Identification of Murr1 as a regulator of the human delta epithelial sodium channel. *J.Biol.Chem.* **279,** 5429-5434.

BIRD,M.K. & LAWRENCE,A.J. 2009. Group I metabotropic glutamate receptors: involvement in drug-seeking and drug-induced plasticity. *Curr.Mol.Pharmacol.* **2,** 83-94.

BIZE,V. & HORISBERGER,J.D. 2007. Sodium self-inhibition of human epithelial sodium channel: selectivity and affinity of the extracellular sodium sensing site. *Am.J.Physiol Renal Physiol* **293,** F1137-F1146.

BLAZER-YOST,B.L. & NOFZIGER,C. 2004. The role of the phosphoinositide pathway in hormonal regulation of the epithelial sodium channel. *Adv.Exp.Med.Biol.* **559,** 359-368.

BOEHMER,C., EMBARK,H.M., BAUER,A., PALMADA,M., YUN,C.H., WEINMAN,E.J., ENDOU,H., COHEN,P., LAHME,S., BICHLER,K.H. & LANG,F. 2004. Stimulation of renal Na+ dicarboxylate cotransporter 1 by Na+/H+ exchanger regulating factor 2, serum and glucocorticoid inducible kinase isoforms, and protein kinase B. *Biochem.Biophys.Res.Commun.* **313,** 998-1003.

BOEHMER,C., WILHELM,V., PALMADA,M., WALLISCH,S., HENKE,G., BRINKMEIER,H., COHEN,P., PIESKE,B. & LANG,F. 2003. Serum and glucocorticoid inducible kinases in the regulation of the cardiac sodium channel SCN5A. *Cardiovasc.Res.* **57,** 1079-1084.

BORON,W. & BOULPAEP,E.L. 2001. *Medical Physiology*. Saunders.

BRAMHAM,C.R. & MESSAOUDI,E. 2005. BDNF function in adult synaptic plasticity: the synaptic consolidation hypothesis. *Prog.Neurobiol.* **76,** 99-125.

BUBIEN,J.K. 2010. Epithelial Na+ channel (ENaC), hormones, and hypertension. *J.Biol.Chem.* **285,** 23527-23531.

BUTTERWORTH,M.B. 2010. Regulation of the epithelial sodium channel (ENaC) by membrane trafficking. *Biochim.Biophys.Acta* **1802,** 1166-1177.

BUTTERWORTH,M.B., EDINGER,R.S., FRIZZELL,R.A. & JOHNSON,J.P. 2009. Regulation of the epithelial sodium channel by membrane trafficking. *Am.J.Physiol Renal Physiol* **296,** F10-F24.

BUTTERWORTH,M.B., EDINGER,R.S., JOHNSON,J.P. & FRIZZELL,R.A. 2005. Acute ENaC stimulation by cAMP in a kidney cell line is mediated by exocytic insertion from a recycling channel pool. *J.Gen.Physiol* **125,** 81-101.

BUTTERWORTH,M.B., EDINGER,R.S., OVAA,H., BURG,D., JOHNSON,J.P. & FRIZZELL,R.A. 2007. The deubiquitinating enzyme UCH-L3 regulates the apical membrane recycling of the epithelial sodium channel. *J.Biol.Chem.* **282,** 37885-37893.

CALDWELL,R.A., BOUCHER,R.C. & STUTTS,M.J. 2004. Serine protease activation of near-silent epithelial Na+ channels. *Am.J.Physiol Cell Physiol* **286,** C190-C194.

CANESSA,C.M. 2007. Structural biology: unexpected opening. *Nature* **449,** 293-294.

CANESSA,C.M., MERILLAT,A.M. & ROSSIER,B.C. 1994a. Membrane topology of the epithelial sodium channel in intact cells. *Am.J.Physiol* **267,** C1682-C1690.

CANESSA,C.M., SCHILD,L., BUELL,G., THORENS,B., GAUTSCHI,I., HORISBERGER,J.D. & ROSSIER,B.C. 1994b. Amiloride-sensitive epithelial Na+ channel is made of three homologous subunits. *Nature* **367,** 463-467.

CARNALLY,S.M., DEV,H.S., STEWART,A.P., BARRERA,N.P., VAN BEMMELEN,M.X., SCHILD,L., HENDERSON,R.M. & EDWARDSON,J.M. 2008. Direct visualization of the trimeric structure of the ASIC1a channel, using AFM imaging. *Biochem.Biophys.Res.Commun.* **372,** 752-755.

CHABOT,H., VIVES,M.F., DAGENAIS,A., GRYGORCZYK,C., BERTHIAUME,Y. & GRYGORCZYK,R. 1999. Downregulation of epithelial sodium channel (ENaC) by CFTR co-expressed in Xenopus oocytes is independent of Cl- conductance. *J.Membr.Biol.* **169,** 175-188.

CHALFANT,M.L., DENTON,J.S., LANGLOH,A.L., KARLSON,K.H., LOFFING,J., BENOS,D.J. & STANTON,B.A. 1999. The NH(2) terminus of the epithelial sodium channel contains an endocytic motif. *J.Biol.Chem.* **274,** 32889-32896.

CHANDRAN,S., LI,H., DONG,W., KRASINSKA,K., ADAMS,C., ALEXANDROVA,L., CHIEN,A., HALLOWS,K.R. & BHALLA,V. 2011. Nedd4-2 Regulation by 14-3-3 Binding at Canonical SGK1 Phosphorylation Sites. *J.Biol.Chem.*

CHANG,C.T., BENS,M., HUMMLER,E., BOULKROUN,S., SCHILD,L., TEULON,J., ROSSIER,B.C. & VANDEWALLE,A. 2005. Vasopressin-stimulated CFTR Cl- currents are increased in the renal collecting duct cells of a mouse model of Liddle's syndrome. *J.Physiol* **562,** 271-284.

CHANG,S.S., GRUNDER,S., HANUKOGLU,A., ROSLER,A., MATHEW,P.M., HANUKOGLU,I., SCHILD,L., LU,Y., SHIMKETS,R.A., NELSON-WILLIAMS,C., ROSSIER,B.C. & LIFTON,R.P. 1996. Mutations in subunits of the epithelial sodium channel cause salt wasting with hyperkalaemic acidosis, pseudohypoaldosteronism type 1. *Nat.Genet.* **12,** 248-253.

CHANG,T., KE,Y., LY,K. & MCDONALD,F.J. 2011. COMMD1 regulates the delta epithelial sodium channel (deltaENaC) through trafficking and ubiquitination. *Biochem.Biophys.Res.Commun.*

CHEN,S.Y., BHARGAVA,A., MASTROBERARDINO,L., MEIJER,O.C., WANG,J., BUSE,P., FIRESTONE,G.L., VERREY,F. & PEARCE,D. 1999. Epithelial sodium channel regulated by aldosterone-induced protein sgk. *Proc.Natl.Acad.Sci.U.S.A* **96,** 2514-2519.

CHOLON,D.M., O'NEAL,W.K., RANDELL,S.H., RIORDAN,J.R. & GENTZSCH,M. 2010. Modulation of endocytic trafficking and apical stability of CFTR in primary human airway epithelial cultures. *Am.J.Physiol Lung Cell Mol.Physiol* **298,** L304-L314.

CHRAIBI,A. & HORISBERGER,J.D. 2002. Na self inhibition of human epithelial Na channel: temperature dependence and effect of extracellular proteases. *J.Gen.Physiol* **120,** 133-145.

CLARK,E.B., JOVOV,B., ROOJ,A.K., FULLER,C.M. & BENOS,D.J. 2010. Proteolytic cleavage of human acid-sensing ion channel 1 by the serine protease matriptase. *J.Biol.Chem.* **285,** 27130-27143.

CLAXTON,N.F., FELLERS,T.J. & DAVIDSON,M.W. 2006. *Encyclopedia of Medical Devices and Instrumentation*. Wiley-Interscience, Inc..

DAAKA,Y. 2011. S-nitrosylation-regulated GPCR signaling. *Biochim.Biophys.Acta*.

DALLE-DONNE,I., ROSSI,R., COLOMBO,G., GIUSTARINI,D. & MILZANI,A. 2009. Protein S-glutathionylation: a regulatory device from bacteria to humans. *Trends Biochem.Sci.* **34,** 85-96.

DEBONNEVILLE,C., FLORES,S.Y., KAMYNINA,E., PLANT,P.J., TAUXE,C., THOMAS,M.A., MUNSTER,C., CHRAIBI,A., PRATT,J.H., HORISBERGER,J.D., PEARCE,D., LOFFING,J & STAUB,O. 2001. Phosphorylation of Nedd4-2 by Sgk1 regulates epithelial Na(+) channel cell surface expression. *EMBO J.* **20,** 7052-7059.

DEVAL,E., GASULL,X., NOEL,J., SALINAS,M., BARON,A., DIOCHOT,S. & LINGUEGLIA,E. 2010. Acid-sensing ion channels (ASICs): pharmacology and implication in pain. *Pharmacol.Ther.* **128,** 549-558.

DIAKOV,A., BERA,K., MOKRUSHINA,M., KRUEGER,B. & KORBMACHER,C. 2008. Cleavage in the {gamma}-subunit of the epithelial sodium channel (ENaC) plays an important role in the proteolytic activation of near-silent channels. *J.Physiol* **586,** 4587-4608.

DONALDSON,S.H. & BOUCHER,R.C. 2007. Sodium channels and cystic fibrosis. *Chest* **132,** 1631-1636.

DONIER,E., RUGIERO,F., JACOB,C. & WOOD,J.N. 2008. Regulation of ASIC activity by ASIC4--new insights into ASIC channel function revealed by a yeast two-hybrid assay. *Eur.J.Neurosci.* **28,** 74-86.

DUGGAN,A., GARCIA-ANOVEROS,J. & COREY,D.P. 2002. The PDZ domain protein PICK1 and the sodium channel BNaC1 interact and localize at mechanosensory terminals of dorsal root ganglion neurons and dendrites of central neurons. *J.Biol.Chem.* **277,** 5203-5208.

DUMONT,J.N. 1972. Oogenesis in Xenopus laevis (Daudin). I. Stages of oocyte development in laboratory maintained animals. *J.Morphol.* **136,** 153-179.

ECKERT,R., RANDALL,D., BURGGREEN,W. & FRENCH,K. 2002. *Tierphysiologie*. Georg Thieme Verlag, Stuttgart.

EDELHEIT,O., HANUKOGLU,I., SHRIKI,Y., TFILIN,M., DASCAL,N., GILLIS,D. & HANUKOGLU,A. 2010. Truncated beta epithelial sodium channel (ENaC) subunits responsible for multi-system pseudohypoaldosteronism support partial activity of ENaC. *J.Steroid Biochem.Mol.Biol.* **119,** 84-88.

EMBARK,H.M., BOHMER,C., VALLON,V., LUFT,F. & LANG,F. 2003. Regulation of KCNE1-dependent K(+) current by the serum and glucocorticoid-inducible kinase (SGK) isoforms. *Pflugers Arch.* **445,** 601-606.

EMBARK,H.M., SETIAWAN,I., POPPENDIECK,S., VAN DE GRAAF,S.F., BOEHMER,C., PALMADA,M., WIEDER,T., GERSTBERGER,R., COHEN,P., YUN,C.C., BINDELS,R.J. & LANG,F. 2004. Regulation of the epithelial Ca2+ channel TRPV5 by the NHE regulating factor NHERF2 and the serum and glucocorticoid inducible kinase isoforms SGK1 and SGK3 expressed in Xenopus oocytes. *Cell Physiol Biochem.* **14,** 203-212.

ESTRADA,F. & SANCHEZ,J.A. 1991. The effect of amiloride on the resting potential and the electrical constants of frog skeletal muscle fibres. *J.Physiol* **433,** 705-717.

FAKITSAS,P., ADAM,G., DAIDIE,D., VAN BEMMELEN,M.X., FOULADKOU,F., PATRIGNANI,A., WAGNER,U., WARTH,R., CAMARGO,S.M., STAUB,O. & VERREY,F. 2007. Early aldosterone-induced gene product regulates the epithelial sodium channel by deubiquitylation. *J.Am.Soc.Nephrol.* **18,** 1084-1092.

FALETTI,C.J., PERROTTI,N., TAYLOR,S.I. & BLAZER-YOST,B.L. 2002. sgk: an essential convergence point for peptide and steroid hormone regulation of ENaC-mediated Na+ transport. *Am.J.Physiol Cell Physiol* **282,** C494-C500.

FELLERS,T.J. & DAVIDSON,M.W. Laser Scanning Confocal Microscopy. 2009. FluoView Resource Centre, Olympus.
Ref Type: Pamphlet

FIRSOV,D., SCHILD,L., GAUTSCHI,I., MERILLAT,A.M., SCHNEEBERGER,E. & ROSSIER,B.C. 1996. Cell surface expression of the epithelial Na channel and a mutant causing Liddle syndrome: a quantitative approach. *Proc.Natl.Acad.Sci.U.S.A* **93,** 15370-15375.

FLORES,S.Y., LOFFING-CUENI,D., KAMYNINA,E., DAIDIE,D., GERBEX,C., CHABANEL,S., DUDLER,J., LOFFING,J. & STAUB,O. 2005. Aldosterone-induced serum and glucocorticoid-induced kinase 1 expression is accompanied by Nedd4-2 phosphorylation and increased Na+ transport in cortical collecting duct cells. *J.Am.Soc.Nephrol.* **16,** 2279-2287.

FOTIA,A.B., DINUDOM,A., SHEARWIN,K.E., KOCH,J.P., KORBMACHER,C., COOK,D.I. & KUMAR,S. 2003. The role of individual Nedd4-2 (KIAA0439) WW domains in binding and regulating epithelial sodium channels. *FASEB J.* **17,** 70-72.

FRONIUS,M. & CLAUSS,W.G. 2008. Mechano-sensitivity of ENaC: may the (shear) force be with you. *Pflugers Arch.* **455,** 775-785.

FULLER,P.J. & YOUNG,M.J. 2005. Mechanisms of mineralocorticoid action. *Hypertension* **46,** 1227-1235.

GAILLARD,E.A., KOTA,P., GENTZSCH,M., DOKHOLYAN,N.V., STUTTS,M.J. & TARRAN,R. 2010. Regulation of the epithelial Na+ channel and airway surface liquid volume by serine proteases. *Pflugers Arch.* **460,** 1-17.

GARTY,H. & PALMER,L.G. 1997. Epithelial sodium channels: function, structure, and regulation. *Physiol Rev.* **77,** 359-396.

GEISLER,C., DIETRICH,J., NIELSEN,B.L., KASTRUP,J., LAURITSEN,J.P., ODUM,N. & CHRISTENSEN,M.D. 1998. Leucine-based receptor sorting motifs are dependent on the spacing relative to the plasma membrane. *J.Biol.Chem.* **273,** 21316-21323.

GELLER,D.S., ZHANG,J., ZENNARO,M.C., VALLO-BOADO,A., RODRIGUEZ-SORIANO,J., FURU,L., HAWS,R., METZGER,D., BOTELHO,B., KARAVITI,L., HAQQ,A.M., COREY,H., JANSSENS,S., CORVOL,P. & LIFTON,R.P. 2006. Autosomal dominant pseudohypoaldosteronism type 1: mechanisms, evidence for neonatal lethality, and phenotypic expression in adults. *J.Am.Soc.Nephrol.* **17,** 1429-1436.

GIRALDEZ,T., AFONSO-ORAMAS,D., CRUZ-MUROS,I., GARCIA-MARIN,V., PAGEL,P., GONZALEZ-HERNANDEZ,T. & ALVAREZ DE LA ROSA,D. 2007. Cloning and functional expression of a new epithelial sodium channel delta subunit isoform differentially expressed in neurons of the human and monkey telencephalon. *J.Neurochem.* **102,** 1304-1315.

GIRALDEZ,T., HUGHES,T.E. & SIGWORTH,F.J. 2005. Generation of functional fluorescent BK channels by random insertion of GFP variants. *J.Gen.Physiol* **126,** 429-438.

GLICKMAN,M.H. & CIECHANOVER,A. 2002. The ubiquitin-proteasome proteolytic pathway: destruction for the sake of construction. *Physiol Rev.* **82,** 373-428.

GONZALEZ,M.C., ABREU,P., BARROSO-CHINEA,P., CRUZ-MUROS,I. & GONZALEZ-HERNANDEZ,T. 2004. Effect of intracerebroventricular injection of lipopolysaccharide on the tuberoinfundibular dopaminergic system of the rat. *Neuroscience* **127,** 251-259.

GOULET,C.C., VOLK,K.A., ADAMS,C.M., PRINCE,L.S., STOKES,J.B. & SNYDER,P.M. 1998. Inhibition of the epithelial Na+ channel by interaction of Nedd4 with a PY motif deleted in Liddle's syndrome. *J.Biol.Chem.* **273,** 30012-30017.

GRANT,B.D. & DONALDSON,J.G. 2009. Pathways and mechanisms of endocytic recycling. *Nat.Rev.Mol.Cell Biol.* **10,** 597-608.

GRUNDER,S., FIRSOV,D., CHANG,S.S., JAEGER,N.F., GAUTSCHI,I., SCHILD,L., LIFTON,R.P. & ROSS-IER,B.C. 1997. A mutation causing pseudohypoaldosteronism type 1 identifies a conserved glycine that is involved in the gating of the epithelial sodium channel. *EMBO J.* **16,** 899-907.

GULLEDGE,A.T., BUCCI,D.J., ZHANG,S.S., MATSUI,M. & YEH,H.H. 2009. M1 receptors mediate cholinergic modulation of excitability in neocortical pyramidal neurons. *J.Neurosci.* **29,** 9888-9902.

HAERTEIS,S., KRUEGER,B., KORBMACHER,C. & RAUH,R. 2009. The delta-subunit of the epithelial sodium channel (ENaC) enhances channel activity and alters proteolytic ENaC activation. *J.Biol.Chem.* **284,** 29024-29040.

HALLOWS,K.R., BHALLA,V., OYSTER,N.M., WIJNGAARDEN,M.A., LEE,J.K., LI,H., CHANDRAN,S., XIA,X., HUANG,Z., CHALKLEY,R.J., BURLINGAME,A.L. & PEARCE,D. 2010. Phosphopeptide screen uncovers novel phosphorylation sites of Nedd4-2 that potentiate its inhibition of the epithelial Na+ channel. *J.Biol.Chem.* **285,** 21671-21678.

HENKE,G., MAIER,G., WALLISCH,S., BOEHMER,C. & LANG,F. 2004. Regulation of the voltage gated K+ channel Kv1.3 by the ubiquitin ligase Nedd4-2 and the serum and glucocorticoid inducible kinase SGK1. *J.Cell Physiol* **199,** 194-199.

HILLE,B. 2001. *Ion Channels of Excitable Membranes, 3rd Edition*. Sinauer Associates.

HORISBERGER,J.D. 1998. Amiloride-sensitive Na channels. *Curr.Opin.Cell Biol.* **10,** 443-449.

HOROWITZ,L.F., HIRDES,W., SUH,B.C., HILGEMANN,D.W., MACKIE,K. & HILLE,B. 2005. Phospholipase C in living cells: activation, inhibition, Ca2+ requirement, and regulation of M current. *J.Gen.Physiol* **126,** 243-262.

HUGHEY,R.P., BRUNS,J.B., KINLOUGH,C.L. & KLEYMAN,T.R. 2004. Distinct pools of epithelial sodium channels are expressed at the plasma membrane. *J.Biol.Chem.* **279,** 48491-48494.

HUGHEY,R.P., MUELLER,G.M., BRUNS,J.B., KINLOUGH,C.L., POLAND,P.A., HARKLEROAD,K.L., CARAT-TINO,M.D. & KLEYMAN,T.R. 2003. Maturation of the epithelial Na+ channel involves proteolytic processing of the alpha- and gamma-subunits. *J.Biol.Chem.* **278,** 37073-37082.

HURLEY,J.H. & STENMARK,H. 2011. Molecular mechanisms of ubiquitin-dependent membrane traffic. *Annu.Rev.Biophys.* **40,** 119-142.

JASTI,J., FURUKAWA,H., GONZALES,E.B. & GOUAUX,E. 2007. Structure of acid-sensing ion channel 1 at 1.9 A resolution and low pH. *Nature* **449,** 316-323.

JI,H.L. & BENOS,D.J. 2004. Degenerin sites mediate proton activation of deltabetagamma-epithelial sodium channel. *J.Biol.Chem.* **279,** 26939-26947.

JI,H.L., BISHOP,L.R., ANDERSON,S.J., FULLER,C.M. & BENOS,D.J. 2004. The role of Pre-H2 domains of alpha- and delta-epithelial Na+ channels in ion permeation, conductance, and amiloride sensitivity. *J.Biol.Chem.* **279,** 8428-8440.

JI,H.L., CHALFANT,M.L., JOVOV,B., LOCKHART,J.P., PARKER,S.B., FULLER,C.M., STANTON,B.A. & BENOS,D.J. 2000. The cytosolic termini of the beta- and gamma-ENaC subunits are involved in the functional interactions between cystic fibrosis transmembrane conductance regulator and epithelial sodium channel. *J.Biol.Chem.* **275,** 27947-27956.

JI,H.L., JOVOV,B., FU,J., BISHOP,L.R., MEBANE,H.C., FULLER,C.M., STANTON,B.A. & BENOS,D.J. 2002. Up-regulation of acid-gated Na(+) channels (ASICs) by cystic fibrosis transmembrane conductance regulator co-expression in Xenopus oocytes. *J.Biol.Chem.* **277,** 8395-8405.

JI,H.L., SU,X.F., KEDAR,S., LI,J., BARBRY,P., SMITH,P.R., MATALON,S. & BENOS,D.J. 2006. Delta-subunit confers novel biophysical features to alpha beta gamma-human epithelial sodium channel (ENaC) via a physical interaction. *J.Biol.Chem.* **281,** 8233-8241.

JOHN INNES CENTRE . Confocal Microscopy. 2011.
Ref Type: Pamphlet

KAMYNINA,E., DEBONNEVILLE,C., BENS,M., VANDEWALLE,A. & STAUB,O. 2001. A novel mouse Nedd4 protein suppresses the activity of the epithelial Na+ channel. *FASEB J.* **15,** 204-214.

KAMYNINA,E. & STAUB,O. 2002. Concerted action of ENaC, Nedd4-2, and Sgk1 in transepithelial Na(+) transport. *Am.J.Physiol Renal Physiol* **283,** F377-F387.

KAPOOR,N., LEE,W., CLARK,E.B., BARTOSZEWSKI,R., MCNICHOLAS,C.M., LATHAM,C.B., BEBOK,Z., PARPURA,V., FULLER,C.M., PALMER,C.A. & BENOS,D.J. 2011. Interaction of ASIC1 and ENaC Subunits in Human Glioma Cells and Rat Astrocytes. *Am.J.Physiol Cell Physiol*.

KARPUSHEV,A.V., LEVCHENKO,V., PAVLOV,T.S., LAM,V.Y., VINNAKOTA,K.C., VANDEWALLE,A., WAKATSUKI,T. & STARUSCHENKO,A. 2008. Regulation of ENaC expression at the cell surface by Rab11. *Biochem.Biophys.Res.Commun.* **377,** 521-525.

KASHLAN,O.B. & KLEYMAN,T.R. 2011. ENaC structure and function in the wake of a resolved structure of a family member. *Am.J.Physiol Renal Physiol*.

KAUFER,D., OGLE,W.O., PINCUS,Z.S., CLARK,K.L., NICHOLAS,A.C., DINKEL,K.M., DUMAS,T.C., FERGUSON,D., LEE,A.L., WINTERS,M.A. & SAPOLSKY,R.M. 2004. Restructuring the neuronal stress response with anti-glucocorticoid gene delivery. *Nat.Neurosci.* **7,** 947-953.

KELLENBERGER,S., GAUTSCHI,I., ROSSIER,B.C. & SCHILD,L. 1998. Mutations causing Liddle syndrome reduce sodium-dependent downregulation of the epithelial sodium channel in the Xenopus oocyte expression system. *J.Clin.Invest* **101,** 2741-2750.

KELLENBERGER,S. & SCHILD,L. 2002. Epithelial sodium channel/degenerin family of ion channels: a variety of functions for a shared structure. *Physiol Rev.* **82,** 735-767.

KIMURA,T., KAWABE,H., JIANG,C., ZHANG,W., XIANG,Y.Y., LU,C., SALTER,M.W., BROSE,N., LU,W.Y. & ROTIN,D. 2011. Deletion of the ubiquitin ligase Nedd4L in lung epithelia causes cystic fibrosis-like disease. *Proc.Natl.Acad.Sci.U.S.A* **108,** 3216-3221.

KLAUSNER,R.D., DONALDSON,J.G. & LIPPINCOTT-SCHWARTZ,J. 1992. Brefeldin A: insights into the control of membrane traffic and organelle structure. *J.Cell Biol.* **116,** 1071-1080.

KLEYMAN,T.R., CARATTINO,M.D. & HUGHEY,R.P. 2009. ENaC at the cutting edge: regulation of epithelial sodium channels by proteases. *J.Biol.Chem.* **284,** 20447-20451.

References

KUNZELMANN,K., BACHHUBER,T., REGEER,R., MARKOVICH,D., SUN,J. & SCHREIBER,R. 2005. Purinergic inhibition of the epithelial Na+ transport via hydrolysis of PIP2. *FASEB J.* **19,** 142-143.

KUNZELMANN,K., SCHREIBER,R., NITSCHKE,R. & MALL,M. 2000. Control of epithelial Na+ conductance by the cystic fibrosis transmembrane conductance regulator. *Pflugers Arch.* **440,** 193-201.

LANG,F., ARTUNC,F. & VALLON,V. 2009. The physiological impact of the serum and glucocorticoid-inducible kinase SGK1. *Curr.Opin.Nephrol.Hypertens.* **18,** 439-448.

LANG,F., BOHMER,C., PALMADA,M., SEEBOHM,G., STRUTZ-SEEBOHM,N. & VALLON,V. 2006. (Patho)physiological significance of the serum- and glucocorticoid-inducible kinase isoforms. *Physiol Rev.* **86,** 1151-1178.

LASSMANN,T. & SONNHAMMER,E.L. 2006. Kalign, Kalignvu and Mumsa: web servers for multiple sequence alignment. *Nucleic Acids Res.* **34,** W596-W599.

LAZRAK,A., JURKUVENAITE,A., CHEN,L., KEELING,K.M., COLLAWN,J.F., BEDWELL,D.M. & MATALON,S. 2011. ENHANCEMENT OF ALVEOLAR EPITHELIAL SODIUM CHANNEL ACTIVITY WITH DECREASED CYSTIC FIBROSIS TRANSMEMBRANE CONDUCTANCE REGULATOR EXPRESSION IN MOUSE LUNG. *Am.J.Physiol Lung Cell Mol.Physiol*.

LEE,I.H., CAMPBELL,C.R., COOK,D.I. & DINUDOM,A. 2008. Regulation of epithelial Na+ channels by aldosterone: role of Sgk1. *Clin.Exp.Pharmacol.Physiol* **35,** 235-241.

LI,S.S. 2005. Specificity and versatility of SH3 and other proline-recognition domains: structural basis and implications for cellular signal transduction. *Biochem.J.* **390,** 641-653.

LIFTON,R.P., GHARAVI,A.G. & GELLER,D.S. 2001. Molecular mechanisms of human hypertension. *Cell* **104,** 545-556.

LIMAN,E.R., TYTGAT,J. & HESS,P. 1992. Subunit stoichiometry of a mammalian K+ channel determined by construction of multimeric cDNAs. *Neuron* **9,** 861-871.

LINGUEGLIA,E., DE WEILLE,J.R., BASSILANA,F., HEURTEAUX,C., SAKAI,H., WALDMANN,R. & LAZDUNSKI,M. 1997. A modulatory subunit of acid sensing ion channels in brain and dorsal root ganglion cells. *J.Biol.Chem.* **272,** 29778-29783.

LISINSKI,I., SCHURMANN,A., JOOST,H.G., CUSHMAN,S.W. & AL HASANI,H. 2001. Targeting of GLUT6 (formerly GLUT9) and GLUT8 in rat adipose cells. *Biochem.J.* **358,** 517-522.

LIU,W., YUEN,E.Y. & YAN,Z. 2010. The stress hormone corticosterone increases synaptic alpha-amino-3-hydroxy-5-methyl-4-isoxazolepropionic acid (AMPA) receptors via serum- and glucocorticoid-inducible kinase (SGK) regulation of the GDI-Rab4 complex. *J.Biol.Chem.* **285,** 6101-6108.

LOFFING,J. & KORBMACHER,C. 2009. Regulated sodium transport in the renal connecting tubule (CNT) via the epithelial sodium channel (ENaC). *Pflugers Arch.* **458,** 111-135.

LU,B., SU,Y., DAS,S., LIU,J., XIA,J. & REN,D. 2007a. The neuronal channel NALCN contributes resting sodium permeability and is required for normal respiratory rhythm. *Cell* **129,** 371-383.

LU,C., PRIBANIC,S., DEBONNEVILLE,A., JIANG,C. & ROTIN,D. 2007b. The PY motif of ENaC, mutated in Liddle syndrome, regulates channel internalization, sorting and mobilization from subapical pool. *Traffic.* **8,** 1246-1264.

LUND,K.A., OPRESKO,L.K., STARBUCK,C., WALSH,B.J. & WILEY,H.S. 1990. Quantitative analysis of the endocytic system involved in hormone-induced receptor internalization. *J.Biol.Chem.* **265,** 15713-15723.

MACDONALD,J.L. & PIKE,L.J. 2005. A simplified method for the preparation of detergent-free lipid rafts. *J.Lipid Res.* **46,** 1061-1067.

MACIA,E., EHRLICH,M., MASSOL,R., BOUCROT,E., BRUNNER,C. & KIRCHHAUSEN,T. 2006. Dynasore, a cell-permeable inhibitor of dynamin. *Dev.Cell* **10,** 839-850.

MALIK,B., PRICE,S.R., MITCH,W.E., YUE,Q. & EATON,D.C. 2006. Regulation of epithelial sodium channels by the ubiquitin-proteasome proteolytic pathway. *Am.J.Physiol Renal Physiol* **290,** F1285-F1294.

MALL,M., GRUBB,B.R., HARKEMA,J.R., O'NEAL,W.K. & BOUCHER,R.C. 2004. Increased airway epithelial Na+ absorption produces cystic fibrosis-like lung disease in mice. *Nat.Med.* **10,** 487-493.

MASILAMANI,S., KIM,G.H., MITCHELL,C., WADE,J.B. & KNEPPER,M.A. 1999. Aldosterone-mediated regulation of ENaC alpha, beta, and gamma subunit proteins in rat kidney. *J.Clin.Invest* **104,** R19-R23.

MAYOR,S. & PAGANO,R.E. 2007. Pathways of clathrin-independent endocytosis. *Nat.Rev.Mol.Cell Biol.* **8,** 603-612.

MIRANDA,P., GIRALDEZ,T., DE LA,P.P., MANSO,D.G., ALONSO-RON,C., GOMEZ-VARELA,D., DOMINGUEZ,P. & BARROS,F. 2005. Specificity of TRH receptor coupling to G-proteins for regulation of ERG K+ channels in GH3 rat anterior pituitary cells. *J.Physiol* **566,** 717-736.

MUSCH,M.W., LUCIONI,A. & CHANG,E.B. 2008. Aldosterone regulation of intestinal Na absorption involves SGK-mediated changes in NHE3 and Na+ pump activity. *Am.J.Physiol Gastrointest.Liver Physiol* **295,** G909-G919.

NEIJSSEN,J., HERBERTS,C., DRIJFHOUT,J.W., REITS,E., JANSSEN,L. & NEEFJES,J. 2005. Cross-presentation by intercellular peptide transfer through gap junctions. *Nature* **434,** 83-88.

NUMBERGER,M. & DRAGUHN,A. 1996. *Patch Clamp Technik*. Spektrum Akademischer Verlag, Heidelberg.

PANDEY,K.N. 2009. Functional roles of short sequence motifs in the endocytosis of membrane receptors. *Front Biosci.* **14,** 5339-5360.

PARK,J., LEONG,M.L., BUSE,P., MAIYAR,A.C., FIRESTONE,G.L. & HEMMINGS,B.A. 1999. Serum and gluco-corticoid-inducible kinase (SGK) is a target of the PI 3-kinase-stimulated signaling pathway. *EMBO J.* **18,** 3024-3033.

PEARCE,D. 2003. SGK1 regulation of epithelial sodium transport. *Cell Physiol Biochem.* **13,** 13-20.

PEARCE,D. & KLEYMAN,T.R. 2007. Salt, sodium channels, and SGK1. *J.Clin.Invest* **117,** 592-595.

POCHYNYUK,O., BUGAJ,V., VANDEWALLE,A. & STOCKAND,J.D. 2008. Purinergic control of apical plasma membrane PI(4,5)P2 levels sets ENaC activity in principal cells. *Am.J.Physiol Renal Physiol* **294,** F38-F46.

POCHYNYUK,O., STARUSCHENKO,A., BUGAJ,V., LAGRANGE,L. & STOCKAND,J.D. 2007. Quantifying RhoA facilitated trafficking of the epithelial Na+ channel toward the plasma membrane with total internal reflection fluo-rescence-fluorescence recovery after photobleaching. *J.Biol.Chem.* **282,** 14576-14585.

PUOTI,A., MAY,A., CANESSA,C.M., HORISBERGER,J.D., SCHILD,L. & ROSSIER,B.C. 1995. The highly selec-tive low-conductance epithelial Na channel of Xenopus laevis A6 kidney cells. *Am.J.Physiol* **269,** C188-C197.

RAIKWAR,N.S., SNYDER,P.M. & THOMAS,C.P. 2008. An evolutionarily conserved N-terminal Sgk1 variant with enhanced stability and improved function. *Am.J.Physiol Renal Physiol* **295,** F1440-F1448.

RAUH,R., DINUDOM,A., FOTIA,A.B., PAULIDES,M., KUMAR,S., KORBMACHER,C. & COOK,D.I. 2006. Stimula-tion of the epithelial sodium channel (ENaC) by the serum- and glucocorticoid-inducible kinase (Sgk) involves the PY motifs of the channel but is independent of sodium feedback inhibition. *Pflugers Arch.* **452,** 290-299.

REITS,E.A. & NEEFJES,J.J. 2001. From fixed to FRAP: measuring protein mobility and activity in living cells. *Nat.Cell Biol.* **3,** E145-E147.

RENARD,S., LINGUEGLIA,E., VOILLEY,N., LAZDUNSKI,M. & BARBRY,P. 1994. Biochemical analysis of the membrane topology of the amiloride-sensitive Na+ channel. *J.Biol.Chem.* **269,** 12981-12986.

RESH,M.D. 2004. Membrane targeting of lipid modified signal transduction proteins. *Subcell.Biochem.* **37,** 217-232.

ROSSIER,B.C. 1998. Mechanosensitivity of the epithelial sodium channel (ENaC): controversy or pseudocontro-versy? *J.Gen.Physiol* **112,** 95-96.

ROSSIER,B.C., PRADERVAND,S., SCHILD,L. & HUMMLER,E. 2002. Epithelial sodium channel and the control of sodium balance: interaction between genetic and environmental factors. *Annu.Rev.Physiol* **64,** 877-897.

ROSSIER,B.C. & STUTTS,M.J. 2009. Activation of the epithelial sodium channel (ENaC) by serine proteases. *Annu.Rev.Physiol* **71,** 361-379.

ROTIN,D. & STAUB,O. 2010. Role of the ubiquitin system in regulating ion transport. *Pflugers Arch.*

RUFFIEUX-DAIDIE,D., POIROT,O., BOULKROUN,S., VERREY,F., KELLENBERGER,S. & STAUB,O. 2008. Deubiquitylation regulates activation and proteolytic cleavage of ENaC. *J.Am.Soc.Nephrol.* **19,** 2170-2180.

RUFFIEUX-DAIDIE,D. & STAUB,O. 2011. Intracellular ubiquitylation of the epithelial Na+ channel controls extracellular proteolytic channel activation via conformational change. *J.Biol.Chem.* **286,** 2416-2424.

SALAUN,C., GREAVES,J. & CHAMBERLAIN,L.H. 2010. The intracellular dynamic of protein palmitoylation. *J.Cell Biol.* **191,** 1229-1238.

SAMBROOK,J., FRITSCH,E.F. & MANIATIS,T. 1989. *Molecular Cloning: A Laboratory Manual*. Cold Spring Harbor Laboratory Pr; 2nd edition (December 1989).

SANDVIG,K., PUST,S., SKOTLAND,T. & VAN DEURS,B. 2011. Clathrin-independent endocytosis: mechanisms and function. *Curr.Opin.Cell Biol.*

SANDVIG,K., TORGERSEN,M.L., RAA,H.A. & VAN DEURS,B. 2008. Clathrin-independent endocytosis: from nonexisting to an extreme degree of complexity. *Histochem.Cell Biol.* **129,** 267-276.

SAXENA,S., SINGH,M., ENGISCH,K., FUKUDA,M. & KAUR,S. 2005. Rab proteins regulate epithelial sodium channel activity in colonic epithelial HT-29 cells. *Biochem.Biophys.Res.Commun.* **337,** 1219-1223.

SAXENA,S.K. & KAUR,S. 2006. Regulation of epithelial ion channels by Rab GTPases. *Biochem.Biophys.Res.Commun.* **351,** 582-587.

SAXENA,S.K., SINGH,M., SHIBATA,H., KAUR,S. & GEORGE,C. 2006. Rab4 GTP/GDP modulates amiloride-sensitive sodium channel (ENaC) function in colonic epithelia. *Biochem.Biophys.Res.Commun.* **340,** 726-733.

SCHILD,L., LU,Y., GAUTSCHI,I., SCHNEEBERGER,E., LIFTON,R.P. & ROSSIER,B.C. 1996. Identification of a PY motif in the epithelial Na channel subunits as a target sequence for mutations causing channel activation found in Liddle syndrome. *EMBO J.* **15,** 2381-2387.

SCHMID,S.L. & FROLOV,V.A. 2011. Dynamin: Functional Design of a Membrane Fission Catalyst. *Annu.Rev.Cell Dev.Biol.*

SEEBOHM,G., STRUTZ-SEEBOHM,N., BALTAEV,R., KORNIYCHUK,G., KNIRSCH,M., ENGEL,J. & LANG,F. 2005. Regulation of KCNQ4 potassium channel prepulse dependence and current amplitude by SGK1 in Xenopus oocytes. *Cell Physiol Biochem.* **16,** 255-262.

SHIGAEV,A., ASHER,C., LATTER,H., GARTY,H. & REUVENY,E. 2000. Regulation of sgk by aldosterone and its effects on the epithelial Na(+) channel. *Am.J.Physiol Renal Physiol* **278,** F613-F619.

SHIMKETS,R.A., LIFTON,R.P. & CANESSA,C.M. 1997. The activity of the epithelial sodium channel is regulated by clathrin-mediated endocytosis. *J.Biol.Chem.* **272,** 25537-25541.

SHIMKETS,R.A., WARNOCK,D.G., BOSITIS,C.M., NELSON-WILLIAMS,C., HANSSON,J.H., SCHAMBELAN,M., GILL,J.R., JR., ULICK,S., MILORA,R.V., FINDLING,J.W. & . 1994. Liddle's syndrome: heritable human hypertension caused by mutations in the beta subunit of the epithelial sodium channel. *Cell* **79,** 407-414.

SHIPSTON,M.J. 2011. Ion channel regulation by protein palmitoylation. *J.Biol.Chem.* **286,** 8709-8716.

SNYDER,P.M. 2005. Minireview: regulation of epithelial Na+ channel trafficking. *Endocrinology* **146,** 5079-5085.

SNYDER,P.M., MCDONALD,F.J., STOKES,J.B. & WELSH,M.J. 1994. Membrane topology of the amiloride-sensitive epithelial sodium channel. *J.Biol.Chem.* **269,** 24379-24383.

SNYDER,P.M., OLSON,D.R., KABRA,R., ZHOU,R. & STEINES,J.C. 2004. cAMP and serum and glucocorticoid-inducible kinase (SGK) regulate the epithelial Na(+) channel through convergent phosphorylation of Nedd4-2. *J.Biol.Chem.* **279,** 45753-45758.

SNYDER,P.M., OLSON,D.R. & THOMAS,B.C. 2002. Serum and glucocorticoid-regulated kinase modulates Nedd4-2-mediated inhibition of the epithelial Na+ channel. *J.Biol.Chem.* **277,** 5-8.

SOUNDARARAJAN,R., PEARCE,D., HUGHEY,R.P. & KLEYMAN,T.R. 2010. Role of epithelial sodium channels and their regulators in hypertension. *J.Biol.Chem.* **285,** 30363-30369.

STARUSCHENKO,A., BOOTH,R.E., POCHYNYUK,O., STOCKAND,J.D. & TONG,Q. 2006. Functional reconstitution of the human epithelial Na+ channel in a mammalian expression system. *Methods Mol.Biol.* **337,** 3-13.

STARUSCHENKO,A., POCHYNYUK,O. & STOCKAND,J.D. 2005. Regulation of epithelial Na+ channel activity by conserved serine/threonine switches within sorting signals. *J.Biol.Chem.* **280,** 39161-39167.

STARUSCHENKO,A., POCHYNYUK,O., VANDEWALLE,A., BUGAJ,V. & STOCKAND,J.D. 2007. Acute regulation of the epithelial Na+ channel by phosphatidylinositide 3-OH kinase signaling in native collecting duct principal cells. *J.Am.Soc.Nephrol.* **18,** 1652-1661.

STAUB,O., DHO,S., HENRY,P., CORREA,J., ISHIKAWA,T., MCGLADE,J. & ROTIN,D. 1996. WW domains of Nedd4 bind to the proline-rich PY motifs in the epithelial Na+ channel deleted in Liddle's syndrome. *EMBO J.* **15,** 2371-2380.

STAUB,O., GAUTSCHI,I., ISHIKAWA,T., BREITSCHOPF,K., CIECHANOVER,A., SCHILD,L. & ROTIN,D. 1997. Regulation of stability and function of the epithelial Na+ channel (ENaC) by ubiquitination. *EMBO J.* **16,** 6325-6336.

STAUB,O. & VERREY,F. 2005. Impact of Nedd4 proteins and serum and glucocorticoid-induced kinases on epithelial Na+ transport in the distal nephron. *J.Am.Soc.Nephrol.* **16,** 3167-3174.

STOCKAND,J.D., STARUSCHENKO,A., POCHYNYUK,O., BOOTH,R.E. & SILVERTHORN,D.U. 2008. Insight toward epithelial Na+ channel mechanism revealed by the acid-sensing ion channel 1 structure. *IUBMB.Life* **60,** 620-628.

STOKES,J.B. 1999. Disorders of the epithelial sodium channel: insights into the regulation of extracellular volume and blood pressure. *Kidney Int.* **56,** 2318-2333.

STRUTZ-SEEBOHM,N., SEEBOHM,G., SHUMILINA,E., MACK,A.F., WAGNER,H.J., LAMPERT,A., GRAHAMMER,F., HENKE,G., JUST,L., SKUTELLA,T., HOLLMANN,M. & LANG,F. 2005. Glucocorticoid adrenal steroids and glucocorticoid-inducible kinase isoforms in the regulation of GluR6 expression. *J.Physiol* **565,** 391-401.

STRYER,L., BERG,J.M. & TYMOCZKO,L. 2003. *Biochemie.* Spektrum Akademischer Verlag GmbH, Heidelberg, Berlin.

SU,Y.R. & MENON,A.G. 2001. Epithelial sodium channels and hypertension. *Drug Metab Dispos.* **29,** 553-556.

TARUNO,A. & MARUNAKA,Y. 2010. Analysis of Blocker-labeled Channels Reveals the Dependence of Recycling Rates of ENaC on the Total Amount of Recycled Channels. *Cell Physiol Biochem.* **26,** 925-934.

THOMAS,S.V., KATHPALIA,P.P., RAJAGOPAL,M., CHARLTON,C., ZHANG,J., EATON,D.C., HELMS,M.N. & PAO,A.C. 2011. Epithelial sodium channel regulation by cell surface associated serum and glucocorticoid regulated kinase 1. *J.Biol.Chem.*

TURNHEIM,K. 1991. Intrinsic regulation of apical sodium entry in epithelia. *Physiol Rev.* **71,** 429-445.

VALLON,V. & LANG,F. 2005. New insights into the role of serum- and glucocorticoid-inducible kinase SGK1 in the regulation of renal function and blood pressure. *Curr.Opin.Nephrol.Hypertens.* **14,** 59-66.

VAN HAM,I.I. & ORON,Y. 2005. Go G-proteins mediate rapid heterologous desensitization of G-protein coupled receptors in Xenopus oocytes. *J.Cell Physiol* **204,** 455-462.

VERREY,F., FAKITSAS,P., ADAM,G. & STAUB,O. 2008. Early transcriptional control of ENaC (de)ubiquitylation by aldosterone. *Kidney Int.* **73,** 691-696.

VUAGNIAUX,G., VALLET,V., JAEGER,N.F., HUMMLER,E. & ROSSIER,B.C. 2002. Synergistic activation of ENaC by three membrane-bound channel-activating serine proteases (mCAP1, mCAP2, and mCAP3) and serum- and glucocorticoid-regulated kinase (Sgk1) in Xenopus Oocytes. *J.Gen.Physiol* **120,** 191-201.

WAGNER,C.A., FRIEDRICH,B., SETIAWAN,I., LANG,F. & BROER,S. 2000. The use of Xenopus laevis oocytes for the functional characterization of heterologously expressed membrane proteins. *Cell Physiol Biochem.* **10,** 1-12.

WALDEGGER,S., BARTH,P., RABER,G. & LANG,F. 1997. Cloning and characterization of a putative human serine/threonine protein kinase transcriptionally modified during anisotonic and isotonic alterations of cell volume. *Proc.Natl.Acad.Sci.U.S.A* **94,** 4440-4445.

WALDMANN,R. 2001. Proton-gated cation channels--neuronal acid sensors in the central and peripheral nervous system. *Adv.Exp.Med.Biol.* **502,** 293-304.

WALDMANN,R., CHAMPIGNY,G., BASSILANA,F., HEURTEAUX,C. & LAZDUNSKI,M. 1997. A proton-gated cation channel involved in acid-sensing. *Nature* **386,** 173-177.

WALDMANN,R., CHAMPIGNY,G., BASSILANA,F., VOILLEY,N. & LAZDUNSKI,M. 1995. Molecular cloning and functional expression of a novel amiloride-sensitive Na+ channel. *J.Biol.Chem.* **270,** 27411-27414.

WANG,H., TRAUB,L.M., WEIXEL,K.M., HAWRYLUK,M.J., SHAH,N., EDINGER,R.S., PERRY,C.J., KESTER,L., BUTTERWORTH,M.B., PETERS,K.W., KLEYMAN,T.R., FRIZZELL,R.A. & JOHNSON,J.P. 2006. Clathrin-mediated endocytosis of the epithelial sodium channel. Role of epsin. *J.Biol.Chem.* **281,** 14129-14135.

WANG,J., BARBRY,P., MAIYAR,A.C., ROZANSKY,D.J., BHARGAVA,A., LEONG,M., FIRESTONE,G.L. & PEARCE,D. 2001. SGK integrates insulin and mineralocorticoid regulation of epithelial sodium transport. *Am.J.Physiol Renal Physiol* **280,** F303-F313.

WEBER,W. 1999. Ion currents of Xenopus laevis oocytes: state of the art. *Biochim.Biophys.Acta* **1421,** 213-233.

WEBSTER,M.K., GOYA,L., GE,Y., MAIYAR,A.C. & FIRESTONE,G.L. 1993. Characterization of sgk, a novel member of the serine/threonine protein kinase gene family which is transcriptionally induced by glucocorticoids and serum. *Mol.Cell Biol.* **13,** 2031-2040.

WESCH,D., MIRANDA,P., AFONSO-ORAMAS,D., ALTHAUS,M., CASTRO-HERNANDEZ,J., DOMINGUEZ,J., MORTY,R.E., CLAUSS,W., GONZALEZ-HERNANDEZ,T., ALVAREZ DE LA ROSA,D. & GIRALDEZ,T. 2010. The neuronal-specific SGK1.1 kinase regulates {delta}-epithelial Na+ channel independently of PY motifs and couples it to phospholipase C signaling. *Am.J.Physiol Cell Physiol* **299,** C779-C790.

WIEMUTH,D., LOTT,J.S., LY,K., KE,Y., TEESDALE-SPITTLE,P., SNYDER,P.M. & MCDONALD,F.J. 2010. Inter-action of serum- and glucocorticoid regulated kinase 1 (SGK1) with the WW-domains of Nedd4-2 is required for epithelial sodium channel regulation. *PLoS.One.* **5,** e12163.

WILKINSON,K.A. & HENLEY,J.M. 2010. Mechanisms, regulation and consequences of protein SUMOylation. *Biochem.J.* **428,** 133-145.

WU,Z. & SIMISTER,N.E. 2001. Tryptophan- and dileucine-based endocytosis signals in the neonatal Fc receptor. *J.Biol.Chem.* **276,** 5240-5247.

XIONG,Z.G., ZHU,X.M., CHU,X.P., MINAMI,M., HEY,J., WEI,W.L., MACDONALD,J.F., WEMMIE,J.A., PRICE,M.P., WELSH,M.J. & SIMON,R.P. 2004. Neuroprotection in ischemia: blocking calcium-permeable acid-sensing ion channels. *Cell* **118,** 687-698.

YAMAMURA,H., UGAWA,S., UEDA,T., NAGAO,M. & SHIMADA,S. 2004a. Capsazepine is a novel activator of the delta subunit of the human epithelial Na+ channel. *J.Biol.Chem.* **279,** 44483-44489.

YAMAMURA,H., UGAWA,S., UEDA,T., NAGAO,M. & SHIMADA,S. 2004b. Protons activate the delta-subunit of the epithelial Na+ channel in humans. *J.Biol.Chem.* **279,** 12529-12534.

YAMAMURA,H., UGAWA,S., UEDA,T., NAGAO,M. & SHIMADA,S. 2005a. Icilin activates the delta-subunit of the human epithelial Na+ channel. *Mol.Pharmacol.* **68,** 1142-1147.

YAMAMURA,H., UGAWA,S., UEDA,T., NAGAO,M. & SHIMADA,S. 2006. A novel spliced variant of the epithelial Na+ channel delta-subunit in the human brain. *Biochem.Biophys.Res.Commun.* **349,** 317-321.

YAMAMURA,H., UGAWA,S., UEDA,T. & SHIMADA,S. 2005b. Evans blue is a specific antagonist of the human epithelial Na+ channel delta-subunit. *J.Pharmacol.Exp.Ther.* **315,** 965-969.

YOO,D., KIM,B.Y., CAMPO,C., NANCE,L., KING,A., MAOUYO,D. & WELLING,P.A. 2003. Cell surface expression of the ROMK (Kir 1.1) channel is regulated by the aldosterone-induced kinase, SGK-1, and protein kinase A. *J.Biol.Chem.* **278,** 23066-23075.

YUE,G., MALIK,B., YUE,G. & EATON,D.C. 2002. Phosphatidylinositol 4,5-bisphosphate (PIP2) stimulates epithelial sodium channel activity in A6 cells. *J.Biol.Chem.* **277,** 11965-11969.

ZECEVIC,M., HEITZMANN,D., CAMARGO,S.M. & VERREY,F. 2004. SGK1 increases Na,K-ATP cell-surface expression and function in Xenopus laevis oocytes. *Pflugers Arch.* **448,** 29-35.

ZHANG,P. & CANESSA,C.M. 2002. Single channel properties of rat acid-sensitive ion channel-1alpha, -2a, and -3 expressed in Xenopus oocytes. *J.Gen.Physiol* **120,** 553-566.

ZHANG,Z.R., CHOU,C.F., WANG,J., LIANG,Y.Y. & MA,H.P. 2010. Anionic phospholipids differentially regulate the epithelial sodium channel (ENaC) by interacting with alpha, beta, and gamma ENaC subunits. *Pflugers Arch.* **459,** 377-387.

ZHOU,R., KABRA,R., OLSON,D.R., PIPER,R.C. & SNYDER,P.M. 2010. Hrs controls sorting of the epithelial Na+ channel between endosomal degradation and recycling pathways. *J.Biol.Chem.* **285,** 30523-30530.

ZHOU,Z., DUERR,J., JOHANNESSON,B., SCHUBERT,S.C., TREIS,D., HARM,M., GRAEBER,S.Y., DALPKE,A., SCHULTZ,C. & MALL,M.A. 2011. The ENaC-overexpressing mouse as a model of cystic fibrosis lung disease. *J.Cyst.Fibros.* **10 Suppl 2,** S172-S182.

VII. Appendix

VII. 1 Abbreviations

General Abbreviations	Denotation
3M3FBS	N-(3-trifluoromethylphenyl)-2,4,6-trimethylbenzenesulfonamide
A/D	analog-to-digital
AMPA	2-amino-3-(5-methyl-3-oxo-1,2- oxazol-4-yl)propanoic acid
ASIC	acid sensing ion channel
ATP	adenosintriphosphat
a.u.	arbitrary unti
BFA	brefeldin A
BK	big Ca^{2+} dependent K^+ channel
bp	base pair
CAP	channel activating protease
cAMP	cyclic adenosine monophosphate
cDNA	DNA-sequence without introns (coding sequence)
CF	cystic fibrosis
CFTR	cystic fibrosis transemembrane regulator
CFP	cyan fluorescent protein
CNS	central nervous systems
COMMD1	copper metabolism Murr1 domain1
cRNA	complementary, revers transcribed RNA of a coding sequence, with a PolyA tail
Ct	threshold cycle
CTP	Cytidintriphosphat
C-terminus	carboxyl-terminus of a peptide
ΔI	current difference
DAG	Diacylglycerol
ddH_2O	double distilled water
DEG	degenerin
$DEPC-H_2O$	0,1% diethylpyrocarbonate-water (nuclease-free)
DIG	digoxigenin
DMEM	Dulbecco's Modified Eagle Medium
DMSO	dimethyl sulfoxide
DNA	desoxyribonucleic acid
ds	double-stranded
DUB	de-ubiquitylating enzyme
Dyn	Dynasore

EAAT	excitatory amino-acid transporters
EDTA	ethylendimintetraacetate
e.g.	for example (*exemplum gratia*)
ENaC	epithelial sodium channel
ERK	extracellular-regulated kinase
et al.	and others (*et alii*)
FBS	fetal bovine serum
Fi	immobile fraction
Fig.	figure
Fm	mobile fraction
FRAP	fluorescence recovery after photo bleaching
g	conductance
GDI	guanosine nucleotide dissociation inhibitor
GDP	guanosine di-phosphate
GFP	green fluorescent protein
Glut8	glucose transporter
GPCR	G-protein coupled receptor
GRE	glucocorticoid response element
GST	glutathion-S-transferase
GTP	guanosine tri-phosphate
HEK293	human embryo kidney 293 cell line
HEPES	N-(2-hydroxyethyl)piperazin-N'-(2-ethansulfonic acid)
HRP	horseradish peroxidase
I	current
I_C	capazitive current
IC_{50}	half maximal inhibitory concentration
i.e.	*id est*
I_i	ion current
I_M	transmembrane current
ISH	*in situ* hybridization
KCNE/Q	voltage gated K^+ channel
LL	dileucine
LPA	lysophosphatidic acid
MEC	mechanosensitive channels from *C. elegans*
MR	mineralcorticoid receptor
MTC	monkey temporal cortex
n	number of experiments
N	number of batches/donors or number of channels
NaDC-1	dicarboxylate transporter
NALCN	non-selective Na^+-leak channel
Nedd4-2	neural precursor cell-expressed, developmentally down-regulated 4-2

NHE3	Na^+/H^+ exchanger 3
n.i.	not injected
NMDG	N-methyl-D-glucamine
NS	nervous system
n.s.	not significant
N-Terminus	amino-Terminus of a peptide
OPTI-MEM	reduced serum medium, modification of Eagle's Minimum Essential Media
OR2	oocyte ringer 2
OR2 w/o Ca^{2+}	calcium-free oocyteringer 2
p	level of significance
PAGE	polyacrylamide gelelectrophoresis
PBS	phosphate buffered saline
PCR	polymerase chain reaction
PD	potential difference
PDK	phosphoinositide dependent kinase
PHA	pseudohypoaldosteronism
PI3K	phosphatidylinositol 3 kinase
PKA	protein kinase A
PLC	phospholipase C
PIP2	phosphatidylinositol-bisphosphate
Po	open probability
PVDF	polyvinylidenfluorid
PY motif	proline tyrosine motif (PPXY, X = any amino acid)
qPCR	quantitative real-time polymerase chain reaction
R	resistance
RFU	relative fluorscence unit
RNA	ribonucleic acid
RT	room temperature
SDS	sodium dodecyl sulfate
SE	standard error of the mean
SGK	serum- and glucocorticoid-induced kinase
SSC	saline sodium citrate buffer
τ	recovery constant
Tab.	Table
TE-buffer	Tris-HCL/EDTA-buffer
TES	TEVC ENaC solution
TEVC	Two-electrode-voltage-clamp
tf	transferrin
tf-AF568	transferrin conjugated to AlexaFluor568
tfr	transferrin receptor
TGN	*trans*-Golgi network

TM	Transmembrane domain
Tm	melting temperature
TNB	Tris-Na$^+$-buffer
TRPV	Transient Receptor Potential Vanilloid
U	voltage
V$_{command}$	clamp potential
Vm	membrane voltage
w/o	without
WW-domain	tryptophan-tryptophan domain
YFP	yellow fluorescent protein
*	significant

Units	Denotation
A	ampere
° C	degree Celcius
F	Faraday = $N_A \cdot e \cdot 1$ mol = 96485,3399 Coulomb
g	gram
h	hour
L	liter
M	molar
m	metre
min	minute
s	second
S	siemens
V	volt
Ω	ohm
%	percent

Order of magnitude	Denotation
G	giga (10^9)
M	mega (10^6)
c	centi ($10^{-2)}$
m	milli (10^{-3})
µ	micro (10^{-6})
n	nano (10^{-9})
p	pico (10^{-12})

VII. 2 Acknowledgements

Finally, I want to say thank you to all the people that contributed to the success of this work:

First, I thank sincerely my directors Diego Alvarez de la Rosa and Teresa Giraldez that they gave me the opportunity to elaborate my PhD thesis in their "small starting up lab" at the University of La Laguna, Tenerife. I'm further grateful to Manolo Feria for his courtesy to not only lend work space, but also an open ear whenever necessary. Last mentioned also accounts for Lina Perez. Gracias ranas, por dejar tocarse los huevos!

For my colleagues, technicians and the other PIs at the ULL/HUNSC I state a huge and overwhelming thank you: foremost Iván and Pablo! Thanx Leni, Ida, Fabian, Lauri, Joni, Laura, Augustin, Natalia, Dani, Ricardo, Chus, Ana, Mayte, Ada, Federico, Jesi, Bea, Miriam, Monica, Yezer, Marta, Judith, Carmen, David, Nacho, Domingo, Javier, Jaime, Tomas, M&Ms, Almut, Mari, Javi, Carlos, Juan, Ana, Ventura, Antonio, Marta & Cristi, Heidi, Adriana, Marta, Eli, Beli, Violenta, Elena, Javi peluki, Felix, Chano, Estefania, Jonay, Oliver, Cristina, Emiliano, Lari, Isa, Cristina, Jonathan, Yared, Chaxi, Felix, David, Raúl, Rosa, Maria, Sonia… ← just in case ;)

And I thank vastly all collaborators, who facilitated me working in their laboratories: at the JLU Giessen my former laboratory – Professor Clauss, Martin Fronius and Mike Althaus; at the National Institutes of Health/NINDS – Miguel Holmgren and Jorge Contreras and at the Max Planck Institute for Experimental Medicine, Göttingen – Walter Stühmer and Luis Pardo. Of course, also the colleagues and technicians over there and not particularly mentioned here deserve a big thank you.

Since nothing works without funding, I deeply acknowledge the assigned grants for conducting my studies during approximately the last decade: FPI from the Spanish Ministry of Science and Innovation, Acción integrada hispano-alemana and Leonardo-Erasmus placements of the EU from the Deutscher Akademischer Austauschdienst and a scholarship from the Geheimrat Jakob Sigle-Salamander Stiftung.

To my old friends at home and new friends on the Canary Islands I owe more than just a thank you on this page. To mention all of them would go beyond the scope, but the most appreciated ones from Tenerife are spotlighted here: Leti, Gabi (to whom I'm not a "guiri"), Ángel (*nomen est omen*), Gio, Mari, Carlos, Luci, Elena, Mila, Tobi, Normis, Eli, Gabi, Maria, Gonzalo, Loli (for being like a sister), Pedri, Alfred, David, Pepillo, Natalia, Jesús, Doro, Dedde, Mike (fürs Erholungsdomizil) and Ina (mi compatriota!).

Last but not least, I say "Danke & Salamat" to my family and beloved ones in heaven and on earth. Though words are insufficient to show how profoundly I feel indebted… I'd never have endured without all the received immense personal effort, constant help and unfailing support, not only financially, but also by endowing me with education, motivation, cheering, faith, persistence, strength, security, attendance, care, affection and love.

Curriculum vitae

Full name: Diana Luise Wesch

Date of birth: February 20, 1983

Place of birth: Heilbronn am Neckar, Germany

Citizenship: German

Education

2002   **Abitur**

Ernst-Sigle-Gymnasium, Kornwestheim, Germany

2002 – 2005   **'Vordiplom' in biology**

Justus-Liebig-Universität, Gießen, Germany

2005 – 2006   **term abroad**

Universidad de Sevilla, Spain

2006 – 2008   **'Diplom' in biology**

'Diplom' thesis with Prof. Dr. W. Clauss,

Department of Animal Physiology,

Justus-Liebig-Universität, Gießen, Germany

2008 – present   **PhD student**

PhD thesis with Diego Alvarez de la Rosa (PhD) & Teresa Giraldez (PhD),

Unit of Pharmacology, Faculty of Medicine & Research Unit of the University Hospital Nuestra Señora de la Candelaria,

Universidad de La Laguna, Tenerife, Spain

Publications

2010   **Wesch, D.**, Miranda, P., Afonso-Oramas, D., Althaus, M., Castro-Hernández, J., Dominguez, J., Morty, R.E., Clauss, W., González-Hernández, T., Alvarez de la Rosa, D. & Giraldez, T. (2010) The neuronal-specific SGK1.1 kinase regulates δ-epithelial Na$^+$ channel independently of PY motifs and couples it to Phospholipase C signaling. *Am J Physiol Cell Physiol*, 299(4):C779-90

under review   **Wesch D.**, Althaus M., Miranda P., Cruz-Moros I., Fronius M., González-Hernández T., Clauss W.G., Alvarez de la Rosa D. & Giraldez T. Differential N-termini in epithelial Na$^+$ channel δ subunit isoforms modulate channel trafficking to the membrane.

under review   Miranda P., Contreras J., **Wesch, D.**, Sigworth F.J., Holmgren M. & Giraldez T. Calcium induces structural rearrangements of the gating ring of the human BK channel.